Expanding Protein Functions by Non-Natural Amino Acid Incorporation and Site-Specific Bioconjugation

---

A Dissertation

Presented to

the faculty of the School of Engineering and Applied Science

University of Virginia

---

in partial fulfillment

of the requirements for the degree

Doctor of Philosophy

by

Sung In Lim

May

2015

APPROVAL SHEET

The dissertation

is submitted in partial fulfillment of the requirements

for the degree of

Doctor of Philosophy

AUTHOR

The dissertation has been read and approved by the examining committee:

Inchan Kwon

Advisor

Roseanne M. Ford

David L. Green

Michael R. Shirts

Young S. Hahn

Accepted for the School of Engineering and Applied Science:

Dean, School of Engineering and Applied Science

May

2015

Acknowledgments

‘My journey is about to end, but it feels like it’s still on the way. A vast expanse to explore lies before me, and I know I have plenty of time.’ This is the first sentence I wrote in acknowledgments of my master’s thesis seven years ago. It’s weird but true that it is the first sentence of my doctoral dissertation acknowledgments again. Yes, now I understand that the journey will come to an end only after my passion for research burns down. I don’t know when the day will be. What matters is to enjoy every step of the itinerary, but to endure when I must.

I agree with the saying that the doctoral course is a lonely battle, only in part. Rather, without backup forces, it’s a losing battle. Almost 1,000 emails are stored in one special subfolder of my inbox. It is labeled ‘Prof. Kwon’. The number shows how cooperatively and enthusiastically ‘we’ have gone through the battle over the past four years. Under supervision of Professor Inchan Kwon, my idea and motivation have gotten sifted, organized, polished, and then become a reality. I would like to express my deepest gratitude to him for training me with all his might. Professors David Green, Roseanne Ford, Michael Shirts, and Young S. Hahn willingly accepted to serve on my dissertation committee, and permitted me to use their names as references. I sincerely appreciate your commitment. My lab mates, Gregoire Simpson, Edward Wong, Jacob Irwin, and Shun Zheng, gave me a lot of assistance with my research and job interview. Thank you, guys.

I definitely remember how I could set off this journey. My parents, parents-in-law and my brother always show respect for my decision with unwavering support and prayers for me. In the opposite side of the world, I feel them every minute. Every single bit of my achievement is a reflection of their love and faith towards me. To my wife, Chanyoung, and son, Geonwoo: You

cover me like the Aegis–an impenetrable shield–in the immediate vicinity. All of my weakness and inability are protected and cured by your sublime sacrifice and sweet innocence. You are a map and compass teaching me how to lead our way together on faith, hope and love. Thank you for being with me on this journey.

Abstract

Conventional approaches to modify a protein function rely on 1) amino acid mutagenesis in which an original amino acid(s) is substituted with any of other natural amino acids, and 2) residue-specific conjugation of a functional molecule to lysine or cysteine. Recent advances in genome engineering and protein evolution have achieved an expanded genetic code, reassigning an amber stop codon to encode a series of non-natural amino acids (NNAA) with high fidelity. Site-specific incorporation of a non-natural amino acid, therefore, should prompt expansion of new protein functions. In particular, incorporation of a NNAA bearing bioorthogonal reactivity can act as a chemoselective handle, enabling generation of a chemically well-defined protein conjugate.

This dissertation details four independent investigations. First, in a quest to engineer long-lived therapeutic proteins with a combined use of NNAA incorporation and site-specific bioconjugation, I investigated the potential of a site-specific fatty acid-conjugation as a tool to extend *in vivo* half-life of proteins. *p*-Ethynyl-L-phenylalanine was incorporated into a predetermined site of superfolder green fluorescent protein, and then reacted with azido-palmitic acid via copper-catalyzed azide-alkyne cycloaddition (CuAAC). The resulting conjugate exhibited binding affinity towards serum albumin and prolonged *in vivo* half-life when injected into mice, opening the possibility of a fatty acid as a half-life extender of therapeutic proteins.

Second, for proteins to which fatty acid-conjugation is not applicable, I developed site-specific albumin conjugation to extend *in vivo* half-life of proteins. Upon genetic incorporation of two *p*-azido-L-phenylalanines into permissive sites, urate oxidase used to treat tumor lysis syndrome was conjugated to human serum albumin through a bifunctional linker using strain-

promoted azide-alkyne cycloaddition (SPAAC) and thiol-maleimide coupling. The conjugate was chemically well-defined with high homogeneity, and showed increased circulation time versus the wild type in mice study.

Third, as a novel application in biocatalysis, dihydrofolate reductase, an enzyme that coverts dihydrofolate to tetrahydrofolate, was site-specifically modified with *p*-ethynyl-L-phenylalanine. Under the optimized CuAAC condition, the enzyme was chemoselectively biotinlyated without loss of enzymatic activity and then bound to a streptavidin plate, demonstrating controllable enzyme immobilization with defined and homogeneous orientation.

Lastly, in order to demonstrate the effect of substrate channeling induced by controlled orientation of the active sites in the multi-enzyme cascade reaction, formate dehydrogenase and mannitol dehydrogenase that perform a coupled enzymatic reaction were conjugated through chemical linkers using mutually orthogonal conjugation chemistries: SPAAC and inverse electron demand Diels-Alder reaction. Positioning of the active site relative to the other was modulated by site-specific incorporation of *p*-azido-L-phenylalanine into the same or the opposite side of the active site in each enzyme. Higher catalytic efficiency was observed when the enzyme pair had the active sites facing each other than oriented outwards, suggesting that processing of the intermediate between enzymes was accelerated by enzyme orientation favorable for substrate channeling.

The significance of dissertation research lies in 1) exploring a protein design scheme that combines the genetic incorporation of NNAAs and the bioorthogonal conjugation chemistries, and 2) its empirical applications to generate truly multifunctional proteins bearing both innate and acquired functionality at their optima with well-defined homogeneity.

Table of Contents

List of Figures

List of Schemes

List of Tables

Chapter 1: Introduction

1.1. Expanded Genetic Code and Incorporation of Non-natural Amino Acids

Successful protein engineering greatly depends on the protein sequence and structure space available for modification. One straightforward way is to increase the number of amino acids available for protein synthesis. Non-natural amino acids (NNAAs) have side chains with distinct polarity, charge, reactivity, or shape from those found in natural amino acids.

Site-specific incorporation technique allows introduction of a NNAA into a specific site(s) of a protein (Figure 1.1) [1]. Since an incorporation site can be flexibly chosen, it is appropriate for local protein modification without perturbing overall protein structure. In order to establish the site-specific incorporation technique, three issues should be addressed. First, a heterologous orthogonal pair of aminoacyl-tRNA/aminoacyl-tRNA synthetase specific for a NNAA should be developed. Second, a new genetic code should be assigned to a NNAA. An amber stop codon (UAG), the least used one in *E. coli* among three stops codons, is employed to encode a NNAA. Third, an endogenous release factor 1 which terminates translation by recognizing an amber codon should be genetically deleted from the expression host E. coli to exclusively assign an amber codon to encode a NNAA. At the same time, all amber codons in the genome must be mutated into other stop codons such as UAA and UGA in order to sustain stable expression of endogenous essential genes.

Our lab has performed a series of NNAA incorporation research using an orthogonal pair of yeast phenylalanyl-tRNA amber suppressor/phenylalanyl-tRNA synthetase which had been developed to incorporate phenylalanine analogs in response to an amber codon [2–4]. Previously, two phenylalanine analogs, *p*-bromo-L-phenylalanine and 2-naphthyl-L-alanine, were successfully introduced into the active site of an enzyme. In this research, the orthogonal pair was used to introduce a terminal alkyne-bearing NNAA, *p*-ethynyl-L-phenylalanine (pEthF).

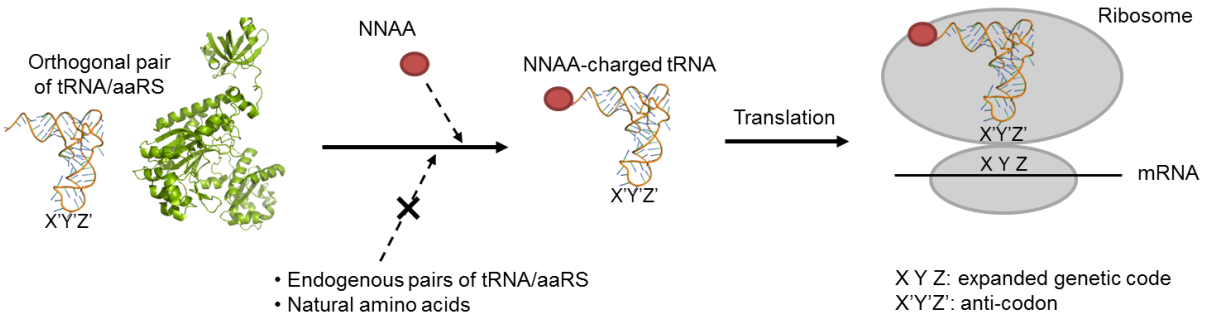

Figure 1.1. Site-specific incorporation of a non-natural amino acid by an orthogonal pair of tRNA amber suppressor and tRNA synthetase.

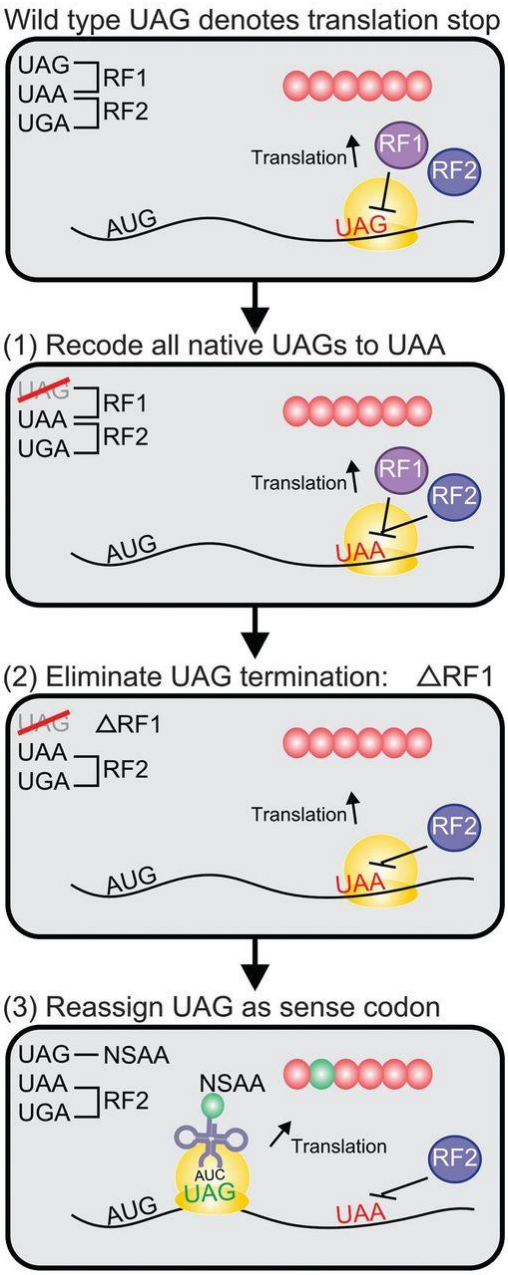

Figure 1.2. Genomically recoded *Escherichia coli*. UAG, amber codon. RF1, release factor 1. RF2, release factor 2 [5]**.** NSAA: Non-standard (non-natural) amino acid.

Moreover, various mutant pairs of tRNA amber suppressor/tRNA synthetase originating from different species have been reported by other groups, and used to incorporate more than 50 NNAAs in *E. coli* [6]. Of particular usefulness to our research is a mutant pair of *Methanococcus jannaschii* tyrosyl-tRNA/tyrosyl-tRNA synthetase which can incorporate *p*-azido-*L*-phenylalaine (pAzF) since the azide functionality in pAzF as well as alkyne functionality in pEthF can participate in bioconjugation known to be bioorthogonal and chemoselective [7].

The mutant tRNA amber suppressor/tRNA synthetase pairs cannot make maximum effectiveness when harbored by a general *E. coli* host. That's because amber codons in the genome are potential off-targets for a tRNA amber suppressor. In addition, an endogenous release factor 1 (RF1) strongly competes with a tRNA amber suppressor for recognition of an amber codon in the target gene, resulting in a translation bias towards an early truncation rather than a full-length product containing a NNAA at an amber site [8,9]. Recently, extensive genome engineering has created genetically RF1-free *E. coli*, C321ΔA.exp, with all amber codons in the genome deleted while exhibiting a normal cell growth (Figure 1.2) [5]. Therefore, the host should truly expand the genetic code for NNAA incorporation. In order to achieve an appreciable expression of a target protein, the strain was utilized to incorporate pAzF in our research.

1.2. Bioorthogonal Chemistry

1.2.1. Azide-Alkyne Cycloaddition

Joining two chemical units in a highly specific manner to generate a new compound is called click chemistry. The azide-alkyne cycloaddition is one of the most popular click chemistry, and can be implemented with or without a catalyst. The copper-catalyzed azide-alkyne cycloaddition (CuAAC) is a reaction in which a terminal alkynyl group (HC≡C-R) and an azido

group (-N=N+=N-R) are united to give a 1,4-di-substituted 1,2,3-triazole in the presence of catalytic copper (I) (Scheme 1.1) [10,11]. Its uniqueness lies in bioorthogonality of both moieties;

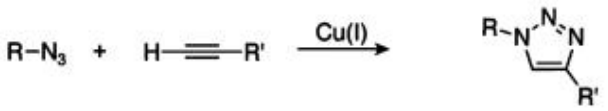

Scheme 1.1. Copper-catalyzed azide-alkyne cycloaddition.

that is, they are absent in all natural amino acids and thus ensure a highly selective reaction [12]. In addition, the CuAAC can be performed in aqueous solutions in which most proteins are kept stable, and, therefore, is useful in protein bioconjugation. For *in situ* generation of Cu(I), the CuAAC is initiated by adding a reductant to a reaction mixture containing Cu(II) as well as reaction partners. To stabilize transient Cu(I) ions, use of a Cu(I)-chelating ligand such as TBTA and THPTA is recommended.

The strain-promoted azide-alkyne cycloaddition (SPAAC) is an alternative bioorthogonal reaction when either or both of reaction partners show sensitivity towards copper ions such as inhibition and degradation [13]. Instead of a terminal alkyne, a ring-strained alkyne is reacted with an azide without copper ions, resulting in a triazole complex (Scheme 1.2). SPAAC has found novel applications in vivo imaging due to its metal-free biocompatibility. In protein bioconjugation, SPAAC is applicable only to an azide-bearing protein, since a bulky ring-strained alkyne cannot be introduced into a protein by a current NNAA incorporation technique. A conjugation partner is modified with a dibenzocyclooctyl (DBCO) or a difluorocyclooctyl (DIFO) motif which readily undergoes a strain-promoted SPAAC with an azide-bearing protein.

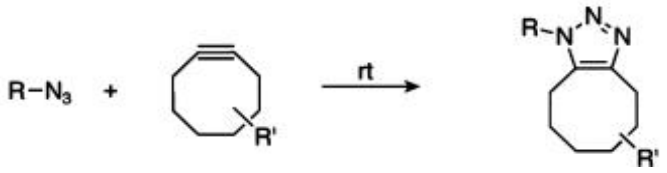

Scheme 1.2. Strain-promoted azide-alkyne cycloaddition.

1.2.2. Inverse Electron Demand Diels-Alder Reaction

Tetrazines irreversibly undergo retro-[4+2]-cycloaddition with activated dienophiles such as trans-cyclooctene [14], norbornene [15], and cyclopropene [16], releasing N_2 as a by-product (Scheme 1.3). The fast rate of inverse electron demand Diels-Alder (IEDDA) reaction is useful for *in vivo* bioconjugation where a target protein is exposed to dynamic biological processes and low in abundance [17–19]. Reactivity of strained alkenes towards tetrazine varies as much as three orders of magnitude with trans-cyclooctene reaching 17,000 $M^{-1}s^{-1}$–the highest reaction rate ever attained in chemoselective bioconjugation [20,21]. IEDDA reaction has been demonstrated to retain the orthogonality towards the azide-alkyne cycloaddition, and therefore applied to a simultaneous, multi-target labeling in combination with CuAAC or SPAAC [22–24].

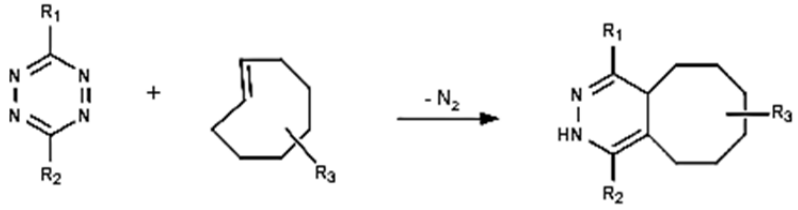

Scheme 1.3. Inverse electron demand Diels-Alder reaction.

1.3. Protein Engineering through Bioconjugation

Protein bioconjugation refers to a covalent linkage between a protein and any molecule that can confer a new or improved function on a protein. Common bioconjugation reactions are mediated by reactive amino acid residues such as lysine and cysteine (Scheme 1.4) [25]. For example, a fluorescent dye activated with N-hydroxysuccinimide ester is coupled to ε-amine in lysine in a slightly basic solution to yield an amide bond. A maleimide-activated reagent reacts with a sulfhydryl group in cysteine to form a thioether linkage at neutral pH. Even though these chemistries are simple and easy to perform, they often lack site-selectivity and end-product homogeneity since positions of natural amino acids cannot be controlled. To attain site-specific protein bioconjugation, installing a bioorthogonal chemical handle onto a protein followed by coupling through bioconjugation chemistry is an emerging strategy [26], and forms the foundation of the dissertation research as described in Chapter 2 through 5.

1.3.1. Extending Serum Half-life of Therapeutic Proteins through Albumin Binding / Conjugation

Advances in protein bioconjugation have witnessed a growing application of proteins in the field of therapeutics. Therapeutic proteins hold an increasing share in number and frequency of use in treating diseases, accounting for 34% (85-billion dollar) of combined worldwide sales of 100 blockbuster drugs in 2010. However, their clinical application is often limited. One major obstacle is their short serum half-life arising from renal filtration, proteolytic degradation, and pinocytosis. The result is a severe clinical shortcoming in that frequent injections give rise to poor patient compliance and high cost, thereby adversely affecting patients' quality of life. The binding/conjugation of therapeutic proteins to serum albumin has become a very effective way to

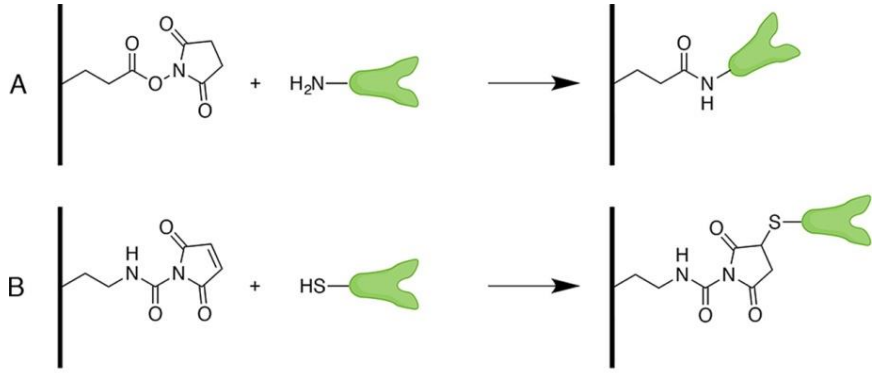

Scheme 1.4. Conventional protein bioconjugation chemistries. (A) Crosslinking of N-hydroxysuccinimide ester with a primary amine in lysine. (B) Crosslinking of maleimide with a sulfhydryl group in cysteine [27].

extend serum half-life of therapeutic proteins. Human serum albumin (HSA) has inherently long serum half-life of 19 days due to the neonatal Fc receptor (FcRn)-mediated recycling as well as its size (67 kDa) large enough to evade renal filtration [28]. Upon fluid-phase endocytosis, HSA is bound to FcRn at a low pH (6.0) of early endosomes and then transported back to the cell surface instead of being degraded in lysosomes. HSA is released back to the blood due to its low affinity to FcRn at pH 7 of the blood [29,30]. Therefore, the FcRn-mediated recycling makes the HSA-binding/conjugation an attractive strategy to extend therapeutic protein half-life. Recently, the conjugation of a natural HSA ligand, fatty acid, has been successfully used to extend serum half-life in vivo of two therapeutic peptides, insulin and glucagon-like peptide-1 agonist (GLP1) via acylation at lysine residues [31,32]. Seven binding sites in HSA have been identified to accommodate saturated fatty acids with 10-18 carbons [33,34]. Compared to direct chemical conjugation of HSA to therapeutic peptides, this approach has the advantage of higher activity to mass ratio [35], while the immunogenicity of original peptides is greatly reduced [36,37]. Moreover, in contrast to the genetic fusion of albumin-binding domain, fatty acid-conjugation is not limited to N-term or C-term of therapeutic proteins. However, fatty acid-conjugation to multiple lysine residues of therapeutic proteins sometimes leads to heterogeneous mixtures of isomers, compromising pharmaceutical activity and downstream processing (Figure 1.3). It was reported that fatty acid-conjugation to multiple lysine residues of interferon-α led to 80% reduction in its antiviral potency [38]. Therefore, fatty acid conjugation has been limited to small peptides with a small number of lysine. I hypothesized that NNAA incorporation to only one permissive site of a therapeutic protein followed by fatty acid-conjugation through CuAAC will overcome these limitations (Figure 1.3). Therefore, I proposed the site-specific fatty acid-

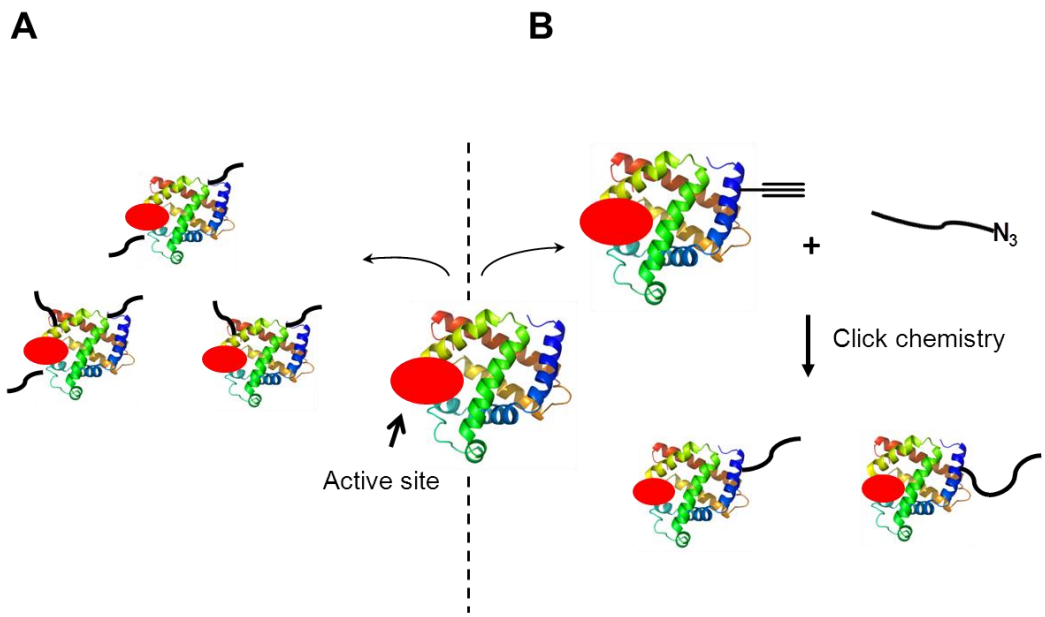

Figure 1.3. Fatty acid conjugation to a therapeutic protein. (A) Conventional chemistry. (B) Site-specific CuAAC.

conjugation as a general strategy to extend serum half-life for a range of therapeutic peptides and proteins without compromising their pharmaceutical activity.

For proteins whose physicochemical properties are incompatible with hydrophobicity of a fatty acid reaction conditions for CuAAC, I propose the site-specific conjugation of human serum albumin through SPAAC as an alternative strategy to prolong *in vivo* half-life of therapeutic proteins.

1.3.2. Construction of Efficient Enzymatic Reaction Systems by Controlling Orientation of Active Sites

Enzymes are a class of proteins that have catalytic activities for conversion of a substrate to a product in a highly selective and fast way, and continue to become increasingly important as biocatalysts for synthesis of valuable compounds. This is because enzymes meet the need for green chemistry in which product formation is maximized while generation of hazardous substances is minimized. Some enzymes that catalyze synthetically useful reactions are dependent upon the availability of cofactors. Unfortunately, cofactor-dependent enzymes are of little use in industrial-scale applications due to high cost of cofactors.

Nicotinamide adenine dinucleotide (NADH) and nicotinamide adenine dinucleotide phosphate (NADPH) are cofactors essential for some enzymes to perform redox reactions, and are found in two forms: reduced or oxidized. They cost about $30 per mmol, which is too expensive to be used in stoichiometric amounts. To overcome the cost obstacle, *in situ* cofactor regeneration system that enzymatically reduces $NAD(P)^+$ to NAD(P)H have been developed in a number of ways [39]. In particular, with increasing environmental consideration, a green and sustainable regeneration method is becoming attractive. Formate dehydrogenase (FDH) readily

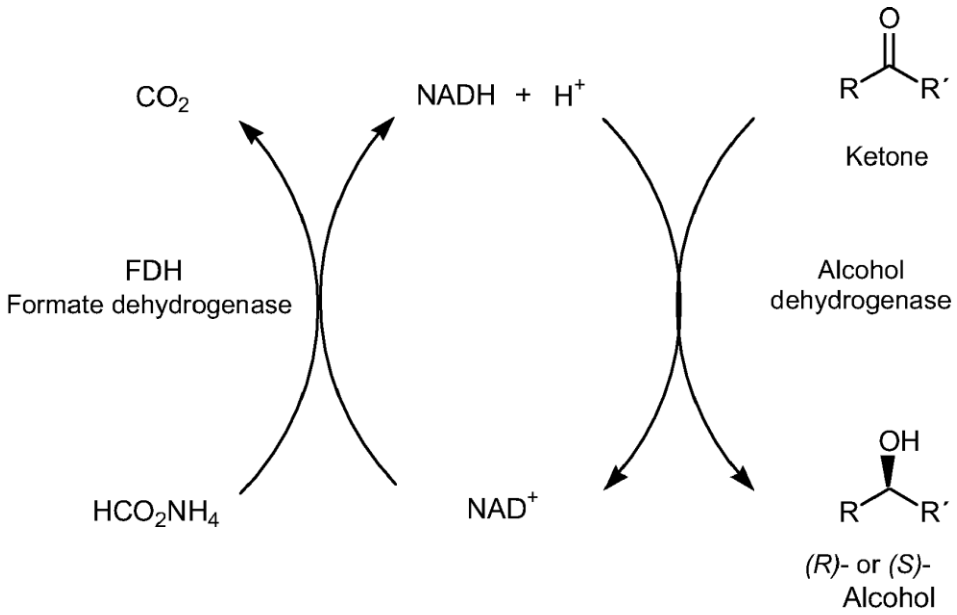

Figure 1.4. Conversion of ketone to alcohol by alcohol dehydrogenase coupled to the enzymatic cofactor regeneration by FDH.

reduces cofactors by concomitantly oxidizing formate to carbon dioxide. Compared to other regeneration methods that utilize organometallic mediator or direct electrochemical transformation, the enzymatic cofactor regeneration shows excellent regioselectivity, i.e. the ability to produce bioactive 1,4-NAD(P)H. By supplementing the cofactor-mediated redox reaction that generates a desired product with FDH, substrates and cofactors, the entire system can operate continuously without depletion of cofactors. For example, the enzymatic production of alcohol from ketone by alcohol dehydrogenase is fueled by continuous regeneration of NADH through FDH-mediated formate oxidation (Figure 1.4).

Nature has evolved the multienzyme cascade reaction system that accelerates the overall reaction rate by preventing the diffusion of an intermediate into the bulk phase but directing it to a subsequent active site. The intermediate can be channeled between two separate enzymes or between two active sites within a single enzyme [40–42]. To understand the effect of spatial organization of each enzyme in the multienzyme system on the overall reaction efficiency, multienzyme scaffolds have been engineered using DNA nanotechnogy or programmed protein-protein interactions [43,44]. Closely spaced enzymes showed enhanced activity of cascade reactions attributed by increased probability of the intermediate transfer between active sites. These studies are important for designing multienzyme nanostructures with optimal pathway flux and kinetics. Nevertheless, it remains elusive how the orientation of an active site relative to a subsequent active site affects enzymatic cascade reaction rates due to technical hurdles for precise control over a conjugation site. I hypothesized that substrate channeling is more pronounced when two cascade enzymes are interlinked with their active sites oriented towards each other. Therefore, I propose that, through site specific incorporation of NNAAs into appropriate positions of paired enzymes followed by bioorthogonal interenzyme conjugation

through a bifunctional linker, diffusion of enzymatically regenerated cofactors is restricted to the active site of the downstream enzyme, thus enhancing the reaction rate.

The enzymatic reaction system is made more efficient by enzyme immobilization. If an enzyme is immobilized onto a solid support, after repeated cycles of cofactor regeneration and enzymatic reactions, an enzyme can be easily separated from products as well as other chemical reagents and may be utilized again. Also, an immobilized enzyme generally exhibits increased stability against changes in temperature and pH. Therefore, it is essential for commercial purposes to recycle an enzyme through immobilization, and this is where protein bioconjugation should play its role. Conventional enzyme immobilization has been mediated by reactions between reactive natural amino acids such (Lys, Cys) and activated reaction partners. As discussed previously, however, conventional methods usually result in randomly oriented conjugations, further leading to reduced enzyme activity and lack of reproducibility (Figure 1.5). Benefits of a controlled orientation and homogenous array of proteins on a support were recently demonstrated by installing an orthogonal functionality into a terminus of an antibody. Antigen-binding sensitivity as well as reproducibility was greatly enhanced due to a controlled orientation of an antigen-binding domain of an antibody. I hypothesize that, with an aid of NNAA incorporation into a permissive site of an enzyme and bioorthogonal chemistry, directed immobilization of an enzyme with well-defined orientation and native activity can be performed to create a highly sensitive and reproducible enzymatic reaction system.

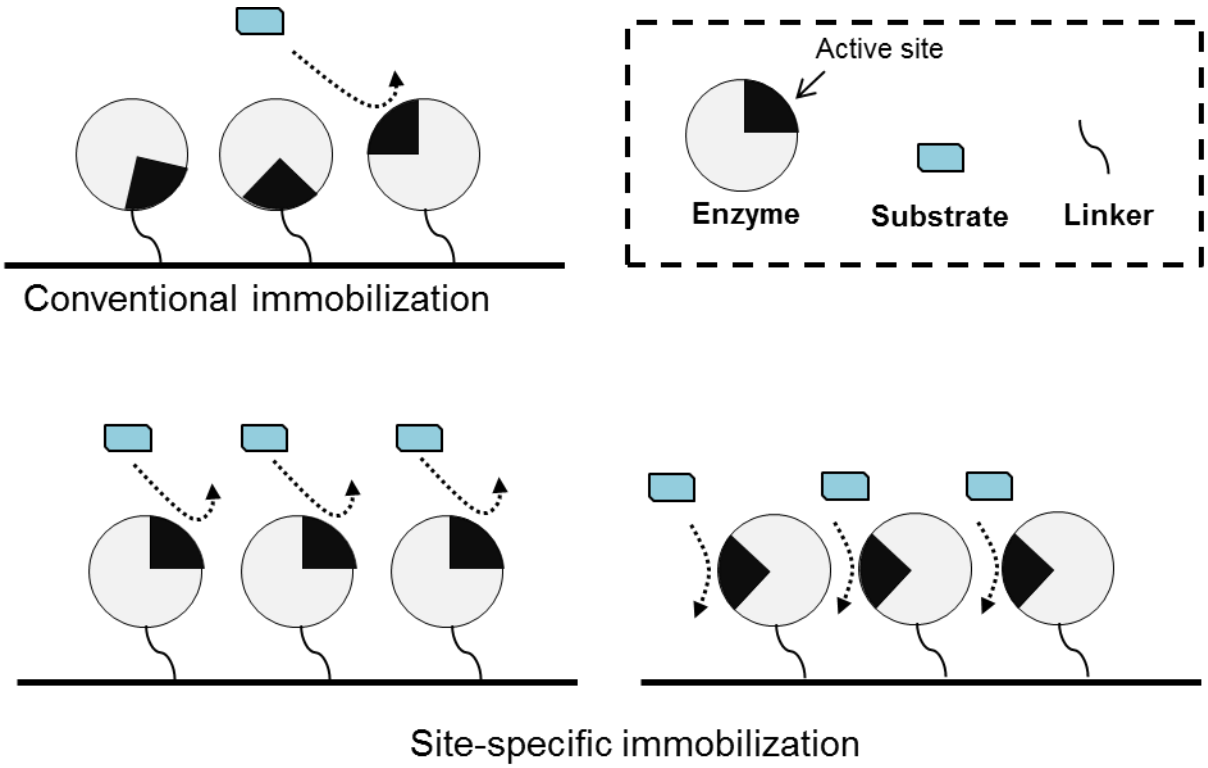

Figure 1.5. Protein immobilization onto a support. (A) Conventional methods. (B) site-specific methods [27]**.**

1.4. Research Objectives

A general goal of the dissertation research is to add a new function to a protein, based on site-specific incorporation of a reactive NNAA and conjugation of a functional molecule through bioorthogonal chemistry. The impact of site-specific bioconjugation was investigated in biotherapeutics and biocatalysis–areas where a protein is a key element governing the performance of the entire system. I hypothesized that site-specific bioconjugation can be used to confer functional benefits that cannot be afforded by conventional bioconjugation on therapeutic proteins and catalytic enzymes.

Specifically, in biotherapeutics, it is of great importance to prolong the circulation time of therapeutic proteins administered intravenously into patients to reduce injection frequency and cost. Although chemical modification with biocompatible molecules have been shown to extend *in vivo* half-lives of proteins, it is hard to retain native protein functions and homogeneity due to inability to control the site of conjugation. In order to generate long-acting therapeutic proteins with native activity and homogeneity, the following research objectives were proposed.

1. **Extension of serum half-life of a protein through site-specific conjugation of a fatty acid with retained protein activity.**
2. **Extension of serum half-life of urate oxidase through site-specific conjugation of human serum albumin with retained therapeutic activity.**

In biocatalysis, it is crucial to construct an enzymatic reaction system that is cost-effective and high-yielding. Enzyme immobilization and co-localization are the most promising approaches to improve enzyme stability, recyclability, and product purity. Since the techniques

usually involve covalent modification of enzymes, site-specific conjugation with controlled enzyme orientation is expected to better improve the biocatalytic performance by retaining enzymatic activity, selectivity and specificity. In order to demonstrate the utility of site-specific bioconjugation in controlling enzyme orientation, the following research objectives were proposed.

3. **Site-specific immobilization of murine dihydrofolate reductase with retained activity and controlled orientation.**
4. **Substrate channeling induced by controlled orientation of active sites of enzymes in a multienzyme reaction cascade**

In the Objective I, I used a superfolder green fluorescent protein as a model to demonstrate that a fatty acid can play as a half-life extender without hampering native activity of a protein when conjugated in a site-specific manner, which is detailed in Chapter 2. The Objective II is described in Chapter 3, where human serum albumin was site-specifically conjugated to urate oxidase through a bifunctional linker to prolong its therapeutic activity *in vivo*. In the Objective III, I used murine dihydrofolate reductase as a model to demonstrate that the systemic optimization of reaction conditions followed by site-specific biotinylation of murine dihydrofolate reductase resulted in homogeneous and orientation-controlled immobilization through streptavidin-biotin interaction, which is detailed in Chapter 4. In Chapter 5, I investigated the substrate channeling effect depending on active site orientation of two coupled enzymes through site-specific tethering achieved by two orthogonal bioconjugation chemistries.

Chapter 2: Site-specific Conjugation of Fatty Acid to Superfolder Green Fluorescent Protein to Prolong In Vivo Half-life through Albumin Binding

Therapeutic proteins are indispensable in treating numerous human diseases. However, therapeutic proteins often suffer short serum half-life. In order to extend the serum half-life, a natural albumin ligand (a fatty acid) has been conjugated to small therapeutic peptides resulting in a prolonged serum half-life via binding to patients' serum albumin *in vivo*. However, fatty acid-conjugation has limited applicability due to lack of site-specificity resulting in the heterogeneity of conjugated proteins and a significant loss in pharmaceutical activity. In order to address these issues, we exploited the site-specific fatty acid-conjugation to a permissive site of a protein, using copper-catalyzed alkyne-azide cycloaddition, by linking a fatty acid derivative to *p*-ethynyl-L-phenylalanine incorporated into a protein using an engineered pair of yeast tRNA/aminoacyl tRNA synthetase (Scheme 2.1).

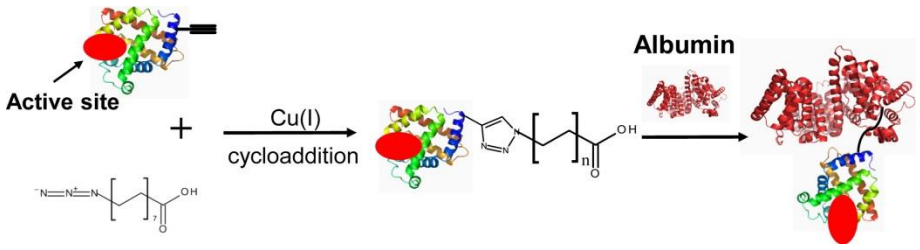

Scheme 2.1. Site-specific palmitic acid-conjugation and albumin binding.

As a proof-of-concept, we show that single palmitic acid conjugated to superfolder green fluorescent protein (sfGFP) in a site-specific manner enhanced a protein's albumin-binding in vitro about 20 times and the serum half-life *in vivo* 5 times when compared to those of the unmodified sfGFP. Furthermore, the fatty acid conjugation did not cause a significant reduction

in the fluorescence of sfGFP. Therefore, these results clearly indicate that the site-specific fatty acid-conjugation is a very promising strategy to prolong protein serum half-life in vivo without compromising its folded structure and activity.

2.1. Background and Motivation

Recombinant proteins with therapeutic activity have become critical for treating numerous diseases, and cover a wide range of therapeutics including monoclonal antibodies, hormones, growth factors, cytokines, and enzymes [45]. However, utility of therapeutic proteins is often hampered by their short serum half-life requiring frequent re-administration resulting in patient discomfort and noncompliance. Therefore, extending the serum half-life of therapeutic proteins will significantly enhance the utility of existing therapeutic proteins and will also enable development of new therapeutic proteins [46,47]. In the quest to extend the serum half-life, binding/conjugation of serum albumin or Fc portion of immunoglobulin G to therapeutic proteins is a very promising emerging strategy [28,48,49].

Human serum albumin (HSA) has an inherently long serum half-life (19 days) due to neonatal Fc receptor (FcRn)-mediated recycling as well as reduced renal filtration [28–30]. HSA-binding/conjugation is a very attractive strategy for extending the serum half-life of a therapeutic protein when compared to conventional poly(ethylene)glycol (PEG) conjugation which mainly relies on renal filtration evasion. Furthermore, although it has long been considered that PEG is non-immunogenic, antibodies raised against PEG were observed in patients administered PEGylated uricase [50]. Therefore, the binding of therapeutic proteins to HSAs in patients' blood is actively investigated to mitigate most immune response issues.

Despite the many benefits of HSA as a binding/conjugation partner, developing a general strategy to bind/conjugate therapeutic proteins to HSA remains a big challenge.

In order to facilitate HSA binding of therapeutic proteins in patients' blood, genetic fusion of an albumin binding domain to N-term or C-term of therapeutic proteins is performed. But this methodology has a potential risk of immunogenicity [51,52]. Furthermore, the end-to-end fusion does not provide steric control or favorable topology that retains both therapeutic efficacy and conformational stability [53–55]. Alternatively, synthetic or natural albumin-binding moieties have been chemically attached to a peptide, preferably to cysteine or lysine residues [56,57]. In particular, the conjugation of a natural HSA ligand, a fatty acid, has been successfully used to extend the serum half-life in vivo of two therapeutic peptides, insulin and glucagon-like peptide-1 agonist (GLP-1) via acylation at lysine residues [31,32]. Seven binding sites in HSA have been identified to accommodate saturated fatty acids with 10–18 carbons [33,34]. Compared to direct fusion/chemical conjugation of HSA to therapeutic proteins, this approach is advantageous for deep penetration into tissues [57], higher activity to mass ratio[35], and greatly reduced immunogenicity [36,37]. However, fatty acid-conjugation to multiple lysine residues of therapeutic proteins likely leads to heterogeneous mixtures of the conjugated proteins, compromising pharmaceutical activity and downstream processing. For instance, fatty acid-conjugation to lysine residues of interferon-alpha led to an 80% reduction in its antiviral potency [38]. Therefore, fatty acid-conjugation has been limited to peptides with a small number of lysine residues. In order to overcome the heterogeneity of the conjugated proteins and the compromised pharmaceutical activity, a fatty acid should be attached to a permissive site of a protein necessitating site-specific fatty acid-conjugation technique. Although therapeutic proteins are dominant over therapeutic peptides in clinical applications, to our knowledge, fatty acid-

conjugation to a protein in a site-specific manner has not been reported. In this report, we describe a novel strategy to achieve site-specific conjugation of the natural albumin ligand, a fatty acid, to a protein with the combined use of copper-catalyzed alkyne-azide cycloaddition (CuAAC) and site-specific incorporation of non-natural amino acid (NNAA) technique. CuAAC is a popular reaction in which a terminal alkynyl group (HC ≡ C − R1) and an azido group (−N = N+ = N − R2) are united to give a 1,4-di-substituted 1,2,3-triazole in the presence of catalytic copper [10,58]. Its uniqueness lies in the bio-orthogonality of both moieties, since they are absent in all natural amino acids and thus ensure a highly selective reaction [12,59,60]. To employ CuAAC in protein engineering, amino acids containing either an alkynyl or azido group should be introduced into a protein. Among several techniques for expanding the chemical diversity of proteins [61–64], the site-specific genetic incorporation of NNAAs is capable of adding new chemistries at a desired site. An orthogonal pair of tRNA amber suppressor and aminoacyl-tRNA synthetase from foreign species needs to be engineered to be specific for each NNAA and utilized to incorporate it in response to an amber codon in the target protein sequence [3,65]. In order to achieve site-specific fatty acid-conjugation to a protein, *p*-ethynyl-*L*-phenylalanine (pEthF) was introduced to a model protein, superfolder green fluorescent protein (sfGFP), using the bacterial cells outfitted with the orthogonal pair of engineered yeast phenylalanyl-tRNA/phenylalanyl-tRNA synthetase. The sfGFP was chosen as a model protein thanks to its favorable properties for our study. First, its fluorescence is directly correlated to its folding [66]. Therefore, perturbation of its folded structure upon fatty acid-conjugation can be estimated by measuring its fluorescence. Second, its spectral properties greatly facilitate quantitative analyses in vitro including HSA binding assay. Third, the family of green fluorescent protein variants is generally known to be non-toxic to animals facilitating

pharmacokinetics testing in vivo [67,68]. The sfGFP variant containing pEthF was coupled to a fatty acid derivative containing an azido group via CuAAC. Finally, using the fatty acid-conjugated sfGFP, we show that the site-specific fatty acid-conjugation to a protein enhances its binding to HSA in vitro and prolongs protein retention in blood when administered in vivo without any significant loss in its intrinsic folded structure and fluorescence.

2.2. Materials and Methods

2.2.1. Materials

p-Ethynylphenylalanine (pEthF) was synthesized as described previously[2]. Ni-NTA agarose and pQE-16 plasmid were obtained from Qiagen (Valencia, CA). Sequencing grade modified trypsin was obtained from Promega Corporation (Madison, WI). Amicon ultra centrifugal filters and ZipTip® with C18 media were purchased from Millipore Corporation (Billerica, MA). NHS-activated agarose and BCA protein assay kit were purchased from Thermo Scientific (Rockford, IL). GFP ELISA kit was purchased from Cell Biolabs, Inc. (San Diego, CA). Coumarin-azide was obtained from Glen Research (Sterling, VA). Palmitic acid-azide was obtained from Invitrogen Corporation (Carlsbad, CA). All other chemicals were purchased from Sigma-Aldrich Corporation (St. Louis, MO).

2.2.2. Plasmid Construction and Strains

Preparation of the plasmids pQE16am-yPheRS^{T415A} and pREP4-ytRNA$^{Phe}_{CUA_UG}$ is described previously [69]. pQE16am-yPheRS^{T415G} encodes the engineered yeast aminoacyl-tRNA synthetase and the murine dihydrofolate reductase (mDHFR) with an amber codon at 38th position and a C-terminal hexahistidine tag. A Phe/Trp/Lys triple auxotrophic Escherichia coli

strain, designated AFWK, was prepared as described previously [69]. AFWK harboring both plasmids was used as an expression host for incorporation of pEthF into murine dihydrofolate reductase (mDHFR). A gene encoding a sfGFP with a C-terminal hexahistidine tag was synthesized from Epoch Life Science, Inc. (Sugar Land, Texas). The expression cassette of the sfGFP was inserted into the AatII/NheI site in pQE16am-yPheRS^{T415A} replacing the coding sequence of the mDHFR and yielding pQE16-sfGFP-yPheRS^{T415A}. An amber codon was generated by PCR mutagenesis in a position between the 214th and the 215th amino acid of the sfGFP resulting in pQE16-sfGFP215Amb-yPheRS^{T415A}. The mutagenic primer sequences were as follows: 215Amb_F, 5′-CCCAACGAAAAGTAGCGTGACCACATGG-3′; 215Amb_R, 5′-CCATGTGGTCACGCTACTTTTCGTTGGG-3′. AFWK was co-transformed with pQE16-sfGFP215Amb-yPheRS^{T415A} and pREP4-ytRNA$^{Phe}_{CUA_UG}$ and then used as an expression host for incorporation of pEthF into the sfGFP.

2.2.3. Expression and Purification of Wild-Type and Mutant Proteins

The wild-type sfGFP (sfGFP-WT) was expressed from AFWK harboring pQE16-sfGFP-yPheRS^{T415A} by 1 mM IPTG induction in LB media containing 100 μg/mL ampicillin at 37 °C. To express the sfGFP mutant containing pEthF at the 215th position (sfGFP-pEthF), AFWK harboring pQE16-sfGFP215Amb-yPheRS^{T415A} and pREP4-ytRNA$^{Phe}_{CUA_UG}$ was used. Saturated overnight cultures grown at 37 °C in M9 minimal medium supplemented with 100 μg/mL ampicillin, 30 μg/mL kanamycin, 0.4% (w/v) glucose, 1 mM $MgSO_4$, 0.1 mM $CaCl_2$, 10 μg/mL thiamine, and 20 amino acids (25 μg/mL each) were diluted 20 fold in the same fresh medium, and grown at 37 ℃ until an OD_{600} of 0.9 was reached. After incubation on ice for 15 min, cells were sedimented by centrifugation at 4000 g for 12 min, and washed with cold 0.9% (w/v) NaCl

by gentle resuspension. After repeating twice, cells were shifted to M9 medium supplemented with the same ingredients described above except for different amino acid compositions: 17 amino acids (35 μg/mL each), 150 μM Lys, 60 μM Phe, 10 μM Trp, and 3 mM pEthF. To maximize the incorporation efficiency in condensed culture, the total volume of M9 medium was 20-fold smaller than the original volume. Upon induction by 1 mM IPTG, cells were incubated with shaking at 30 ℃ for 15 h before harvest. Expression of the wild-type mDHFR (mDHFR-WT) or the mDHFR mutant with pEthF (mDHFR-pEthF) at the 38th position was performed similarly except that the plasmid pQE16 for mDHFR-WT or pQE16am-yPheRS^{T415G} for mDHFR-pEthF was used instead of pQE16-sfGFP^{215Amb}-yPheRS^{T415A}. Cells were pelleted by centrifugation, and the protein was purified by gravity-flow affinity chromatography using Ni-NTA agarose beads under native (sfGFP-WT and sfGFP-pEthF) or denaturing (mDHFR-WT and mDHFR-pEthF) condition according to the supplier's instructions (Qiagen). Purified proteins were directly used or buffer-exchanged using PD-10 desalting columns to appropriate buffers. If necessary, the protein solutions were concentrated using centrifugal filters.

2.2.4. CuAAC-Mediated Dye Labeling and Fatty Acid-Conjugation

Palmitic acid-azide was reacted with the mDHFR-pEthF under the following condition yielding the mDHFR-Pal: 30 μM mDHFR-pEthF in the denaturing elution buffer (8 M urea, 10 mM Tris, 100 mM NaH_2PO_4, pH = 4.5), 150 μM palmitic acid-azide, 1 mM $CuSO_4$, 2 mM sodium ascorbate, and at room temperature for 2 h. sfGFP-pEthF was conjugated to palmitic acid-azide or fluorogenic coumarin-azide under the following condition generating sfGFP-Pal or sfGFP-CM: 30 μM sfGFP-pEthF in 20 mM potassium phosphate (pH 8) and 35% (v/v) DMSO, 150 μM palmitic acid-azide or coumarin-azide, 1 mM TBTA, 1.5 mM $CuSO_4$, 2 mM DTT, and

at 25 ℃ for 10 h. Reactions were quenched by adding 200 mM imidazole and 5 mM EDTA. Upon completion of reaction, the reaction mixture was desalted and buffer-exchanged using PD-10 desalting columns to appropriate buffers for downstream uses. Protein concentrations were determined by BCA assay.

2.2.5. Verification of pEthF Incorporation and Fatty Acid-Conjugation by Mass Spectrometry

Tryptic digestion of the mDHFR-WT, the mDHFR-pEthF or the mDHFR-Pal in the denaturing elution buffer (8 M urea, 10 mM Tris, 100 mM NaH2PO4, pH = 4.5) was performed by diluting 10 μL of a protein with 90 μL of NH4HCO3 and then adding 0.5 μL of modified trypsin (0.1 μg). Following incubation at 37 °C for 2 h, the reaction mixture was mixed with 12 μL of 5% (v/v) trifluoroacetic acid (TFA) to quench the reaction and then desalted on a ZipTip® C18. The site-specific incorporation of pEthF into mDHFR and palmitic acid-conjugation was confirmed by MALDI-TOF mass spectrometry (MS) analysis of the tryptic digests of mDHFR. The MS analysis was performed using 20 mg/mL of 2,5-dihydroxybenzoic acid and 2 mg/mL of l-(−)-fucose dissolved in 10% ethanol as a matrix by MicroflexTM MALDI-TOF MS (Bruker Corporation, Billerica, MA). LC–MS/MS analyses of tryptic digests of mDHFR were conducted on a thermo electron LTQ VelosOrbitrap mass spectrometer. The tryptic digests of mDHFR were separated on a reverse phase column (75 μm) with acetonitrile gradient. The column eluent was introduced to the microspray source, and amino acid sequence analysis was carried out by fragmentation of the precursor ion corresponding to the Peptide_Z38. The site-specific incorporation of pEthF into sfGFP and palmitic acid-conjugation were confirmed by LC–MS coupled with electron spray ionization (ESI). The chromatographic separation was performed

using a BEH C4 (2.1 × 100 mm, 1.7 μm) column at a flow rate of 0.4 μL/min with mobile phase consisting of water and n-propanol. The eluent was introduced into the ion source of the LTQ-Orbitrap mass spectrometer operated in a positive mode at a spray voltage of 3.0 kV. The data were acquired by XCalibur (Thermo Scientific) and processed using ProMass deconvolution (Thermo Scientific).

2.2.6. In Vitro Albumin-Binding Assay

N-hydroxysuccinimide-activated agarose was coated with HSA according to the supplier's protocol or inactivated by adding an excess amount of glycine to generate HSA-coated and inactivated resin, respectively. The resins were mixed with the sfGFP-WT, the sfGFP-pEthF, or the sfGFP-Pal and incubated at room temperature for 1 h. After washing with PBS multiple times, the fluorescence images and intensities of the resins were obtained at λ_{ex} = 480 nm and λ_{em} = 510 nm using the Biospectrum imaging system (UVP Inc., Upland, CA) and the Biotek fluorescence plate reader, respectively. For membrane-based binding assay, the HSA solution (10 mg/mL) was spotted on the nitrocellulose membrane. After extensive washing with PBS, the membrane was blocked with casein solution. Two microliters of protein solutions (2 mg/mL) was overlaid on the HSA spot, and the membrane was washed with PBS and analyzed by the imaging system.

2.2.7. In Vivo Studies of the sfGFP-WT and sfGFP-Pal

The animal protocol was approved by the Institutional Animal Care and Use Committee (IACUC) at the University of Virginia. Pharmacokinetic properties of sfGFP-WT and sfGFP-Pal were investigated by injecting 50 μg of each sfGFP sample in 200 μL PBS into the tail vein of

young female C57BL/6 mice (n = 4). The blood was sampled at 0 (10 min), 3, and 6 h post-injection for the sfGFP-WT, and at 0 (10 min), 3, 6, 18, 24, and 30 h post-injection for the sfGFP-Pal.

2.3. Results and Discussion

2.3.1. Site-Specific Incorporation of p-Ethynyl-L-Phenylalanine into the Murine Dihydrofolate Reductase and the CuAAC-Mediated Dye Labeling

In order to investigate site-specific fatty acid-conjugation to a protein via CuAAC (Figure 2.1A), we introduced pEthF into murine dihydrofolate reductase (mDHFR) in a site-specific manner. Since the expression and purification of DHFRs in *E. coli* are well established [69,70], we routinely used mDHFR to study site-specific incorporation of a NNAA. pEthF is a phenylalanine analog with an alkyne moiety at para-position of the phenyl ring (Figure. 2.1B) and expected to act as a molecular handle for CuAAC with azide-functionalized molecules. Previously, the yeast-originated pair of phenylalanine-tRNA suppressor/phenylalanyl-tRNA synthetase variant ($ytRNA^{Phe}_{CUA\_UG}$/$yPheRS^{T415A}$) was designed to incorporate a Phe analog into mDHFR in E. coli expression system [69,71]. The relaxed substrate specificity of $yPheRS^{T415A}$ also allows recognition of a panel of Phe and Trp analogs with a bulky functional group at para-position of the phenyl ring. Therefore, we hypothesize that the $ytRNA^{Phe}_{CUA\_UG}$/$yPheRS^{T415A}$ pair will also allow efficient site-specific incorporation of pEthF in response to an amber codon at the 38th position of the mDHFR mutant (mDHFR-38Am). The mDHFR-38Am was expressed in the presence of 3 mM pEthF, purified under denaturing condition, and trypsin-digested for MALDI-TOF analysis as described previously with minor alterations [69,70]. The mDHFR

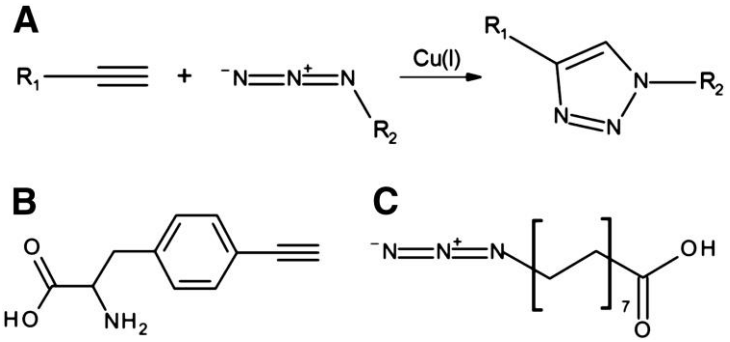

Figure 2.1. Reaction scheme and chemical structures. (A) Copper-catalyzed alkyne-azide cycloaddition. Structures of p-ethynylphenylalanine (B) and palmitic acid-azide (C).

mutant containing pEthF at the 38th position is designated as mDHFR-pEthF. For wild-type mDHFR (mDHFR-WT), peptide F38 (residues 26-39; NGDLPWPPLRNEAFK), one of the tryptic digests, was detected with a monoisotopic mass of 1682.7 Da, in accord with its theoretical mass (Figure 2.2A). Peptide Z38 of the mDHFR-pEthF (residue 26–39; NGDLPWPPLRNEAmK where Am indicates an amber codon) was detected with a strong signal at a mass of 1706.8 Da, supporting the incorporation of pEthF in response to the amber codon.

To validate orthogonal reactivity of the alkyne end group of pEthF with an azide moiety via CuAAC, fluorogenic coumarin azide was reacted with the purified mDHFR-pEthF or mDHFR-WT in a $CuSO_4$/ascorbate system. Since the reaction of the coumarin azide with an alkyne group produces a strongly fluorescent triazole-linked conjugate [72], the evolution of fluorescence is an indicator of pEthF reactivity for CuAAC. In SDS-PAGE analysis, the protein gel under UV exposure (λ_{ex} = 390 nm) clearly exhibited the fluorescence confirming the formation of a triazole linkage between coumarin azide and the alkynyl group of the mDHFR-pEthF (Figure 2.2B) as well as a strong protein band stained with Coomassie blue dye, whereas the mDHFR-WT did not exhibit any fluorescence despite a strong protein band stained with Coomassie blue dye. The combined results of the mass spectrometric analysis and the fluorogenic dye conjugation strongly support the idea that pEthF was site-specifically incorporated into a protein using the E. coli expression system containing the orthogonal pair of $ytRNA^{Phe}_{CUA\_UG}$/$yPheRS^{T415A}$, and the pEthF introduced into a protein is reactive for bio-orthogonal CuAAC.

2.3.2. Site-Specific Fatty Acid-Conjugation to the mDHFR-pEthF

Next, we tested if a fatty acid with an intrinsic affinity for HSA can be grafted to the

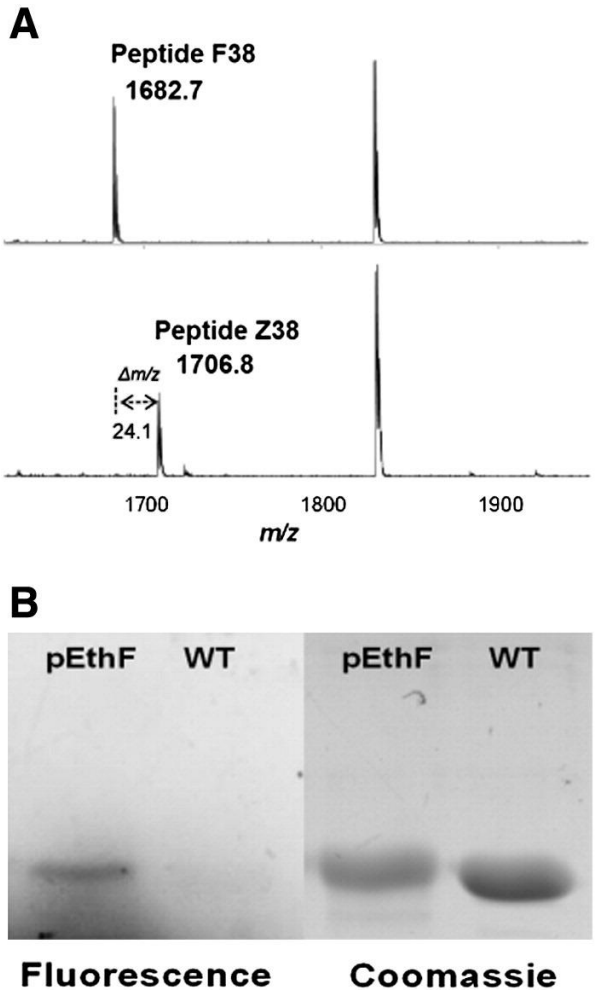

Figure 2.2. Site-specific incorporation of pEthF into the mDHFR-38Am and CuAAC-mediated coumarin-labeling. (A) MALDI-TOF analysis of trypsin-digested mDHFR-WT and mDHFR-pEthF. Peptide F38 (top) of the mDHFR-WT and Peptide Z38 of the mDHFR-pEthF (bottom). (B) Protein gel images of the fluorogenic dye-treated mDHFR-pEthF (pEthF) and mDHFR-WT (WT). The gel was subjected to UV (390 nm) irradiation to excite the fluorophore (fluorescence panel), and then stained with Coomassie brilliant blue (Coomassie panel) to visualize proteins.

mDHFR-pEthF through CuAAC. Palmitic acid-azide (15-azidopentadecanoic acid), a palmitic acid analog containing an azide moiety at the end of the carbon chain (Figure 2.1C), was used for for this purpose. The mDHFR-pEthF was reacted with palmitic acid-azide, and then subjected to tryptic digestion. The MALDI-TOF mass spectrum of the tryptic digests shows that a new signal with a monoisotopic mass of 1989.9 appears whereas Peptide Z38 signal is substantially reduced (Figure 2.3). Considering that palmitic acid-azide conjugation will add 283.4 Da to the mass of Peptide Z38 (the actual mass shift of 283.2 in the spectrum), the new peak is considered as palmitic acid-conjugated Peptide Z38 (Peptide Z38-PAL). This result clearly indicates that palmitic acid-azide has been conjugated to the mDHFR-pEthF in a site-specific manner.

2.3.3. Site-Specific Fatty Acid-Conjugation to Superfolder Green Fluorescent Protein without Compromising Its Folded Structure and Intrinsic Fluorescence

To investigate site-specific fatty acid-conjugation to a native protein without compromising intrinsic properties, we examined the site-specific fatty acid-conjugation to superfolder green fluorescent protein (sfGFP) [66]. Intrinsic fluorescence of sfGFP correlated to its folding facilitates the estimation of the extent of structure perturbation during CuAAC and the determination of sfGFP quantity in the following characterization steps. In order to allow efficient fatty acid-conjugation with least protein structure perturbation, we chose a position between the 214th and the 215th amino acid as pEthF incorporation site by using a server-based solvent accessibility calculation program (ASAView) [73]and examining the crystal structure of sfGFP. This position is located in a loop region with high solvent accessibility (0.72 score in the ASAView) and distal from the chromophore (Figure 2.4). Furthermore, it was reported that

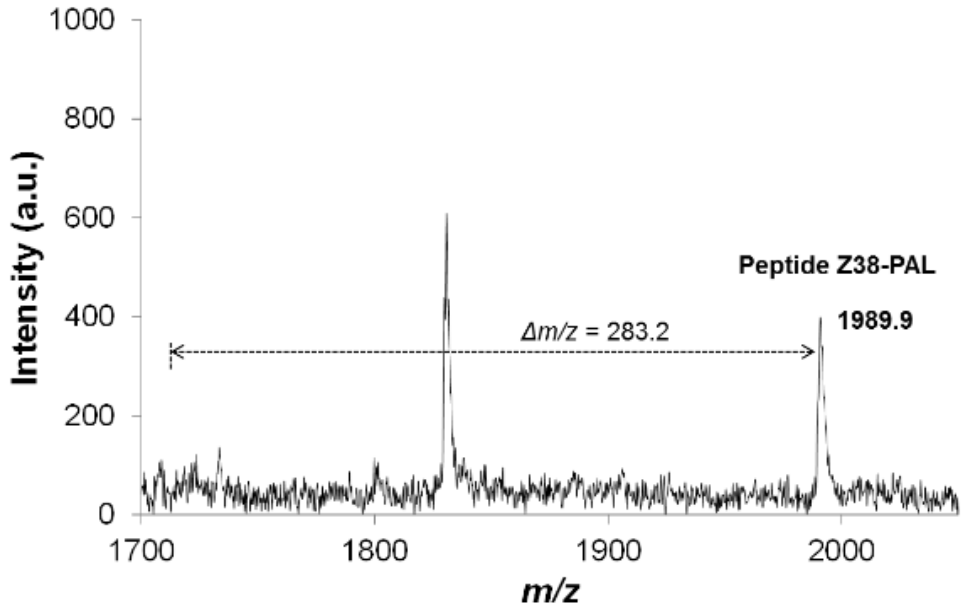

Figure 2.3. Confirmation of the palmitic acid-conjugation to the mDHFR-pEthF by MALDI-TOF MS. Peptide Z38-PAL, one of tryptic digests of the mDHFR-Pal, was detected at a mass of 1989.9.

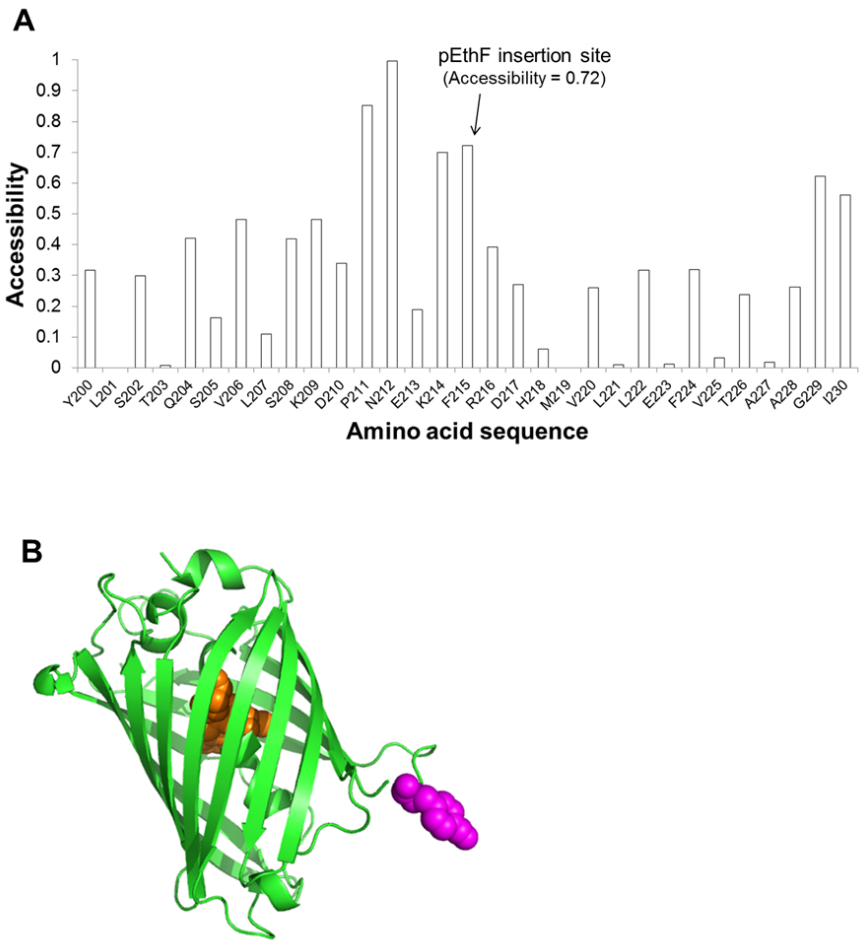

Figure 2.4. Determination of an optimal site for mutagenesis. (A) Residue-based solvent accessibility of the sfGFP-pEthF. ASAView [73], an online tool for a graphical representation of solvent accessibility, was used to calculate the relative solvent accessibility of all residues including pEthF at 215th position, based on the PDB file (ID: 2B3P) of sfGFP and a fully automated protein structure homology-modeling server for mutation [74]. (B) Three-dimensional structure of the sfGFP-pEthF generated by Pymol [75]. The chromophore (orange) and pEthF incorporated at the 215th position (magenta) are represented by spheres.

another NNAA at this position can be used for CuAAC [59]. pEthF was introduced into the amber codon site using the E. coli expression host harboring ytRNA$^{Phe}_{CUA_UG}$/yPheRS^{T415A} orthogonal pair. The sfGFP variant containing pEthF at position 215 (sfGFP-pEthF) was purified via metal-ion affinity chromatography using a six-histidine tag. Based on the expression medium volume, about 80 mg/L of purified sfGFP-pEthF was obtained. Site-specific incorporation of pEthF into wild-type sfGFP (sfGFP-WT) was confirmed by mass spectrometry coupled with electron spray ionization (ESI-MS) (Figure 2.5). The measured mass of the full length sfGFP variant (sfGFP-pEthF) is 27,755.2 Da, which is consistent with the calculated mass of 27,755.8 Da. The sfGFP-pEthF was then subjected to CuAAC-mediated palmitic acid-conjugation in a native condition using a $CuSO_4$/dithiothreitol (DTT)/Tris[(1-benzyl-1H-1,2,3-triazol-4-yl)methyl]amine (TBTA) system where TBTA acts as an accelerating ligand as well as a radical scavenger [58]. The palmitic acid-conjugate (sfGFP-Pal) was analyzed by ESI-MS and found to have a molecular weight greater than that of the sfGFP-pEthF by 281.2 Da, strongly indicating site-specific conjugation at a stoichiometry of one palmitic acid per protein. As reported previously [76,77], the N-terminal methionine was cleaved in a portion of the sfGFP-pEthF (ΔM-sfGFP-pEthF) generating a peak with 27,624.1 m/z (Figure 2.5). However, an additional peak corresponding to the palmitic acid-conjugated ΔM-sfGFP-pEthF (27,905.7 m/z) was also detected, indicating that both the intact and the methionine-cleaved sfGFPs are successfully conjugated to the palmitic acid.

Next, we investigated whether the fatty acid-conjugation perturbs the sfGFP folded structure. As an indicator of the portion of correctly folded sfGFPs, the fluorescence intensity of sfGFPs was monitored (Fig. 2.6). The fluorescence intensity of the sfGFP-pEthF is 25% higher than that of the sfGFP-WT. Even after the sfGFP-pEthF was conjugated to a fatty acid,

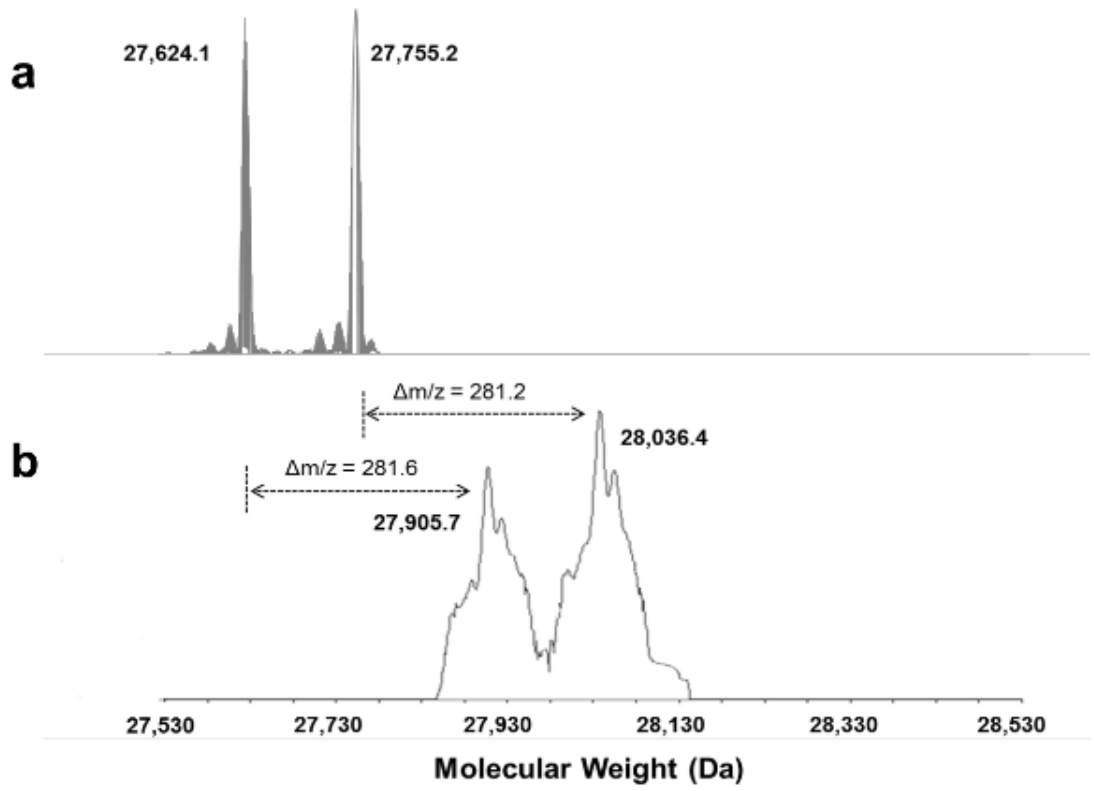

Figure 2.5. Confirmation of the palmitic acid-conjugation to the sfGFP-pEthF by ESI-MS. ESI-MS spectrum of the sfGFP-pEthF (A) and the sfGFP-Pal (B). Following the reversed-phase high performance chromatography using BEH C4 column (2.1 × 100 mm, 1.7 μm), the molecular weight of a full length protein was analyzed on an LTQ-Orbitrap XL mass spectrometer.

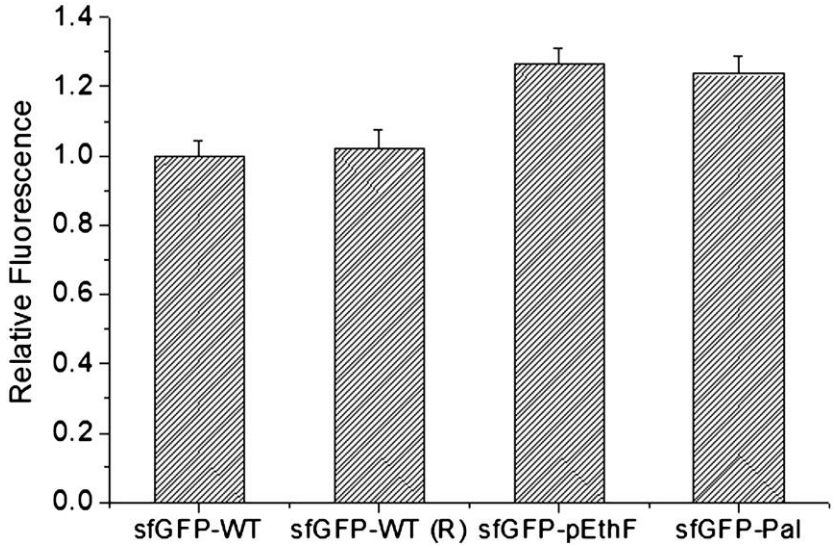

Figure 2.6. The relative fluorescence of the sfGFP-WT and sfGFP variants. Protein solutions (20 μg/mL) were loaded onto a 96-well microplate at 100 μL per well, and read on the plate reader at λ_{ex} = 480 nm and λ_{em} = 510 nm. Values were averaged for each protein (n = 5 originating from the same batch in different aliquots), and normalized to the fluorescence of the sfGFP-WT. In order to investigate the effect of reagents used in CuAAC, the sfGFP-WT was treated in parallel with the sfGFP-pEthF subjected to the fatty acid-conjugation, and designated sfGFP-WT (R). Error bars represent standard error of the mean.

the fluorescence intensity of the sfGFP-Pal remains unchanged. Similarly, the incubation of the sfGFP-WT under the same condition used for the fatty acid-conjugation of the sfGFP-pEthF did not significantly alter the fluorescence intensity. These results clearly demonstrate that neither the site-specific incorporation of pEthF at position 215 of sfGFP nor the fatty acid-conjugation via CuAAC compromises the intrinsic fluorescence and thereby folded structure of sfGFP.

2.3.4. HSA-Binding of the sfGFP-Pal In Vitro

To investigate whether the fatty acid-conjugation to a protein generates albumin-binding affinity, the sfGFP-WT and the sfGFP-Pal were mixed with HSA-coupled agarose beads or, as a control, inactivated beads in which amine-reactive N-hydroxysuccinimide groups had been blocked by glycine. After washing the beads multiple times with PBS on a gravity-flow column, the fluorescence intensity of the beads were qualitatively or quantitatively analyzed by using a fluorescence imager and a fluorescence microplate reader, respectively (Figure 2.7A). The HSA-coupled beads mixed with the sfGFP-Pal exhibit significant fluorescence while the HSA-coupled beads mixed with the sfGFP-WT display negligible fluorescence. Furthermore, the inactivated beads mixed with the sfGFP-Pal exhibit negligible fluorescence. These results strongly support the idea that the sfGFP-Pal binds the HSA-coupled beads via HSA-specific interactions. In order to quantitatively compare the binding affinities of the sfGFP-WT and the sfGFP-Pal to HSA, the fluorescence intensities of the HSA-coupled beads mixed with the sfGFP-WT and the sfGFP-Pal were measured. The HSA-coupled beads mixed with the sfGFP-Pal exhibit about 20-fold greater fluorescence than those with the sfGFP-WT. The inactivated beads mixed with the sfGFP-WT and the sfGFP-Pal exhibit 1.7- and 1.3-fold greater fluorescence than that of the HSA-coupled

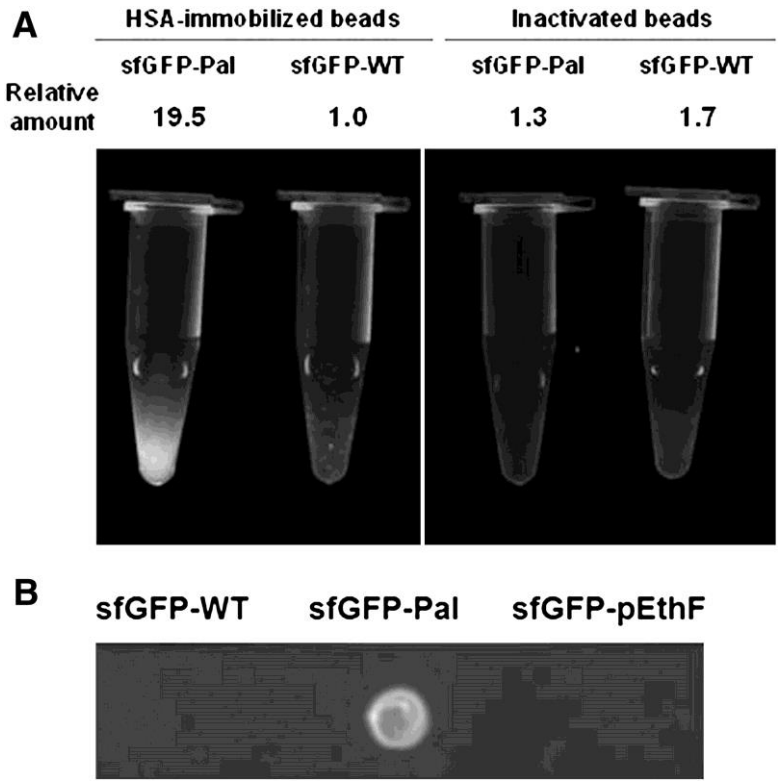

Figure 2.7. Relative albumin-binding affinity of sfGFP-variants. (A) Inactivated (amine-reactive functional groups blocked by glycine) or HSA-immobilized agarose beads were mixed with the sfGFP-WT and the sfGFP-Pal. After washing extensively with PBS, the fluorescence image was taken on the UV epi-illuminator at λ_{ex} = 480 nm, and emitted light above 510 nm was captured. For a quantitative fluorescence measurement, the same amounts of agarose beads were loaded on a 96-well microplate and read on the plate reader at λ_{ex} = 480 nm and λ_{em} = 510 nm. The relative amounts of sfGFP samples were calculated from the relative fluorescence intensities. (B) Four micrograms of each protein in 2 μL of PBS were dotted onto the HSA-coated nitrocellulose membrane and air-dried. After washing in PBS for 5 min and air-dry, the membrane was epi-illuminated at λ_{ex} = 480 nm, and emitted light above 510 nm was captured.

beads mixed with the sfGFP-WT, likely because the sfGFP-WT and the sfGFP-Pal reacted with a small amount of residual amine-reactive *N*-hydroxysuccinimide groups in the inactivated beads. Without any significant structural perturbation, the fluorescence intensity is directly correlated to the amount of sfGFP. Therefore, these results suggest that the fatty acid-conjugation leads to a substantial increase in albumin-binding affinity. To eliminate the possibility that the fluorescence increase is caused by aggregation of the sfGFP-Pal leading to its retention in the column during the HSA-coupled bead binding assay, the binding was also examined using the nitrocellulose membrane blot which was subjected to extensive washing. In contrast to the sfGFP-WT and the sfGFP-pEthF that were washed away after being spotted on HSA-coated membrane, the sfGFP-Pal was tightly bound to HSA as confirmed using fluorescence image analysis (Figure 2.7B). These results indicate unambiguously that the site-specific palmitic acid-conjugation remarkably enhances HSA-binding affinity of the sfGFP compared to the unmodified sfGFP.

2.3.5. Pharmacokinetic Study of the sfGFP-Pal

In order to evaluate clinical benefits from albumin-binding capacity generated from the site-specific fatty acid-conjugation, a single dose of either the sfGFP-WT or the sfGFP-Pal was intravenously administered to mice (n=4), and the sfGFP serum concentrations in the serum samples taken at different time points were measured by using GFP-specific ELISA kit. Assuming one-compartment distribution and first-order elimination of the sfGFP in the serum [78,79], its logarithmic residual serum concentrations versus time were plotted, and the data were fit to a straight line to calculate the serum half-life (Figure 2.8). The serum half-life of the sfGFP-Pal calculated (5.2 h) is approximately 5-fold longer than that of the sfGFP-WT (1.0 h).

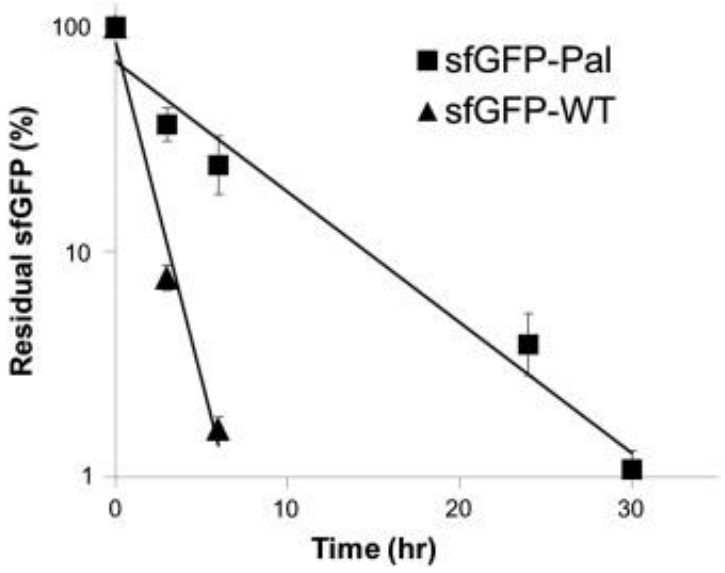

Figure 2.8. Pharmacokinetics of the sfGFP-WT and the sfGFP-Pal. Four mice were intravenously administered the sfGFP-Pal (square) or the sfGFP-WT (triangle), respectively, and serum concentrations were measured by ELISA at different time points (mean ± s.d.): 0 (10 min), 3, and 6 h for the sfGFP-WT; 0 (10 min), 3, 6, 24, and 30 h for the sfGFP-Pal. Data were normalized with regard to the initial value, plotted in a logarithmic scale versus time post-injection, and fitted into a straight line (R^2 = 0.98 for the sfGFP-WT and 0.97 for the sfGFP-Pal).

2.3.6. Discussion

The fatty acid-conjugation is an attractive methodology for developing long-acting protein therapeutics. A natural occurrence of a fatty acid in the blood greatly reduces the risk of immunogenicity and toxicity when it is used as an albumin-binding tag. In addition, its small size relative to other albumin-binding motifs [80,81], including albumin-binding domain, is less likely to impair protein folded structure and function upon conjugation. The recently FDA-approved long-acting peptide analogs in which a fatty acid has been chemically linked to a lysine residue represent the potential of a fatty acid as a safe and reliable half-life extender in clinical settings. To render it broadly applicable to large-sized proteins as well as small peptides, new protein conjugation chemistry is required to prevent the production of positional isomers and detrimental loss of inherent activity arising from random coupling to multiple lysine residues.

Since its advent in 2002, CuAAC has found numerous applications in diverse fields, providing highly selective reactivity. To implement CuAAC for the site-specific attachment of a fatty acid to a protein, pEthF was introduced by using the engineered orthogonal pair of $ytRNA^{Phe}_{CUA\_UG}$/$yPheRS^{T415A}$ with the yield of approximately 80 mg/L based on the volume of protein expression medium. Research efforts witnessed over the past couple of years have demonstrated near-optimal expression of a NNAA-incorporated protein (up to 800 mg/L) comparable to that of its wild-type, thereby showing great promise for its expanded application to protein therapeutics [8,82,83]. Successful bioconjugation via CuAAC is critically dependent on stabilizing catalytically active Cu(I) oxidation state while simultaneously preventing generation of reactive byproducts leading to undesirable protein aggregation. We discovered that the $CuSO_4$/DTT/TBTA system is suitable for the fatty acid-conjugation to a protein resulting in a high yield with minimal side products. The use of TBTA ligand was essential for a high yield

and an optimal reaction rate, but its low solubility in water required the addition of a polar solvent, DMSO, in the CuAAC reaction. Newly-developed water-soluble ligands such as THPTA and BTTAA might be alternatives for bioconjugation of proteins intolerant to DMSO [84].

We report here the utility of a fatty acid as an albumin-binding tag attached to a large protein with absolute site selectivity. Site-specificity is the key advantage of our technique over other albumin-binding strategies relying on the genetic fusion of affinity motifs or random chemical attachment of synthetic binding molecules. Another key to exploiting this technology is imparting albumin-binding capability to a protein with minimal perturbation of its native activity and stability. As demonstrated in this paper, the site-specific fatty acid-conjugation via CuAAC does not cause any significant loss of the sfGFP fluorescence, strongly indicating that the native sfGFP structure was not perturbed. Based on examination of a crystal structure of a target protein and the solvent accessibility prediction, optimal sites for NNAA incorporation and subsequent fatty acid-conjugation can be chosen, which has not been possible previously. Furthermore, the utility of this technology to modulate pharmacokinetics can be easily expanded by varying carbon chain lengths or by adding distinct chemical linkers between a fatty acid and a target protein. Tailoring the half-life of a therapeutic protein offers the advantage of being able to optimize the requirements of its intended clinical application [85,86].

The animal study has clearly revealed the significance of albumin-binding effect on in vivo half-life extension. Five-fold longer retention of the sfGFP-Pal in blood compared to the sfGFP-WT is most likely attributed to FcRn-mediated recycling of the sfGFP-HSA complex, which is supported by in vitro HSA-binding assay. Previously, a GFP variant C-terminally attached to a PEG-like polymer exhibited only 2 h of serum half-life when injected intravenously

into mice [87]. Similarly, a single-chain diabody (scDb) C-terminally fused to an albumin-binding domain showed 2.6 h of serum half-life despite the 13-fold half-life extension compared to that of an unmodified one [88]. Therefore, the half-lives of the GFP and the scDb conjugates were found to be smaller than that of the sfGFP-Pal (5.2 h). Although differences in dose, concentration measurement, and data analysis complicate a direct comparison between half-life extension technologies, it is evident that the technique and approach described in this paper constitutes a significant impact on the optimization of therapeutic efficacy of a protein by virtue of unique features including immuno-safety and orthogonal chemistry unrestricted in site of modification, and thereby has broad applications to short-lived proteins.

2.4. Conclusion

In this study, we successfully demonstrated that a fatty acid can be conjugated to a pEthF site of a recombinant protein via CuAAC leading to an increase in HSA binding in vitro and in serum half-life in vivo by 20-fold and 5-fold, respectively. To our knowledge, this is the first time to show the site-specific conjugation of a biomolecule into a single pEthF site of a protein via CuAAC. Furthermore, a careful choice of the pEthF incorporation site in a protein allows the successful fatty acid-conjugation without any significant perturbation of the folded protein. In the future, development of an orthogonal tRNA/aaRS pair for pEthF incorporation into a protein expressed in yeasts and mammalian cells will extend the application of the technique described here to broader ranges of recombinant proteins.

Chapter 3: Site-Specific Albumination of a Therapeutic Protein with Multi-Subunit to Prolong Activity *In Vivo*

Albumin fusion/conjugation (albumination) has been an effective method to prolong in vivo half-life of therapeutic proteins. However, its broader application to proteins with complex folding pathway or multi-subunit is restricted by incorrect folding, poor expression, heterogeneity, and loss of native activity of the proteins linked to albumin. We hypothesized that the site-specific conjugation of albumin to a permissive site of a target protein will expand the utilities of albumin as a therapeutic activity extender to proteins with a complex structure. We show here the genetic incorporation of a non-natural amino acid (NNAA) followed by chemoselective albumin conjugation to prolong therapeutic activity in vivo. Urate oxidase (Uox), a therapeutic enzyme for treatment of hyperuricemia, is a homotetramer with multiple surface lysines, limiting conventional approaches for albumination. Incorporation of p-azido-L-phenylalanine into two predetermined positions of Uox allowed site-specific linkage of dibenzocyclooctyne-derivatized human serum albumin (HSA) through strain-promoted azide-alkyne cycloaddition (SPAAC). The bio-orthogonality of SPAAC resulted in the production of a chemically well-defined conjugate, Uox-HSA, with a retained enzymatic activity. In mice, Uox-HSA lost the half of enzymatic activity in serum every 8.8 h post-administration, while wild-type Uox lost the half of enzymatic activity every 1.3 h post-administration. These results clearly demonstrated that site-specific albumination led to the prolonged enzymatic activity of Uox in vivo. Site-specific albumination enabled by NNAA incorporation and orthogonal chemistry demonstrates its promise for the development of long-acting protein therapeutics with high potency and safety.

3.1. Background and Motivation

The past three decades have witnessed the clinical success of therapeutic proteins for treatment of numerous diseases, and the momentum continues overriding even the growth of overall pharmaceutical sectors [89]. One of major considerations in protein therapeutics development is to increase the circulation time to avoid frequent injections. Since therapeutic proteins administered to patients are continuously removed, engineering efforts have been made to shield proteins from glomerular filtration, pinocytosis, and immune response. Employing human serum albumin (HSA) as a drug carrier is one of the effective modifications for prolonging *in vivo* half-life of a drug. HSA has unusually long circulation time (over two weeks) attributed by electrostatic repulsion in kidneys and FcRn-mediated recycling in endothelium [28,49,90,91]. Furthermore, its long serum half-life can be used to increase serum half-lives of other proteins through genetic fusion or chemical conjugation, termed together as albumination. Peptides and small-sized proteins have been successfully albuminated, thereby displaying prolonged circulation and enhanced pharmacodynamics [92–97]. However, there are still challenges to fuse albumin with a therapeutic protein with multi-subunit and complex folded structure due to poor expression and misfolding resulting in a significant therapeutic activity loss [98–100]. The chemical conjugation of albumin to a therapeutic protein generates heterogeneous mixture of the conjugates making the downstream process very difficult, limiting its application to small peptides with a very restricted number of reactive functional groups available for albumin conjugation [91]. Such long-standing hurdles that the conventional methods of albumination have suffered may be overcome by site-specific protein conjugation. A flexible choice of incorporation sites and a site-directed reaction would allow essentially any therapeutic

protein to be linked to HSA regardless of folding pathway, multimerization, and abundance of reactive natural amino acids.

The expanded genetic code has made a breakthrough in protein conjugation, allowing the incorporation of non-natural amino acids (NNAAs), in particular those having bio-orthogonal reactivity, into any position of a target protein site-specifically in diverse expression hosts including *E. coli*, yeast, and CHO cells [65,69,101–105]. Upon incorporation, the reactive NNAA serves as a chemical handle to which any molecule of interest with a cognate functional group can be attached without cross-reaction with other natural amino acids [106,107]. Of noteworthy significance is its emerging application to protein therapeutics, e.g., site-specific PEGylation and antibody-drug conjugate [82,108–111]. It has been shown that combined use of NNAA incorporation and chemoselective chemistry, i.e., site-specific protein conjugation, produces a highly homogenous end product with a minimal loss of native functions, streamlining the manufacturing process and adding greater clinical benefits. Although click chemistry was proven a powerful tool to modify proteins containing an NNAA [10,112], to our knowledge, it was not reported that the combined use of NNAA incorporation and click chemistry can be used to site-specifically conjugate albumin to a therapeutic protein with multi-subunit. Here we demonstrate that albumination through site-specific incorporation of *p*-azido-L-phenylalanine and bio-orthogonal strain-promoted azide-alkyne cycloaddition (SPAAC) (Figure 2.9E) [113,114] can readily improve the duration of *in vivo* activity of urate oxidase (Uox)–a therapeutic enzyme with multi-subunit.

Uox originating from *Aspergillus flavus* is a 135 kDa homotetramer with a large central tunnel with both N- and C-termini in close proximity, and has four active sites located at the interfaces between subunits [115]. Uox catalyzes degradation of a poorly soluble uric acid into a

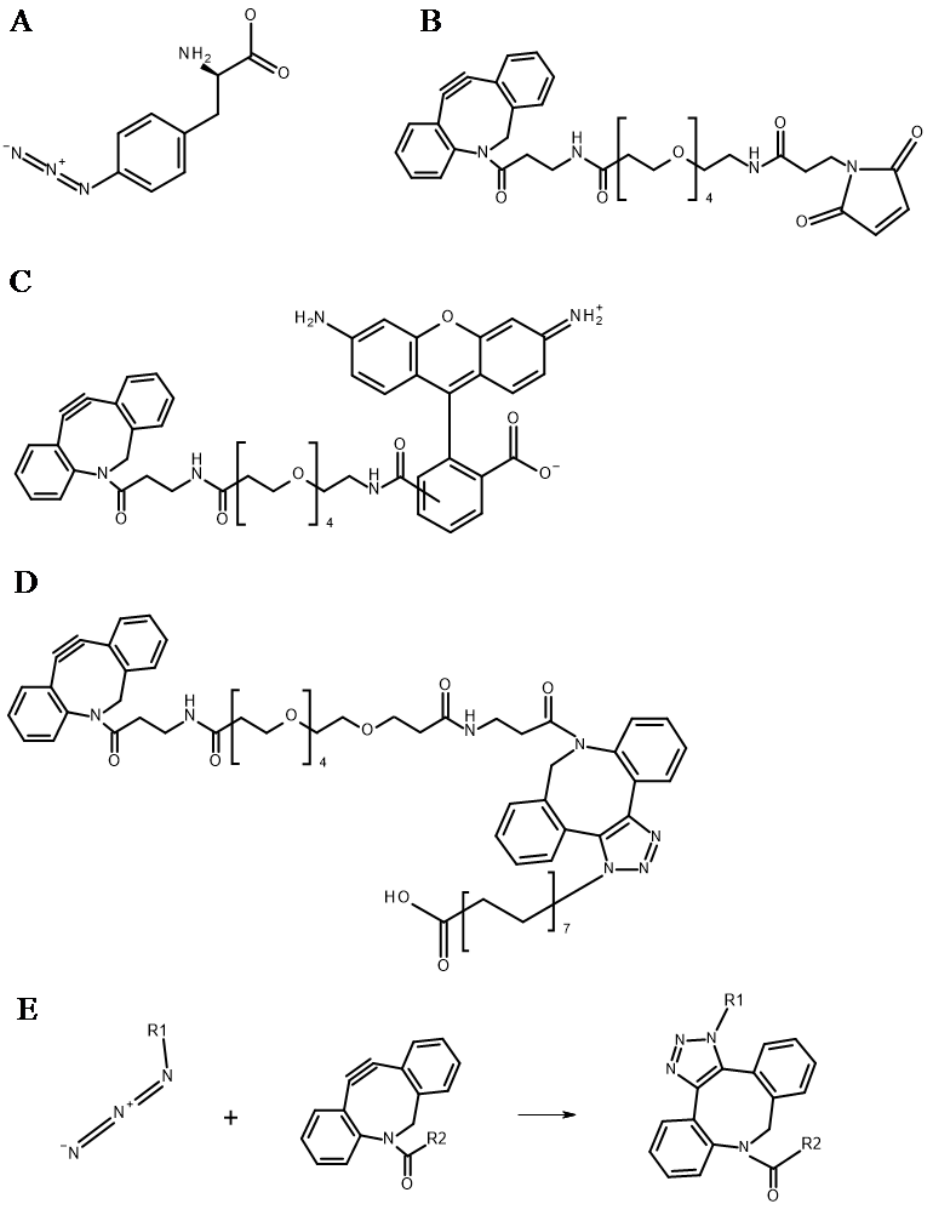

Figure 3.1. Chemical structures and reaction scheme. (A) *p*-azido-L-phenylalanine. (B) DBCO-PEG_4-MAL. (C) DBCO-PEG_4-carboxyrhodamine. (D) DBCO-PEG_4-palmitic acid. (E) Strain-promoted azide-alkyne cycloaddition (SPAAC).

soluble allantoin, thus lowering serum uric acid level, and is used to treat patients suffering from hyperuricemia [116–118]. It suffers rapid clearance upon injection narrowing its applicability to short-term treatment of tumor lysis syndrome [119,120]. Although PEGylation of Uox through random coupling to lysine residues achieved a significant extension of serum half-life [121–124], non-specific and excessive modification raises concerns of heterogeneity, immune responses against PEGs [125], and reduced efficacy [126,127]. Therefore, in order to circumvent these concerns, developing alternative strategies to prolong *in vivo* activity of Uox is required.

Alternative to PEG conjugation, the genetic fusion of HSA to a therapeutic protein is a popular method to generate a long-acting bio-better. However, close proximity between N- or C-termini of each subunit and the multimeric nature of Uox likely prevent a stable formation of a native three-dimensional structure upon fusion to HSA due to steric hindrance and different folding behavior such as disulfide bond formation. We therefore investigate whether site-specific albumination could be a novel approach to construct a Uox-HSA conjugate with the prolonged activity. Considering that a tetrameric Uox has a size of 135 kDa exceeding the renal filtration cutoff of 70 kDa, FcRn-mediated recycling in endothelium was expected to mainly contribute to the prolonged activity *in vivo*. Uox variants developed for therapeutic applications have a non-human origin and have varying degrees of immune responses [128]. Prolonged activity of Uox by HSA conjugation is expected to reduce immune response of Uox due to less frequent injections with efficacy comparable to the conventional Uox therapy. Although Uox obtained from A. flavus was used in this study, the use of a recently found ‘human-like’ Uox [128] would further lessen a potential immunogenic concern in the treatment of gout and tumor lysis syndrome. Broadly, this strategy should make it possible to empower long-lived property of HSA to ‘hard-to-fuse’ therapeutic proteins that form multi-subunit complex or have termini

important to their native structure/function. An additional advantage lies in the modulation of protein conjugate topology such that the relative orientation between a cargo protein and HSA can be controlled for optimal performance towards their respective biological targets.

3.2. Materials and Methods

3.2.1. Materials

p-Azido-L-phenylalanine (AzF) was obtained from Chem-Impex International (Wood Dale, IL) and dissolved in 0.2 M NaOH to make 100 mM stock solution. Ni-NTA agarose and pQE80 plasmid were obtained from Qiagen (Valencia, CA). Vivaspin centrifugal concentrators with a MWCO of 50 kDa were purchased from Sartorius Corporation (Bohemia, NY). ZipTip with C18 resin was purchased from Millipore Corporation (Billerica, MA). Sequencing grade modified trypsin was obtained from Promega Corporation (Madison, WI). DBCO-PEG_4-carboxyrhodamine, DBCO-PEG_4-MAL, and DBCO-PEG_4-DBCO were purchased from Bioconjugate Technology Company (Scottsdale, AZ). 15-azidopentadecanoic acid was obtained from Life Technologies (Gaithersburg, MD). PD-10 desalting columns, HiTrap SP HP cation exchange column, and Superdex 200 10/300 GL size exclusion column were obtained from GE Health care (Piscataway, NJ). UNO Q1 anion exchange column and Biologic DuoFlow chromatography system were obtained from Bio-Rad (Hercules, CA). All chemicals were obtained from Sigma-Aldrich Corporation (St. Louis, MO) unless otherwise stated.

3.2.2. Plasmid Construction and Bacterial Strains

A plasmid pEVOL-pAzF [7] encoding an AzF-specific engineered pair of tyrosyl-tRNA synthetase/amber suppressor tRNA derived from *Methanococcus jannaschii* (Plasmid ID: 31186)

was obtained from Addgene (Cambridge, MA), and used without modification. To construct a bacterial expression vector for C-terminally His×6-tagged recombinant urate oxidase (Uox) originating from *Aspergillus flavus*, its coding sequence was amplified from pCG62-Uox [118], a kind gift from Dr. Weber (University of Freiburg, Germany), and cloned into pQE80 to give pQE80-Uox. Site-directed mutagenic PCR was performed with pQE80-Uox as a template to replace tryptophan codons at positions 160 and 174 with amber codons (UAG), yielding pQE80-Uox_W160.174amb. All DNA cloning in this study were performed by the restriction-free cloning technique [129]. *E. coli* TOP10 was transformed with pQE80-Uox for expression of the wild-type Uox (Uox-WT), affording TOP10 [Uox]. As an expression host for AzF-incorporated Uox (Uox-W160.174AzF), genomically engineered *E. coli* C321.ΔA.exp [5] was obtained from Addgene (ID: 49018), and co-transformed with pEVOL-pAzF and pQE80-UoxW160.174amb, affording C321.ΔA.exp [Uox-W160.174amb].

3.2.3. Site-Specific Incorporation of AzFs into Uox and Purification

The saturated culture of C321.ΔA.exp [Uox-W160.174amb] was inoculated into fresh 2×YT medium containing 100 μg/mL ampicillin and 35 μg/mL chloramphenicol at 1:100 (v/v) dilution, and was subjected to vigorous shaking (220 rpm) at 37°C. When the OD_{600} of 0.5 was reached, AzF solution was added to a final concentration of 1 mM. After 10 min, protein expression was induced by 1 mM IPTG and 0.2% (w/v) *L*-(+)-arabinose. Cells were harvested after 5 h, and pelleted by centrifugation at 5,000 rpm for 10 min before storage at -20°C. To extract and purify UoxW160.174AzF, cell pellets were resuspended with the lysis buffer consisting of 50 mM sodium phosphate (pH 7.5), 0.3 M NaCl, 10 mM imidazole, 1 mg/mL lysozyme, DNase, RNase, and protease inhibitor cocktail, and mixed by rotation at 37°C for 1 h

followed by at 4°C for 2 h. After centrifugation at 11,000 rpm for 30 min, the clear supernatant was recovered, mixed with Ni-NTA agarose for 1 h, and then washed with the washing buffer consisting of 50 mM sodium phosphate (pH 7.5), 0.3 M NaCl, and 20 mM imidazole on a gravity-flow column to remove impurities. Proteins were eluted by the elution buffer consisting of 50 mM sodium phosphate (pH 7.5), 0.3 M NaCl, and 250 mM imidazole, and then buffer-exchanged to a storage buffer consisting of 50 mM HEPES (pH 8.2) and 0.2 M NaCl by a PD-10 column. Expression and purification of Uox-WT were performed similarly except that TOP10 [Uox] was used as an expression host without adding AzF and *L*-(+)-arabinose.

3.2.4. Spectrometric Quantification of Uox-WT and Uox-W160.174AzF

The molar absorbance of AzF at 280 nm was measured by NanoDrop Spectrometer (Thermo Scientific, Wilmington, DE), and found to be 2,620 $M^{-1}cm^{-1}$ (data not shown). The molar absorption coefficients, ε_{280} ($M^{-1}cm^{-1}$), of Uox-WT and Uox-W160.174AzF were calculated using the following equation [130],

$$\varepsilon_{280} = (5500 \times n_{Trp}) + (1490 \times n_{Tyr}) + (2620 \times n_{AzF})$$

where the molar absorbances of Trp, Tyr, and AzF are multiplied by the number of each residue ($n_{residue}$), and then combined. ε_{280} of Uox-WT and Uox-W160.174AzF were determined to be 53,400 $M^{-1}cm^{-1}$ and 47,640 $M^{-1}cm^{-1}$, respectively. The concentrations were measured by the Beer-Lambert Law [131].

3.2.5. MALDI-TOF Mass Spectrometry

Proteins in the storage buffer at 0.5 mg/mL were digested with trypsin at 37℃ overnight, and then desalted on a ZipTip C18 according to the manufacturer's protocol. Purified tryptic digests mixed with DHB matrix (20 mg/mL of 2,5-dihydroxybenzoic acid and 2 mg/mL of *L*-(−)-fucose dissolved in 10% ethanol) at 1:1 (v/v) were subjected to mass characterization by Microflex MALDI-TOF M/S (Bruker Corporation, Billerica, MA).

3.2.6. Labeling of Uox-W160.174AzF by SPAAC

Uox-WT and Uox-W160.174AzF at 30 μM in the storage buffer were separately reacted with DBCO- PEG_4-carboxyrhodamine at 100 μM at RT for 2 h, and then loaded onto SDS-PAGE to measure in-gel fluorescence in a BioSpectrum imaging system (UVP, Upland, CA). Upon illumination at λ_{ex} = 480 nm, the emitted light above 510 nm was captured. Conjugation of DBCO-PEG_4-palmitic acid was performed by reacting Uox-W160.174AzF at 30 μM in the storage buffer with DBCO-PEG_4-DBCO at 150 μM at RT for 6 h, affording Uox-PEG_4-DBCO. After desalting on a PD-10, five equivalents of 15-azidopentadecanoic acid was added to Uox-PEG_4-DBCO, and then reacted at RT for 2 h to give Uox-PEG_4-palmitic acid.

3.2.7. Circular Dichroism (CD) and Data Analysis

The secondary structures of Uox-WT and Uox-W160.174AzF in 10 mM sodium phosphate (pH 7.0) were evaluated using a Jasco 710 spectropolarimeter with 1-mm path length quartz cuvette at room temperature at a protein concentration of 0.03 mg/mL. The background-subtracted sample spectra were then deconvoluted to obtain numerical estimations of secondary

structure content using the DichroWeb online CD analysis software server [132,133], employing the SELCON3 analysis program along with 'Set #4'reference sets [134,135].

3.2.8. Generation of Uox-HSA Conjugate

Lyophilized human serum albumin (HSA) was dissolved in PBS, and purified on an anion exchange column, UNO Q1, to remove high-molecular-weight impurities. The purified HSA at 50 μM was conjugated to DBCO-PEG_4-MAL at 200 μM by thiol-maleimide coupling in PBS buffered at pH 7.0 for 2 h, and then buffer-exchanged to 20 mM sodium phosphate (pH 6.0), yielding HSA-PEG_4-DBCO. To synthesize Uox-HSA conjugate by SPAAC, Uox-W160.174AzF was mixed with HSA-PEG_4-DBCO at 1:1 molar ratio in 20 mM sodium phosphate (pH 6.0), and then concentrated to a final protein concentration of 10 mg/mL. After 7 h incubation at room temperature, the mixture was subjected to the two-step column chromatography consisting of a cation exchange one removing unreacted HSA-PEG_4-DBCO and an anion exchange one removing unreacted Uox-W160.174AzF to obtain a purified Uox-HSA conjugate. The cation exchange chromatography was run on a HiTrap SP-HP equilibrated in 20 mM sodium phosphate (pH 6.0) with NaCl gradient elution. The eluate containing Uox-HSA conjugate and residual Uox-W160.174AzF was desalted and buffer-exchanged to 20 mM bis-tris (pH 6.5) on a centrifugal filter with MWCO of 50 kDa, and then loaded onto the anion exchanger, UNO Q1, equilibrated with 20 mM bis-tris (pH 6.5). Pure Uox-HSA conjugate was eluted by applying NaCl gradient. Proteins were analyzed by SDS-PAGE in tris/glycine buffer system after reduction by DTT or subjected to size-exclusion chromatography using Superdex 200 10/300 GL column, equilibrated with PBS (pH 7.4).

3.2.9. Enzymatic Activity Assay

The spectrophotometric method was used to determine the kinetic constants of Uox-WT and Uox-HSA [128]. After determining concentrations by BCA protein assay (Thermo Scientific, Wilmington, DE) and the densitometric analysis of subunit composition, Uox-WT or Uox-HSA at 60 nM was reacted with uric acid at various concentrations in 200 µL of the assay buffer consisting of 50 mM sodium borate (pH 9.5) and 0.2 M NaCl. Reduction in absorbance at 293 nm attributed by conversion of uric acid to 5-hydroxyisourate was monitored in triplicate at 25˚C in a standard 96-well plate on the Synergy^{TM} four multimode microplate reader (BioTek, Winooski, VT). The consumption rate of uric acid (nmol/min) was obtained by dividing the rate of OD change (min^{-1}) by a molar absorptivity of uric acid (12,300 $M^{-1}cm^{-1}$) [136] and a path length (0.56 cm), and then multiplying an assay volume (2.0×10^5 nL). Average consumption rates at each substrate concentration were fitted to a typical Michaelis–Menten curve to yield V_{max} and K_m. In order to evaluate the enzymatic activity in blood, 10 µL of serum was mixed with 190 µL of the assay buffer containing 100 µM of uric acid, and then monitored as described above. The enzymatic activity was obtained in an arbitrary unit (mU/mL) by dividing the consumption rate of uric acid by the volume of serum (10^{-2} mL) used in the assay, where one unit (mU) is defined as the amount of an enzyme used to catalyze the oxidation of 1 nmole of uric acid per minute at 25˚C.

3.2.10. In vivo Study of Residual Uox Activity in Serum

The animal protocol was approved by the Institutional Animal Care and Use Committee (IACUC) at the University of Virginia. Enzymatic activities of Uox-WT and Uox-HSA *in vivo* were investigated by injecting 5.7 nmole (based on a monomeric Uox) of each protein in 200 µL

PBS into the tail vein of young female C57BL/6 mice (n = 4). Female C57BL/6 mice were chosen in this study, because they have been successfully used for the PK studies including one in our laboratory [111,137,138]. The blood was sampled at 0.5, 1, 2, and 4 h post-injection for Uox-WT, and at 0.5, 1, 2, 4, 8, 12 and 24 h post-injection for Uox-HSA.

3.3. Results and Discussion

3.3.1. Site-Specific Double Incorporation of AzFs into Permissive Sites of Uox

In order to take advantage of an unusually long serum half-life of HSA, we chose to conjugate the Uox variant containing AzFs (Figure 3.1A) with HSA using a hetero-bifunctional hydrophilic linker, DBCO-PEG_4-MAL (Figure 3.1B), to ensure chemoselectivity and native activity of Uox and HSA. Cysteine at position 34 (C34) of HSA can be readily utilized for thiol-maleimide crosslinking since C34 is the only free cysteine and located away from FcRn-binding domain (Figure 3.2) [139,140]. DBCO can be chemoselectively conjugated to an azide functional group via SPAAC. AzF is a non-natural amino acid containing an azide group. Uox can be made reactive towards DBCO by genetically incorporating AzFs into permissive sites of Uox. Predetermined sites in Uox not critical for native activity could be targeted for chemically well-defined conjugation with HSA. To determine mutation sites which are least likely to perturb the native structure and function of Uox upon substitution by AzFs, amino acids bearing an aromatic group, Phe, Trp, and Tyr, were chosen as potential targets for their structural similarity with AzF. Next, ten Phes, seven Trps, and ten Tyrs in the primary structure of Uox were screened for their solvent accessibility by ASA-View server [73] (Figure 3.3A). A residue with higher solvent accessibility is preferred for AzF incorporation since subsequent conjugation with

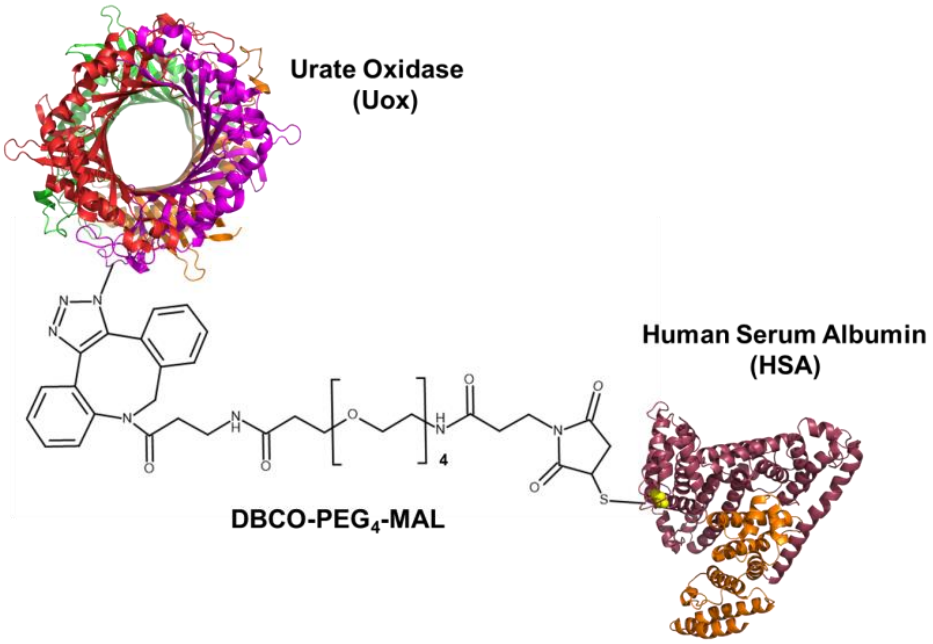

Figure 3.2. Schematic representation of Uox-HSA conjugate. C34 (yellow sphere) of HSA is located remote from the FcRn-binding domain (colored orange), and linked to DBCO-PEG_4-MAL through thiol-maleimide coupling to yield HSA-DBCO. Uox is a homotetramer each of which is colored differently. Strain-promoted azide-alkyne cycloaddition (SPAAC) mediates site-specific albumination between Uox-W160.174AzF and HSA- PEG_4-DBCO.

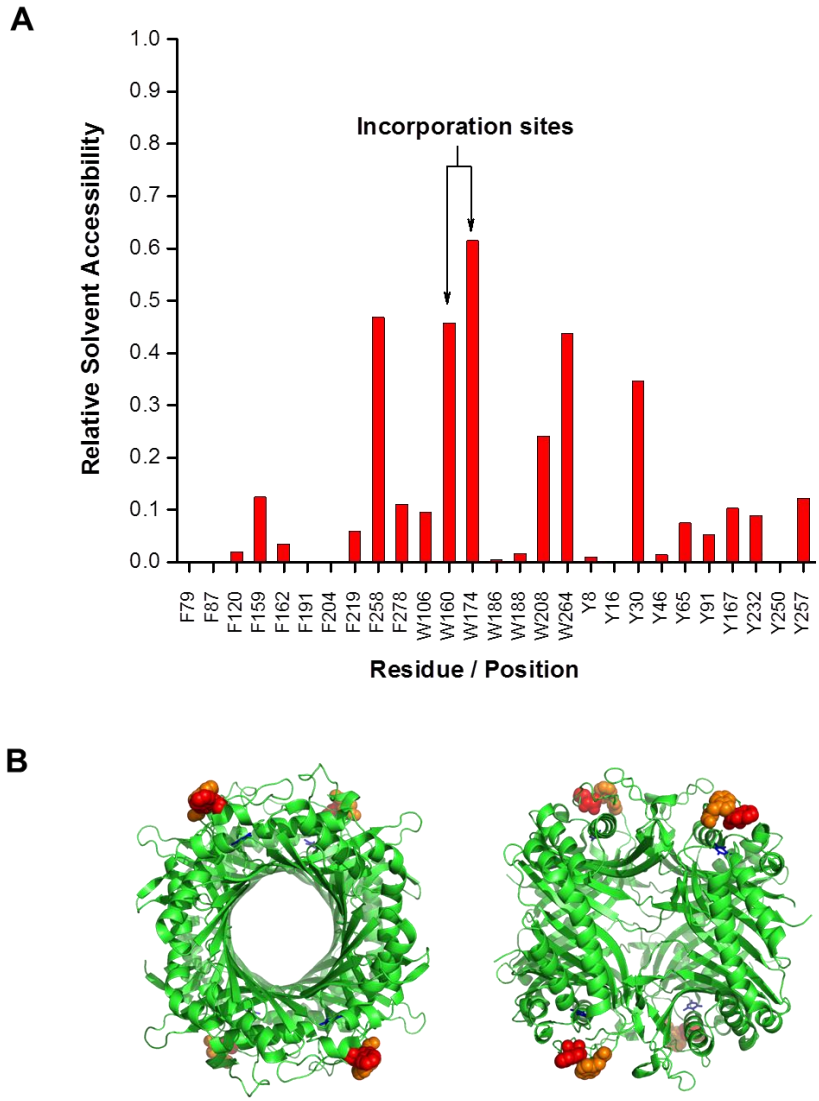

Figure 3.3. Determination of AzF incorporation sites. (A) Residue-based solvent accessibility of Uox-WT. ASA-View, an online server for a graphical representation of solvent accessibility, was used to calculate the relative solvent accessibility of Phe, Trp, and Tyr residues based on the PDB file (ID#: 1WS2). (B) Three-dimensional structure of Uox-WT (front view, left; side view, right) generated by Pymol. AzF incorporation sites (W160, red; W174, orange) are represented by spheres.

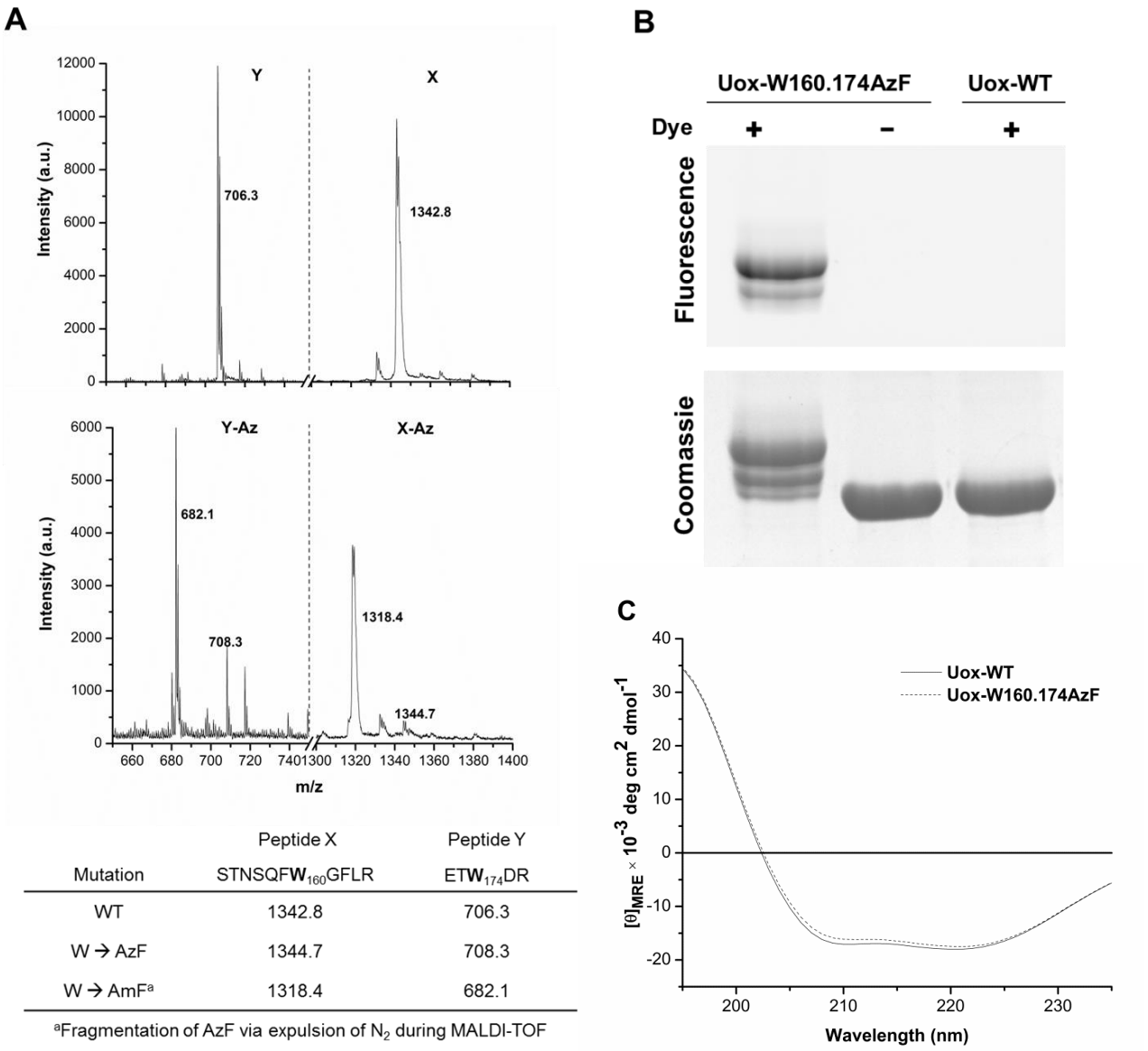

Mutation	Peptide X STNSQF**W**$_{160}$GFLR	Peptide Y ET**W**$_{174}$DR
WT	1342.8	706.3
W → AzF	1344.7	708.3
W → AmF[a]	1318.4	682.1

[a]Fragmentation of AzF via expulsion of N_2 during MALDI-TOF

Figure 3.4. Validation of site-specific incorporation of AzFs into Uox. (A) MALDI-TOF M/S analyses of trypsin-digested Uox-WT (top) and Uox-W160.174AzF (bottom). Peptide Y (residues 172-176; ETWDR) contains the 174th Trp which is substituted by AzF in Peptide Y-Az. Peptide X (residues 154-164, STNSQFWGFLR) contains the 160th Trp which is substituted by AzF in Peptide X-Az. (B) Protein gel images of Uox-W160.174AzF and Uox-WT treated with a fluorescent dye, DBCO-PEG_4-carboxyrhodamine. The gel was subjected to UV (390 nm) irradiation to excite the fluorophore (fluorescence panel), and then stained with Coomassie blue (Coomassie panel) to visualize proteins. (C) CD spectra of Uox-WT (solid) and Uox-W160.174AzF (dotted).

DBCO moiety would be made effective by increased chance of collisions. Four sites (W160, W174, F258, and W264) showed relatively high solvent accessibility. Two conjugation sites–Trps at positions 160 (W160) and 174 (W174) with high solvent accessibility of 0.46 and 0.62–were selected for double AzF incorporation (Figure 3.3B) to achieve an appreciable HSA conjugation yield. When AzF was incorporated into a single site (W160), the yield was too low to obtain a sufficient amount of conjugates for downstream purposes (data not shown). F258 and W264, despite their high solvent accessibility, were excluded since they are located in subunit interfaces and so the conjugation at those sites will likely lead to substantial perturbations of the Uox subunit assembly. Importantly, W160 and W174 have not been reported to play a role in structural/functional integrity of Uox. In the preliminary experiments, we first tested single AzF incorporation at W160, which led to the conjugation efficiency below 10% (data not shown). Therefore, we chose to incorporate two AzFs into Uox, eventually providing eight reactive sites per tetrameric Uox, in order to enhance conjugation efficiency between two macromolecules–Uox and HSA. It has been reported that C321.ΔA.exp strain can incorporate an NNAA at multiple sites without compromising protein production yield [5]. Uox-W160.174AzF was expressed from C321.ΔA.exp [Uox-W160.174amb] in the presence of 1 mM AzF, and then purified by His-tag affinity chromatography with a yield of 8 mg/L of culture medium.

Fidelity of double AzF incorporation was analyzed by tryptic digestion of Uox-W160.174AzF, along with Uox-WT as a control, followed by MALDI-TOF mass spectrometry. For Uox-WT, two tryptic digests, X and Y, containing W160 and W174, respectively, were found at 1342.8 m/z (theoretical m/z = 1342.7) and 706.3 m/z (theoretical m/z = 706.3) (Figure 3.4A, top). The replacement of tryptophan (204.2 Da) with AzF (206.2 Da) is expected to yield

m/z change of +2, i.e., 1344.7 m/z for X-Az and 708.3 m/z for Y-Az. However, major shifts were detected at 1318.4 m/z and 682.1 m/z, respectively (Fig. 3.4A, bottom).

It was previously reported that an aryl and an aliphatic azide is unusually susceptible to fragmentation via expulsion of N_2 during matrix-assisted laser desorption ionization leading to the generation of amine group [141–144], which is evidenced by the major shifts corresponding to a substitution of Trp by amino-phenylalanine (AmF, 180.20 Da). To further verify that the mass discrepancy had resulted from fragmentation during MALDI-TOF analysis, not from metabolic conversion of AzF during cell culture, Uox-W160.174AzF was reacted with a DBCO-functionalized polymer, DBCO-PEG_4-palmitic acid (1138.4 Da, Figure 3.1D). New m/z signals corresponding to conjugates formed by SPAAC between DBCO-PEG_4-palmitic acid and X-Az or Y-Az were observed at 2482.5 (theoretical = 2483.0) and 1846.6 (theoretical = 1846.7), respectively (Figure 3.5). Furthermore, no or substantially reduced intensity of original m/z values were detectable, indicating the high SPAAC reactivity of two AzFs incorporated. The orthogonal reactivity of SPAAC was visualized by dye-labeling. DBCO-PEG_4-carboxyrhodamine (880.9 Da, Figure 3.1C) reacted with Uox-WT and Uox-W160.174AzF, separately, and then analyzed by in-gel fluorescence and migration. In contrast to undetectable fluorescence of Uox-WT, Uox-W160.174AzF exhibited high fluorescence upon excitation and slower migration resulting from dye conjugation (Figure 3.4B). In addition, double bands in Fluorescence panel as well as triple bands in Coomassie panel demonstrate double incorporation and progressive labeling of both azide groups.

Circular dichroism spectroscopy (CD) has been successfully used to investigate secondary structural changes in a target protein [133,145]. Therefore, in order to determine

A

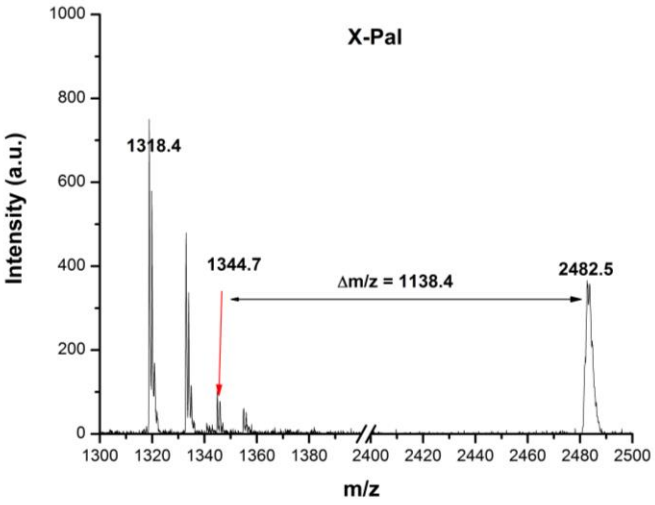

B

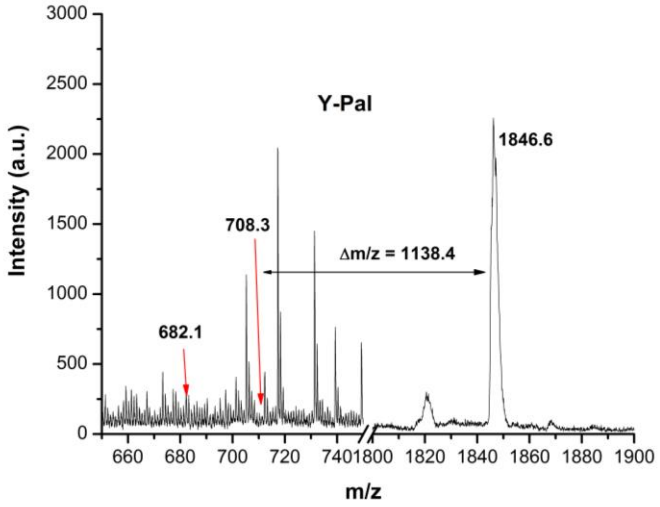

Figure 3.5. MALDI-TOF mass spectra of trypsin-treated Uox conjugated to DBCO-PEG$_4$-palmitic acid. (A) Upon conjugation, Peptide X containing W160AzF exhibited a new signal at 2482.5 contributed by m/z increase as much as the MW of DBCO-PEG$_4$-palmitic acid (1138.4), a shift from 1344.7 corresponding to W160AzF, not W160AmF (1318.4). (B) Upon conjugation, Peptide Y containing W174AzF exhibited a new signal at 1846.6 contributed by m/z increase as much as the MW of DBCO-PEG$_4$-palmitic acid (1138.4), a shift from 708.3 corresponding to W174AzF, not W174AmF (682.1).

Table 3.1. Secondary structure contents of Uox-WT and Uox-W160.174AzF

	α-helix	β-sheet	β-turn	unordered
Uox-WT	0.557	0.093	0.124	0.237
Uox-W160.174AzF	0.549	0.097	0.126	0.227

whether there are any structural changes in Uox upon AzF incorporation, CD was employed to characterize and compare the secondary structures of Uox-WT and Uox-W160.174AzF. The CD spectrum of Uox-W160.174AzF showed no significant deviation from that of Uox-WT (Figure 3.4C). The secondary structure contents analyzed from the CD spectra also supported that the structural perturbation of Uox by AzF double incorporation was negligible (Table 3.1).

3.3.2. Synthesis and characterization of Uox-HSA

To append DBCO functionality to HSA, a bifunctional linker, DBCO-PEG_4-MAL, was attached to C34 through Michael addition between a thiol and a maleimide, affording HSA-PEG_4-DBCO. Site-specific conjugation of Uox to HSA through SPAAC was performed by mixing Uox-W160.174AzF with HSA-PEG_4-DBCO, and confirmed by a new band at 150 kDa (Figure 3.6, lane 3). After removing residual HSA-PEG_4-DBCO by cation exchange chromatography (Figure 3.7A), the partially purified Uox-HSA solution was subjected to anion exchange chromatography and then the purified Uox-HSA conjugate was obtained (Figure 3.7B). The absence of HSA band in the purified Uox-HSA sample indicates that any residual unreacted HSA molecules were effectively removed during the purification process (Figure. 3.6, lane 4). The band of Uox monomer in the purified Uox-HSA sample can be explained by the disruption of non-covalent subunit interaction of the tetrameric Uox-HSA in the presence of denaturing SDS.

The molar ratio of an unreacted Uox monomer to a monomeric Uox conjugated to HSA was calculated on the basis of the Coomassie-stained band intensities, and found to be approximately 2.5 (Figure 3.8A). In order to investigate the subunit stoichiometry in a native tetrameric form, Uox-HSA was subjected to size exclusion chromatography. In comparison to

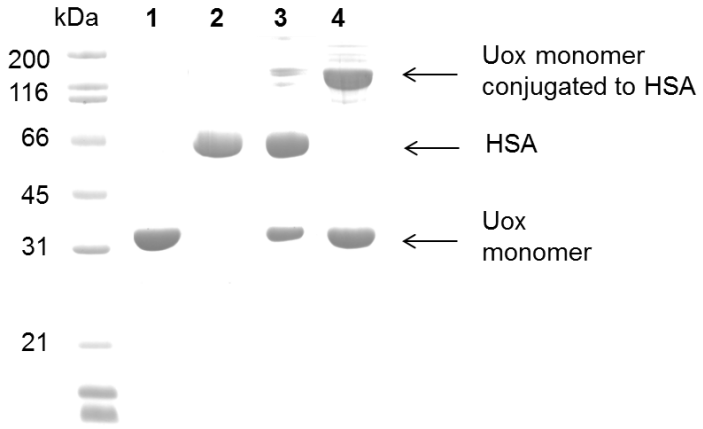

Figure 3.6. Coomassie blue-stained SDS-PAGE. Lane 1, Uox-W160.174AzF; Lane 2, HSA-PEG_4-DBCO; Lane 3, reaction mixture; Lane 4, column-purified Uox-HSA.

A

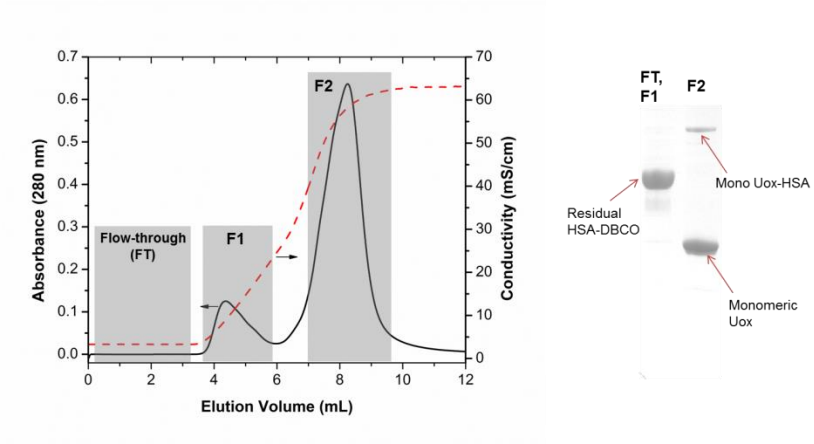

B

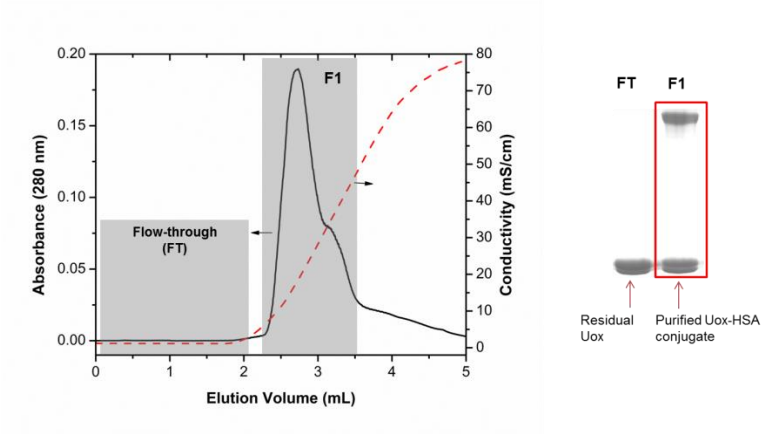

Figure 3.7. Purification of Uox-HSA. (A) Cation exchange chromatogram and SDS-PAGE analysis. The reaction mixture was loaded onto a SP-HP (1 mL) cation exchanger equilibrated with 20 mM sodium phosphate (pH 6.0) and eluted with NaCl gradient. Unreacted Uox and Uox-HSA (fraction 2) were isolated from unreacted HSA-PEG_4-DBCO (flow-through and fraction 1) as shown in SDS-PAGE. (B) Anion exchange chromatogram and SDS-PAGE analysis. Upon desalting, the fraction 2 from the cation exchange chromatography was loaded onto a UNO-Q1 anion exchanger equilibrated with 20 mM bis-tris (pH 6.5) and eluted with NaCl gradient. Uox-HSA was collected at the fraction 1 while unreacted Uox was found in the flow-through. In SDS-PAGE, tetrameric Uox-HSA was resolved into two discrete bands: monomeric Uox-HSA conjugate, upper band; monomeric Uox, lower band.

A

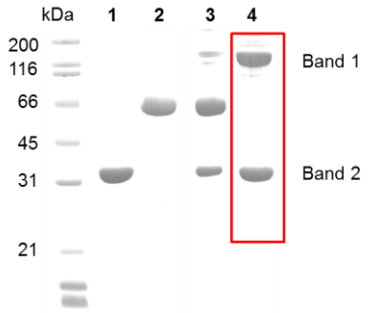

Band	Identity	Intensity (a.u.)	MW (Da)	Mole (Intensity / MW, a.u.)	Mole (rel.)
1	Uox monomer conjugated to HSA	83,926	102,000	0.82	10
2	Uox monomer	71,170	35,000	2.03	25

B

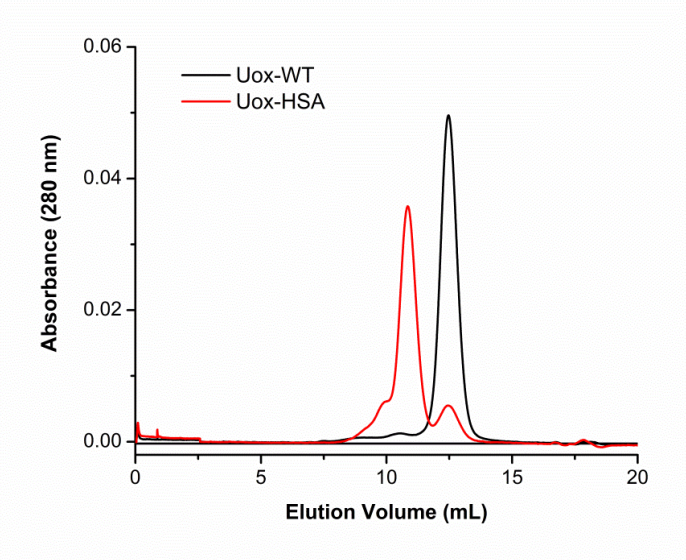

Figure 3.8. Characterization of Uox-HSA. (A) Densitometric determination of the molar subunit composition of denatured Uox-HSA. Uox-HSA was loaded onto SDS-PAGE to resolve Uox monomers conjugated to HSA (band 1) and unconjugated Uox monomers (band 2). The same gel image presented in Fig. 3 was analyzed by Image J to estimate band intensity. The MW of the monomeric Uox-HSA conjugate (102,000 Da) is the sum of MWs of monomeric Uox (35,000 Da) and HSA (67,000 Da). (B) Size exclusion chromatography of Uox-HSA and Uox-W160.174AzF in a native condition.

the unmodified Uox-W160.174AzF tetramer which eluted as a single symmetric peak, Uox-HSA displayed a major peak at an earlier elution volume followed by a smaller peak corresponding to the unmodified tetramer (Figure 3.8B). The major peak is likely to represent Uox tetramer carrying one HSA while a small poorly resolved peak observed at the elution front appears to contain Uox tetramer carrying mostly two or more HSAs. This is supported by a simple random combination analysis of the subunit stoichiometry of Uox-HSA based upon the molar ratio determined by densitometry, in which Uox tetramer having one HSA has been found to be the most probable tetrameric assembly of subunits, provided that HSA-conjugated Uox monomers has the same subunit interaction with unconjugated Uox monomers (Table 3.2).

The effect of HSA conjugation on enzymatic activity was evaluated by Michaelis-Menten kinetics (Figure 3.9). The catalytic rates of both Uox-HSA and Uox-WT were determined at varying concentrations of uric acid. Uox-HSA had a V_{max} comparable to that of Uox-WT (Table 3.3). Although Uox-HSA had a lower K_m for uric acid than that of Uox-WT, the difference was not substantial due to relatively large standard errors of regression. These kinetic analysis results clearly indicated that the enzymatic activity of Uox was fully retained upon HSA conjugation.

3.3.3. In vivo study

In order to evaluate pharmacological benefits from site-specific albumination, a single dose of either Uox-WT or Uox-HSA was intravenously administered to mice (n = 4), and their enzymatic activities in serum samples taken at different time points were measured by the uric acid-degradation assay. Assuming the one-compartment distribution with first-order elimination [78,111], the logarithmic residual activity versus time post-injection was fitted to a mono-exponential decay to calculate a serum activity half-life ($t_{1/2}$) and area under the curve (AUC)

Table 3.2. Statistical analysis of subunit composition of tetrameric Uox-HSA

Uox monomer	Uox monomer conjugated to HSA	[a]Probability	[b]Elution volume (mL)
4	0	${}_{25}C_4 \times {}_{10}C_0 / {}_{35}C_4 = 0.24$	12.8
3	1	${}_{25}C_3 \times {}_{10}C_1 / {}_{35}C_4 = 0.44$	11.0
2	2	${}_{25}C_2 \times {}_{10}C_2 / {}_{35}C_4 = 0.26$	10.0
1	3	${}_{25}C_1 \times {}_{10}C_3 / {}_{35}C_4 = 0.06$	< 10.0
0	4	${}_{25}C_0 \times {}_{10}C_4 / {}_{35}C_4 = 0.0004$	< 10.0

[a]Tetrameric assembly by random combination based upon the molar ratio obtained by densitometry in Fig. 3.8A.

[b]Obtained from size exclusion chromatogram in Fig. 3.8B.

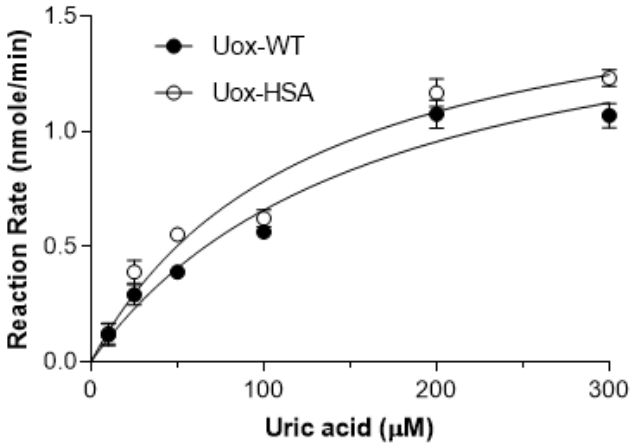

Figure 3.9. Michaelis-Menten plots. The uric acid-degrading assay was performed at various substrate concentrations with a fixed enzyme concentration of 60 nM. Means (n = 3) ± SE of Uox-WT or Uox-HSA was fit to a curve to calculate kinetic parameters.

Table 3.3. Kinetic parameters

	V_{max} (nmol/min)	K_m (μM)
Uox-WT	1.74 ± 0.18	164.6 ± 35.2
Uox-HSA	1.76 ± 0.16	125.5 ± 25.6

Values ± standard errors of regression obtained by fitting to the Michaelis-Menten equation

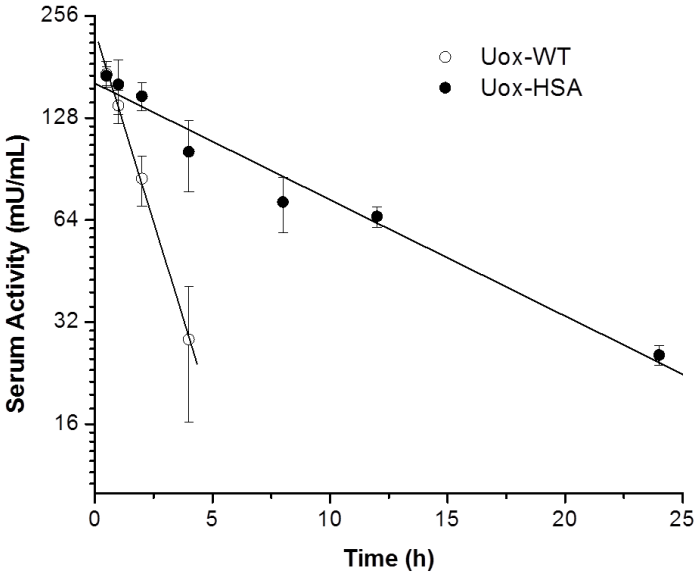

Figure 3.10. Residual enzymatic activity in serum of intravenously injected Uox-WT and Uox-HSA in mice (n = 4). Uric acid-degrading activities of Uox-WT and Uox-HSA were measured from blood samples drawn at different time points: 0.5, 1, 2, 4 h for Uox-WT; 0.5, 1, 2, 4, 8, 12, 24 h for Uox-HSA. The catalytic reaction rate per mL of serum on a logarithmic scale over time was plotted to give a linear fit. Each data point represents the mean (n = 4) ± SE.

Table 3.4. In vivo study results

	$t_{1/2}$ (h)	AUC (mU/mL × h)
Uox-WT	1.3	[a]302.9
Uox-HSA	8.8	[b]1656.9

[a]From 0.5 to 4 h
[b]From 0.5 to 24 h

(Figure. 3.10). In contrast to rapid elimination of Uox-WT with a $t_{1/2}$ of 1.3 h, Uox-HSA exhibited a prolonged activity with a $t_{1/2}$ of 8.8 h (Table 3.4).

3.4. Discussion

Site-specific albumination of a therapeutic protein with complex structures, i.e. multi-subunit, was successfully demonstrated by the combination of site-specific incorporation of AzF and SPAAC. The high fidelity reassignment of a UAG codon to encode AzF was achieved by exploiting a genomically engineered *E. coli* equipped with an engineered pair of tyrosyl-tRNA synthetase/amber suppressor tRNA [7,146]. The absence of release factor 1 (RF1) and genomic UAG codons in the expression host rendered the pair strictly targeted to amber mutations of Uox-encoding gene without unwanted truncation by RF1, allowing stable expression of Uox containing AzFs at two distinct sites.

A careful selection of NNAA incorporation sites lies at the core of successful site-specific albumination. First, incorporation should be made at a surface-exposed position for high-yielding conjugation. It has been reported that higher solvent-accessibility of a NNAA generally ensures higher conjugation efficiency [147–149]. However, it should be noted that NNAA substitution for an original amino acid with a fairly different structure and charge may undermine the accessibility-efficiency correlation [150]. Therefore, AzF incorporation sites, W160 and W174, were chosen out of amino acids bearing an aromatic ring, i.e., Phe, Trp, and Tyr, as well as high solvent accessibility. Judging from mass spectra of Uox conjugated to DBCO-PEG_4-palmitic acid (Figure 3.5) and the SDS-PAGE analysis upon dye conjugation (Figure 3.4B), our scheme seems to be suitable for selecting incorporation site with high conjugation efficiency. Second, the incorporation site should not be critically involved in native

function of a target protein. Combining the literature search and three-dimensional structure analysis, the best incorporation sites can be predicted from candidates screened by the solvent accessibility.

The prolonged activity of Uox-HSA relative to Uox-WT demonstrates the benefits of site-specific albumination. Random PEGylation onto multiple lysine residues of Uox resulted in severe heterogeneity in the conjugates and reduced activity, though the serum half-life was significantly extended [50]. In particular, PEGylation extended the serum activity half-life of Uox obtained from *Candida utilis* from 1 h to 8 h in mice [151]. Although Uox from *A. flavus* was used in this study, single HSA conjugation to Uox led to the prolonged activity comparable to PEGylation.

Emerging concerns over immunogenicity of the methoxy terminus of PEG should not be overlooked [152,153]. Tetra(ethylene glycol) (PEG_4) used here as a backbone of the heterobifunctional linker, DBCO-PEG_4-MAL, has no exposed terminus upon conjugation, and its short length greatly minimizes the immunogenic potential [152]. Moreover, if PEG in the linker causes any immune response issue, the linker can be easily modified not to include PEG without altering the overall site-specific albumination scheme. Therefore, site-specific albumination is a promising platform for developing long acting versions of large and complex proteins. The elimination kinetics of Uox-HSA activity observed in the mice study resulted in 6.8-fold increase in serum activity half-life, in comparison to Uox-WT. Furthermore, it is very likely that the effect of FcRn-mediated recycling of Uox-HSA would be more pronounced in higher animal models since the murine FcRn is known to exhibit binding affinity towards HSA substantially lower than that between human FcRn and HSA [154]. Introduction of HSA variants

with higher FcRn affinity in site-specific albumination might contribute to a much longer extension of activity *in vivo* [155].

3.5. Conclusion

We show here the site-specific conjugation of HSA to Uox with multi-subunit is a promising approach to prolonging *in vivo* efficacy, which is challenging to achieve by conventional bioconjugation or genetic fusion techniques. Genetic incorporation of NNAAs into permissive positions of Uox followed by albumination through bio-orthogonal chemistry generated a well-defined conjugate with retained enzymatic activity and longer duration *in vivo*. The platform may find diverse applications for delivery of therapeutic proteins.

Chapter 4: Site-specific Immobilization of a Murine Dihydrofolate Reductase by Copper(I)-catalyzed Azide-alkyne Cycloaddition with Retained Enzymatic Activity

Cu(I)-catalyzed azide-alkyne cycloaddition (CuAAC) is an efficient reaction linking an azido and an alkynyl group in the presence of copper catalyst. Incorporation of a non-natural amino acid (NNAA) containing either an azido or an alkynyl group into a protein allows site-specific bioconjugation in mild conditions via CuAAC. Despite its great potential, bioconjugation of an enzyme has been hampered by several issues including low yield, poor solubility of a ligand, and protein structural/functional perturbation by CuAAC components. In the present study, we incorporated an alkyne-bearing NNAA into an enzyme, murine dihydrofolate reductase (mDHFR), in high cell density cultivation of Escherichia coli, and performed CuAAC conjugation with fluorescent azide dyes to evaluate enzyme compatibility of various CuAAC conditions comprising combination of commercially available Cu(I)-chelating ligands and reductants. The condensed culture improves the protein yield 19-fold based on the same amount of non-natural amino acid, and the enzyme incubation under the optimized reaction condition did not lead to any activity loss but allowed a fast and high-yield bioconjugation. Using the established conditions, a biotin-azide spacer was efficiently conjugated to mDHFR with retained activity leading to the site-specific immobilization of the biotin-conjugated mDHFR on a streptavidin-coated plate. These results demonstrate that the combination of reactive non-natural amino acid incorporation and the optimized CuAAC can be used to bioconjugate enzymes with retained enzymatic activity.

4.1. Background and Motivation

Enzymes play important roles in biocatalysis to produce value-added compounds, as well as in the diagnostics and therapeutics to improve human health. In order to further expand the utility of enzymes, bioconjugation has been actively explored. The conjugation of polyethylene glycol (pegylation) to therapeutic enzymes leads to prolonged circulation time in vivo [156]. The conjugation of fluorescence dye facilitates the studies on protein trafficking inside cells/tissues or protein structural changes [157–159]. The covalent attachment of enzymes on solid surface (enzyme immobilization) leads to an enhanced thermostability [160]. For these applications, amino acids with reactive residues such as lysine and cysteine have been common targets for bioconjugation [161,162]. However, the bioconjugation to multiple lysine residues of an enzyme often leads to heterogeneous mixtures of isomers, compromising the catalytic properties probably due to modification of an active site. In order to overcome this issue, the site-specific bioconjugation of an enzyme has been investigated. Although cysteine can be used to achieve site-specific bioconjugation in some cases, its application is limited in cases where there is an additional free cysteine residue or a disulfide bond(s) is critical for protein folding. In order to achieve absolute site-specificity, we and several other groups employed the bioconjugation strategy utilizing site-specific incorporation of a reactive non-natural amino acid (NNAA) [163–165]. To attain an efficient site-specific incorporation, an expression host is equipped with an orthogonal pair of suppressor tRNA and aminoacyl-tRNA synthetase that have been modified to be specific for a NNAA of interest but not to cross-talk with 20 natural amino acids as well as endogenous sets of tRNA and tRNA synthetase [65,166]. The orthogonal pair incorporates a NNAA in response to an expanded genetic code, usually stop codons or four-base codons [167,168]. In particular, site-specific incorporation of a NNAA is of interest for protein

bioconjugation, because it allows a flexible selection of an incorporation site and subsequent chemo-selective conjugation, affording a conjugate with high homogeneity and minimal loss of native protein function.

In order to achieve the site-specific bioconjugation using a NNAA, bioorthogonal protein chemistry is also required. We chose Cu(I)-catalyzed azide-alkyne cycloaddition (CuAAC) in this study, since it is a high-yielding and reliable reaction forming a stable triazole linkage between biologically inert azide and terminal alkyne groups [12], and readily compatible with aqueous and mild conditions beneficial for protein bioconjugation [169,170]. CuAAC has been embraced for numerous biomolecular conjugation applications since its discovery in 2002 [10,171,172]. To employ CuAAC, a NNAA functionalized with an azide or an alkyne group is incorporated into a target protein in a residue- or a site-specific manner [3,111,173].

Efficient protein bioconjugation has been the primary goal for optimizing CuAAC conditions generating varying compositions of reaction components [84,174–178]. Although the retained stability of a viral capsid protein and the fluorescence of superfolder fluorescent protein after bioconjugation were investigated [60,111,176], it has not yet been reported that CuAAC systems can be used to bioconjugate enzymes with retention of most activities which can be affected by even a subtle perturbation in the folded structure and chemical modification. It was reported that the lipase conjugated to nanoparticles via CuAAC exhibited catalytic activity [179]. However, the extent of activity retention upon the conjugation was not presented. Since CuAAC reaction components or conditions may damage catalytic properties of enzymes, the optimized CuAAC conditions achieving a high bioconjugation yield may not be ideal for the bioconjugation of enzymes, For instance, Candida antarctica lipase B exhibited significant loss of activity when overnight-incubated with CuAAC reagents including $CuSO_4$, ascorbate, and

bathophenanthroline ligand [180]. More recently, Escherichia coli dihydrofolate reductase with a site-specifically incorporated tyrosine analog was subjected to direct protein-protein conjugation through CuAAC, and the authors reported complete loss of activity resulting from detrimental effects of the Cu(I) complex [59]. Considering the great potential of CuAAC in bioconjugation of enzymes and therapeutic proteins, it is timely and important to determine whether CuAAC conditions can be optimized to efficiently bioconjugate enzymes with retained enzymatic activity.

As a model system to study site-specific bioconjugation of enzymes via CuAAC, we chose murine dihydrofolate reductase enzyme (mDHFR), an enzyme that converts dihydrofolate (DHF) to tetrahydrofolate (THF). Here we first evaluated effects of CuAAC reaction components on retention of the catalytic activity as well as reaction efficiency in order to identify optimal CuAAC reaction conditions for enzyme bioconjugation. Furthermore, varying bioconjugation yields at different conjugation sites were also investigated. Since not all residues of an enzyme are readily accessible for bioconjugation, a choice of conjugation site is important to achieve high bioconjugation yield. Based on the solvent accessibility of amino acid residues in the mDHFR calculated by the ASA-View program [73], two residues (one with a high solvent accessibility and another with a low solvent accessibility) were selected. Then, the conjugation yield at the two sites was compared. Finally, with the optimized CuAAC conditions and conjugation site, we investigated whether an enzyme can be directly immobilized on the surface with preserved catalytic activity. Directed immobilization of a protein is one important topic in the fields of biosensing and biocatalysis, because it may increase the biosensor's sensitivity and biocatalyst's stability [181]. In order to mediate enzyme immobilization, a biotin/streptavidin pair with strong affinity and high selectivity was utilized. A biotin derivative containing an azide

functional group was site-specifically conjugated to the mDHFR and then subjected to binding to a streptavidin-coated plate.

4.2. Materials and Methods

4.2.1. Materials

p-Ethynylphenylalanine (pEthF) was synthesized as described previously [2]. Ni-NTA agarose and pQE16 plasmid were obtained from Qiagen (Valencia, CA). Endoproteinase Lys-C was obtained from Promega Corporation (Madison, WI). Amicon ultra centrifugal filters with a molecular weight cutoff of 10 kDa and ZipTip® with C_{18} media were purchased from Millipore Corporation (Billerica, MA). Sulforhodamine-azide and Biotin-PEG3-azide were purchased from Bioconjugate Technology Company (Scottsdale, AZ). Azidocoumarin was obtained from Glen Research (Sterling, VA). Streptavidin Coated High Sensitivity Plate was obtained from Thermo Scientific (Rockford, IL). All other chemicals were purchased from Sigma-Aldrich Corporation (St. Louis, MO).

4.2.2. Plasmid Construction and Strains

Preparation of the plasmids pQE16-yPheRS^{T415A} and pREP4-ytRNA$^{Phe}_{CUA_UG}$ is described elsewhere [69]. pQE16$_{am43}$-yPheRS^{T415A} or pQE16$_{am179}$-yPheRS^{T415A} encodes the yeast phenylalanyl-tRNA synthetase variant and the murine dihydrofolate reductase (mDHFR) with an amber codon at the 43rd or 179th position and a C-terminal hexahistidine tag. An amber codon was introduced by PCR mutagenesis replacing the 43rd valine codon or the 179th phenylalanine codon. The mutagenic primer sequences were as follows: V43 Forw, 5′-CACAACCTCTTCATAGGAAGGTAAACAG-3′; V43 Rev, 5′-

CTGTTTACCTTCCTATGAAGAGGTTGTG-3′; F179 Forw, 5′-CATCAAGTATAAGTAGGAAGTCTACGAG-3′; F179 Rev, 5′-CTCGTAGACTTCCTACTTATACTTGATG-3′. pREP4-ytRNA$^{Phe}_{CUA_UG}$ encodes the mutant yeast amber suppressor tRNA engineered to have minimal cross-reactivity with the *E. coli* aminoacyl-tRNA synthetases. A Phe/Trp/Lys triple auxotrophic *Escherichia coli* strain, AFWK, was prepared as described previously [69]. AFWK harboring both plasmids was used as an expression host for site-specific incorporation of pEthF into the amber codon.

4.2.3. Expression and Purification of Proteins

The wild-type mDHFR (mDHFR-WT) was expressed from E. coli XL1-Blue harboring pQE16 by 1 mM IPTG induction in LB media containing 100 μg/mL ampicillin at 37 °C. To express the mDHFR mutant containing pEthF at the 43rd position (mDHFR-43pEthF), AFWK harboring pQE16$_{am43}$-yPheRS^{T415A} and pREP4-ytRNA$^{Phe}_{CUA_UG}$ was used. Saturated overnight cultures grown at 37 °C in M9 minimal medium supplemented with 100 μg/mL ampicillin, 30 μg/mL kanamycin, 0.4% (w/v) glucose, 1 mM $MgSO_4$, 0.1 mM $CaCl_2$, 10 μg/mL thiamine, and 20 amino acids (25 μg/mL each) were diluted 20-fold in the same fresh medium, and grown at 37 °C until an OD_{600} of 0.9 was reached. After incubation on ice for 15 min, cells were sedimented by centrifugation at 4000 g for 12 min, and washed with cold 0.9% (w/v) NaCl by gentle resuspension. After repeating twice, cells were shifted to M9 medium supplemented with the same ingredients described above except for different amino acid compositions: 17 amino acids (35 μg/mL each), 150 μM Lys, 60 μM Phe, 20 μM Trp, and 3 mM pEthF. To maximize the incorporation efficiency in condensed culture, the total volume of M9 expression medium was

20-fold smaller than the original volume. Upon induction by 1 mM IPTG, cells were incubated with shaking at 30 ℃ for 15 h before harvest. Cells were pelleted by centrifugation, and the protein was purified by gravity-flow affinity chromatography using Ni-NTA agarose beads under native condition according to the supplier's instructions (Qiagen). Purified proteins were directly used or buffer-exchanged using PD-10 desalting columns to appropriate buffers. If necessary, the protein solutions were concentrated using centrifugal filters. The mDHFR mutant containing pEthF at the 179th position (mDHFR-179pEthF) was obtained as described above except that $pQE16_{am179}$-$yPheRS^{T415A}$ was used instead of $pQE16_{am43}$-$yPheRS^{T415A}$.

4.2.4. Mass Characterization by MALDI-TOF Mass Spectrometry

To the mDHFR-WT or the mDHFR-pEthF in 20 mM potassium phosphate (pH 8.0) was added endoproteinase Lys-C to a final protease:mDHFR ratio of 1:50 (w/w). Following incubation at 37 ℃ overnight, the reaction mixture was mixed with 0.5% (v/v) trifluoroacetic acid (TFA) to quench the reaction and then desalted on a ZipTip® C_{18}, and then analyzed by MALDI-TOF mass spectrometry (MS) to confirm site-specific incorporation of pEthF into the desired position of the mDHFR. The MS analysis was performed using 20 mg/mL of 2,5-dihydroxybenzoic acid and 2 mg/mL of L-(−)-fucose dissolved in 10% ethanol as a matrix by Microflex™ MALDI-TOF MS (Bruker Corporation, Billerica, MA).

4.2.5. Kinetic Studies

Stock solutions were prepared as follows: 80 μM mDHFR-pEthF in 20 mM potassium phosphate (pH 8.0), 20 mM $CuSO_4$ in DW, 20 mM tris[(1-benzyl-1H-1,2,3-triazol-4-yl)methyl] amine (TBTA) in dimethyl sulfoxide (DMSO), 20 mM tris(3-hydroxypropyltriazolylmethyl)

amine (THPTA) in DW, 1 mM azidocoumarin in DMSO, and 40 mM reductant in DW. For CuAAC in the TBTA/DMSO system, the mDHFR-pEthF at a final concentration of 30 μM was mixed with an appropriate concentration of DMSO, 1 mM $CuSO_4$, 1 mM TBTA, 60 μM of azidocoumarin, and 2 mM reductant in 70 μL reaction volume (listed in the order of addition). For CuAAC in the THPTA system, the mDHFR-pEthF at a final concentration of 30 μM was mixed with 1 mM $CuSO_4$, 1 mM THPTA, 60 μM of azidocoumarin, and 2 mM reductant in 70 μL reaction volume. Evolution of fluorescence was monitored at λ_{ex} = 400 nm, λ_{em} = 470 nm in standard 96-well plates on the SynergyTM four multimode microplate reader (BioTek, Winooski, VT) at appropriate time intervals at 25^{o}C. To quench the reaction, 10 mM ethylenediaminetetraacetic acid (EDTA) was added.

4.2.6. Enzymatic Activity Assay

To measure enzymatic activity of the mDHFR-pEthF, nicotinamide adenine dinucleotide phosphate (NADPH)-dependent reduction of dihydrofolate (DHF) was monitored at $A_{340\ nm}$ by the SynergyTM four multimode microplate reader according to the protocol provided by the dihydrofolate reductase assay kit (Sigma) with slight modification as follows. The reaction was initiated by mixing 100 μL of the assay buffer (50 mM 2-(N-morpholino)ethanesulfonic acid (Mes), 25 mM tris(hydroxymethyl)aminomethane (Tris), 25 mM ethanolamine, and 100 mM sodium chloride, pH 7.5, containing 120 μM NADPH and 100 μM DHF) with 100 μL of the assay buffer containing an appropriate concentration of the mDHFR-pEthF. All measurements were made in triplicate at 25 ^{o}C. The change in absorbance after 10 min was taken as a measure of catalytic activity.

4.2.7. Immobilization and Activity Assay of the Biotinylated mDHFR

Biotinylation of the mDHFR-43pEthF was conducted for 20 min in the following condition: 50 μM mDHFR-43pEthF, 1 mM $CuSO_4$, 1 mM THPTA, 150 μM of biotin-PEG3-azide, and 2 mM ascorbate in 20 mM potassium phosphate (pH 8.0) / 0.1M NaCl. After adding EDTA at a final concentration of 10 mM to quench the reaction, the reaction mixture was desalted by a PD-10 column, and concentrated by ultrafiltration to 1 mg/mL of the biotinylated mDHFR (mDHFR-43biotin). Fifty microliter of the mDHFR-43biotin was added to each well in a streptavidin-coated plate, and incubated at room temperature for 30 min. After washing three times with 200 μL of 20 mM potassium phosphate (pH 8.0) / 0.1M NaCl / 0.05% Tween 20, 150 μL of the assay buffer was added to each well. Absorbance at 340 nm was monitored at appropriate time points by the microplate reader.

4.3. Results and Discussion

4.3.1. Incorporation of p-Ethynyl-L-Phenylalanine into the mDHFR

To minimize structural perturbation upon incorporation of hydrophobic phenylalanine analog, p-ethynylphenylalanine (pEthF) (Figure 4.1A), the valine at the 43rd position was chosen as a target because it is away from the active site (Figure 4.2), and exhibits hydrophobic index similar to that of phenylalanine [182] and substantial solvent accessibility (Figure 4.3). Residues were numbered based on the amino acid sequence of the mDHFR in the Protein Data Bank (PDB ID: 3D80) [183]. We introduced an amber codon at the 43rd position of the mDHFR to replace valine with pEthF (mDHFR-43pEthF). Protein expression in a site-specific incorporation system generally suffers from low protein yield because an exogenous suppressor tRNA should compete with endogenous release factor 1 for the recognition of an amber stop codon [8], necessitating a

large volume of culture to secure an appreciable amount of a target protein. In addition, a high NNAA concentration, typically in mM range, is required to maximize the fraction of a suppressor tRNA charged with a NNAA [71,184], which is expensive or commercially not available. To increase expression yield of the mDHFR containing a site-specifically incorporated pEthF with its minimal consumption, cells were harvested by centrifugation before IPTG induction, and then resuspended with M9 expression medium containing 3 mM pEthF, the volume of which was 20-fold less than the original volume. Previously, condensed E. coli cultures in the NNAA incorporation system employing an evolved pyrrolysyl-tRNA synthetase/$tRNA_{CUA}$ pair from Methanosarcina species significantly enhanced the expression yield of proteins containing a NNAA [185,186]. The methodology has been found to be effective with the yeast phenylalanyl-tRNA synthetase/suppressor tRNA machinery we used here. When the culture volume was condensed by a factor of 20 but the pEthF concentration was not changed, the amount of the mDHFR-43pEthF obtained per milligram of pEthF (65.2 µg) was approximately 19-fold higher than that in the uncondensed culture (3.5 µg). These results successfully demonstrate that the production of the mDHFR-pEthF in a condensed volume of cell culture greatly minimizes the waste of a valuable NNAA.

To verify the substitution of the 43rd valine by pEthF, endoproteinase Lys-C digests of the mDHFR-43pEthF and the wild-type mDHFR (mDHFR-WT) were analyzed by MALDI-TOF. Peptide V43 (residue 33–46; YFQRMTTTSSVEGK) derived from the mDHFR-WT, was detected with a monoisotopic mass of 1634.9 Da, in accord with its theoretical mass (Figure 4.4A, top). For the mDHFR-43pEthF, Peptide Z43 (residue 33–46; YFQRMTTTSSAmEGK where Am indicates an amber codon) was observed at 1706.8 Da, while no signal was found at

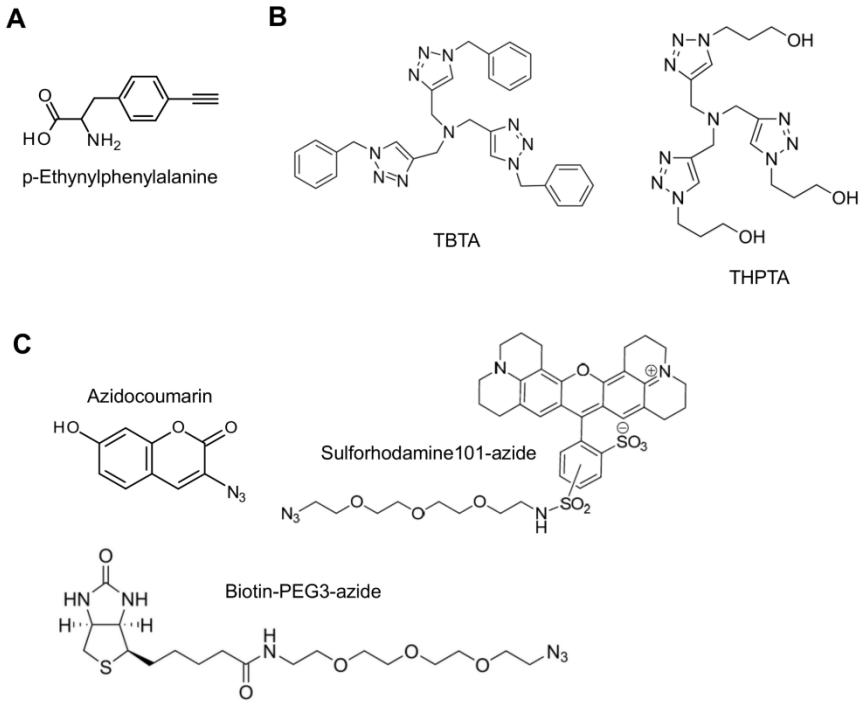

Figure 4.1. Chemical structures. (A) *p*-ethynylphenylalanine, (B) Cu(I)-chelating ligands, and (C) azide-functionalized reagents.

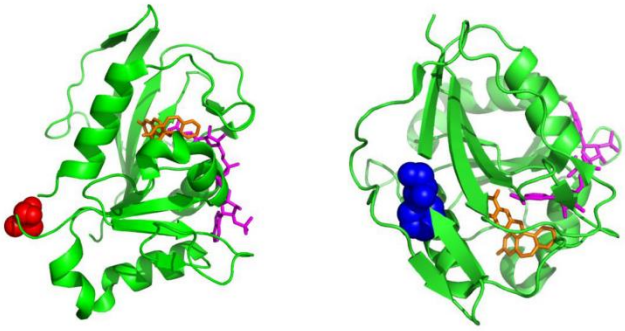

Figure 4.2. Locations of selected residues for pEthF incorporation in the three-dimensional structure of the mDHFR-WT. Valine at the 43rd position and phenylalanine at the 179th position are highlighted in red (left) and blue (right), respectively. The cofactor NADPH (magenta) and the inhibitor (orange) are shown in stick representation (PDB ID: 3D80).

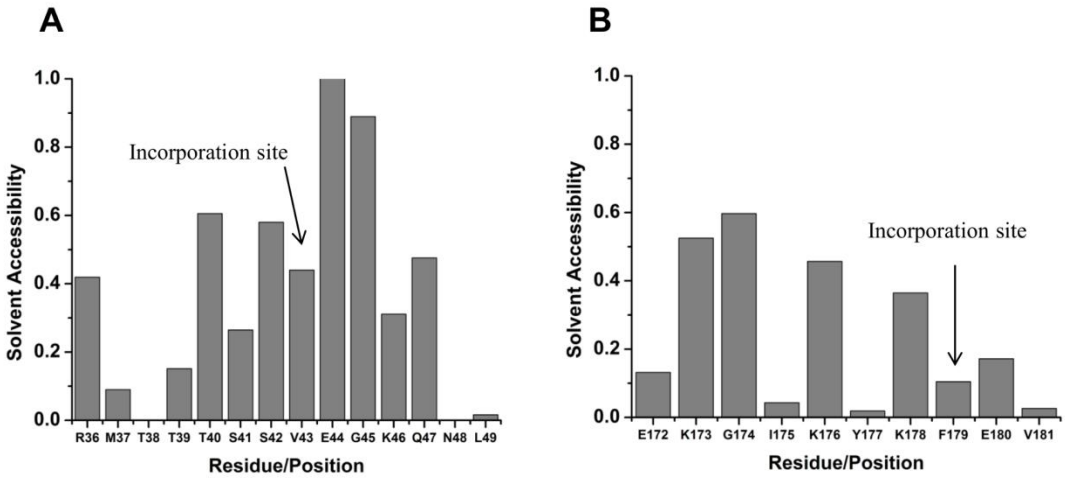

Figure 4.3. Solvent accessibility of pEthF incorporation sites, V43 (A) and F179 (B), and their neighboring residues calculated by the ASA-View program. Relative values of absolute surface area of each residue were derived from the crystal structure of the mDHFR (PDB ID: 3D80).

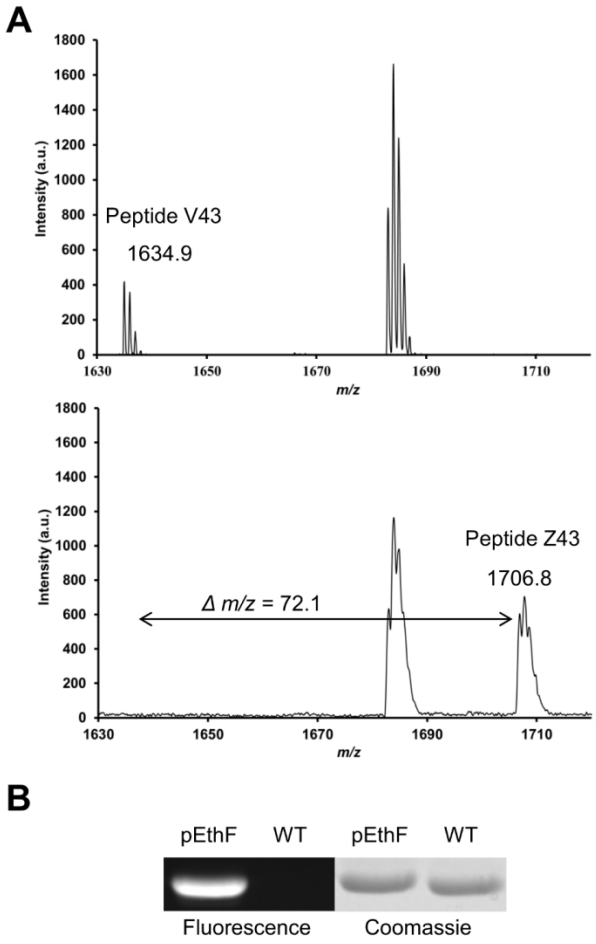

Figure 4.4. Incorporation of pEthF into the 43rd position of the mDHFR and its orthogonal reactivity. (A) MALDI-TOF spectra of Lys-C-digested fragments derived from the mDHFR-WT (top) and the mDHFR-pEthF (bottom). (B) SDS-PAGE of the mDHFR-pEthF (pEthF) and the mDHFR-WT (WT) reacted with sulforhodamine-azide. The reaction was performed at 25 ^{o}C by mixing the protein (30 μM) with the dye (60 μM), $CuSO_4$ (1 mM), TBTA (1 mM), and ascorbate (2 mM) in 20 mM phosphate (pH 8.0) plus 30% (v/v) DMSO. The gel was illuminated by the excitation light at 550 nm (fluorescence panel), and then stained with Coomassie brilliant blue (Coomassie panel).

1634.9 Da (Figure 4.4A, bottom), strongly supporting the incorporation of pEthF in response to the amber codon.

To validate orthogonal reactivity of the alkynyl group at the para-position of pEthF, the mDHFR-43pEthF, along with the mDHFR-WT as a control, was incubated with a fluorescent probe, sulforhodamine-azide (Figure 4.1C), in the presence of $CuSO_4$, ascorbate, and TBTA. In-gel fluorescence analysis showed that only the mDHFR-43pEthF was reactive toward the azide group via CuAAC (Figure 4.4B).

4.3.2. Effect of CuAAC in TBTA/DMSO System on Enzymatic Activity

The catalytic function of an enzyme is sensitive to the chemical environment, and often severely hampered by suboptimal reaction conditions. There are several reasons for such a loss of catalytic activity. First, the addition of DMSO or SDS to solvate hydrophobic surfaces and chelating ligands may lead to irreversible deformation of the three-dimensional structure [174,176,186]. Second, harmful byproducts formed from a reductant can adversely modify proteins [103,176]. Finally, lack of CuAAC kinetic studies when a protein serves as a reaction target obscures an optimal reaction time that meets both maximum yield and minimal exposure to the abovementioned potential risk factors. Therefore, to ensure enzyme-friendly applications of CuAAC, proper choices of the chelating ligand, the reductant, and duration of reaction should be addressed.

TBTA (Figure 4.1B) stabilizes Cu(I) ions which are susceptible to disproportionation, and has been commonly used as an accelerating ligand for CuAAC. However, due to its low water-solubility, it tends to become precipitated in aqueous media in which most protein conjugations are conducted. To increase TBTA solubility, we incrementally added a polar

organic solvent, DMSO, to the CuAAC reaction mixture while holding all others fixed, and explored its effect on reaction yield. A milky turbidity observed in the CuAAC reaction mixture dropped in proportion to DMSO concentration. In order to evaluate reaction efficiency, we employed fluorogenic assay using azidocoumarin (Figure 4.1C) which, initially non-fluorescent, becomes highly fluorescent upon its conjugation to terminal alkyne through CuAAC, thereby enabling spectroscopic tracking of the reaction progress [187]. Higher DMSO concentration allowed higher conjugation efficiency, indicating that solubility of TBTA is important to a high-yielding CuAAC reaction (Figure 4.5A). DMSO-dependent labeling efficiency was also evident by in-gel fluorescence assay (Figure 4.5B). As quantified by fluorescence intensity, the CuAAC reaction in 30% (v/v) DMSO exhibited 13.6% stronger fluorescence than that in 10% (v/v) DMSO.

It was previously reported that DMSO exerts inhibitory effects on catalytic enzymes [188–190]. In particular, E. coli dihydrofolate reductase lost 17% of its native enzymatic activity after incubation in the CuAAC reaction buffer containing 20% (v/v) DMSO [191]. To investigate the effect of DMSO on enzymatic activity of the mDHFR-43pEthF, we measured NADPH-dependent reduction of DHF catalyzed by the mDHFR-43pEthF after 15 min incubation with 30% (v/v) DMSO and 36-fold dilution with the assay buffer (Figure 4.5C). The mDHFR-43pEthF exhibited 86.7% of its original activity after incubation, indicating that 30% (v/v) DMSO essential for maximum yield irreversibly impairs the enzymatic activity and, therefore, the TBTA/DMSO system for CuAAC is not compatible with the mDHFR.

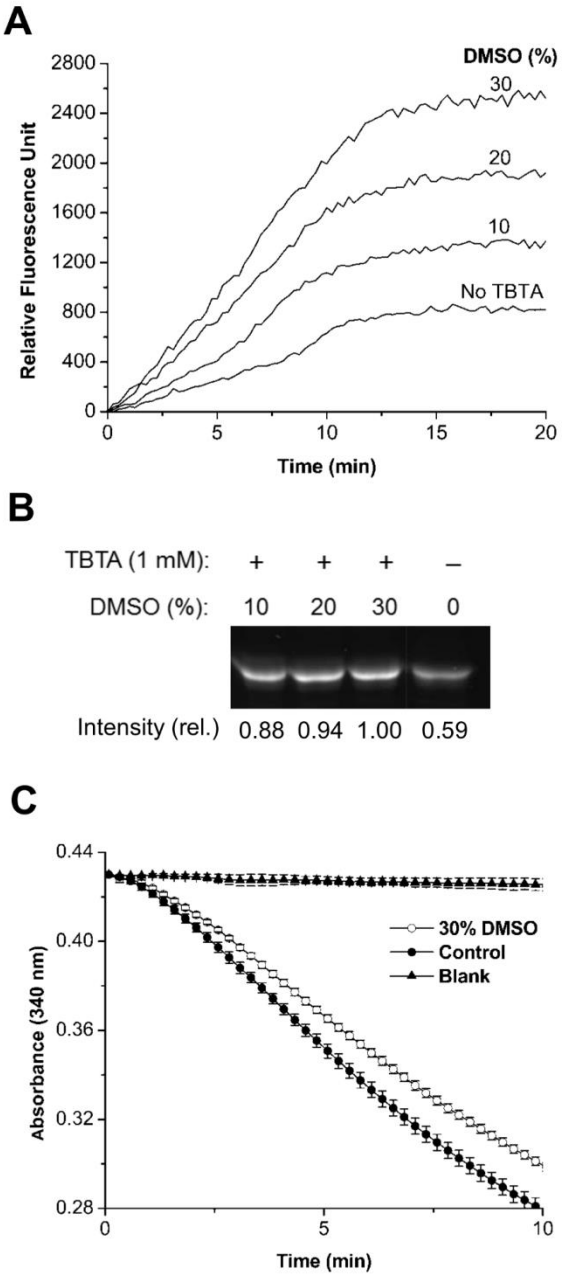

Figure 4.5. Performance of TBTA-assisted CuAAC reactions under various DMSO concentrations and their effects on the enzymatic activity. (A) Kinetic traces detected at various DMSO volume concentrations in the presence of TBTA or in a DMSO-free buffer without TBTA. Reactions were initiated at 25 ^{o}C by adding ascorbate (2 mM) to a phosphate-buffered (pH 8.0) mixture containing 30 µM of the mDHFR-43pEthF, 60 µM of azidocoumarin,

1 mM of $CuSO_4$, 1 mM TBTA, and appropriate DMSO contents. Fluorescence evolution was recorded at λ_{ex} = 400 nm and λ_{em} = 470 nm. (B) In-gel fluorescence of an equal amount of reaction products. Relative intensities were quantified by densitometry. (C) Effect of DMSO incubation on activity of the mDHFR-43pEthF. After incubation of 30 μM protein in 10 μl of DMSO-free (closed circle) or 30% (v/v) DMSO-containing phosphate buffer (pH 8.0) (open circle) for 15 min at 25 ^{o}C, the mixture was diluted 36-fold with the assay buffer for activity assay as described in Materials and Methods. Relative activity was calculated based on changes in absorbance for 10 min after initiation of the enzymatic reaction. Error bars represent standard errors (n=3).

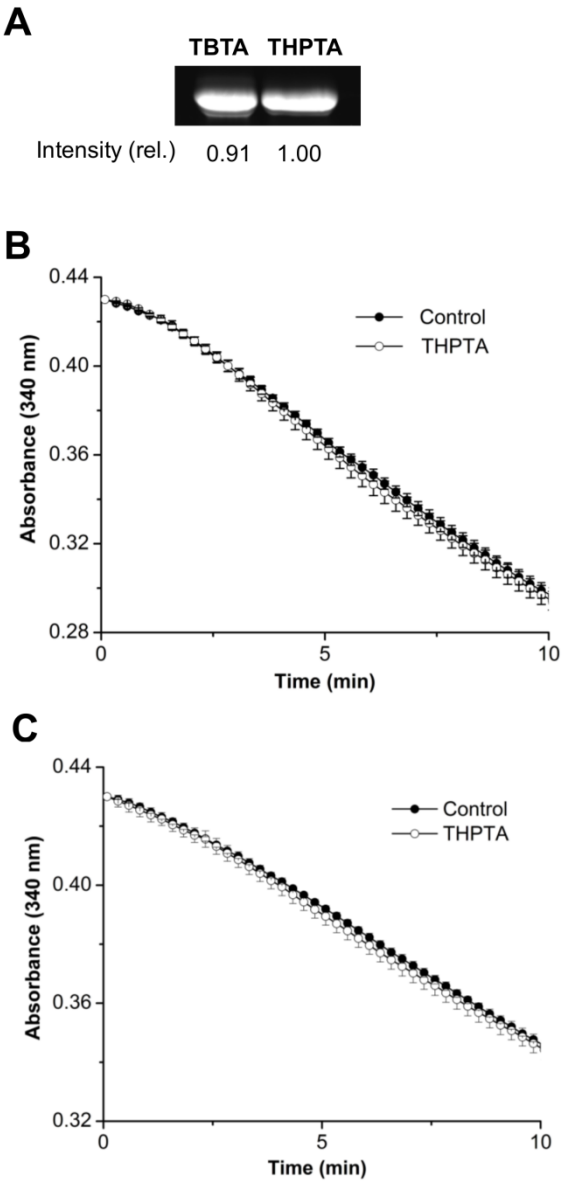

Figure 4.6. THPTA-assisted CuAAC reaction and its effect on the enzymatic activity. (A) In-gel fluorescence of reaction products from TBTA- and THPTA-assisted dye labeling via CuAAC. The mDHFR-pEthF (30 μM) was reacted at 25 ^{o}C for 15 min with sulforhodamine-azide (60 μM) in the presence of 1 mM $CuSO_4$, 1 mM TBTA, 2 mM ascorbate in a phosphate buffer (pH 8.0) containing 30% (v/v) DMSO or in the presence of 1 mM $CuSO_4$, 1 mM THPTA, 2 mM ascorbate in a DMSO-free phosphate buffer (pH 8.0). (B) Effect of THPTA incubation on

activity of the mDHFR-43pEthF. After incubation of 30 μM protein with (open circle) or without (close circle) 1 mM THPTA in 10 μl of DMSO-free phosphate buffer (pH 8.0) for 15 min at 25 ^{o}C, the mixture was diluted 36-fold with the assay buffer for activity assay. Error bars represent standard errors (n=3). (C) Effect of THPTA incubation on activity of the mDHFR-179pEthF (n=3).

4.3.3. CuAAC with the Water-soluble Chelating Ligand, THPTA

To circumvent the use of DMSO, which is essential for TBTA-mediated CuAAC but adversely affects the enzymatic activity, we employed a water-soluble ligand, THPTA (Figure 4.1B) [58], and tested its performance as a chelating ligand. At the same concentration of 1 mM, the CuAAC labeling using THPTA in an aqueous buffer was as efficient as the labeling using TBTA in 30% DMSO (Figure 4.6A). In contrast to the TBTA/DMSO system, the catalytic activity of the mDHFR-43pEthF was preserved after incubation with THPTA in DMSO-free reaction buffer (Figure 4.6B). The same condition could be applied to the other mDHFR mutant bearing a site-specifically incorporated pEthF at the 179th position (mDHFR-179pEthF) without harming its native activity (Figure 4.6C). These results indicate that THPTA is a relevant substitute for TBTA as a chelating ligand for enzyme bioconjugation via CuAAC.

4.3.4. Optimization of CuAAC with Various Reductants

We explored relative compatibility of various reductants in terms of their effects on the reaction rate and enzymatic activity of the mDHFR-43pEthF. We chose three reductants: tris(2-carboxyethyl)phosphine (TCEP), a highly water-soluble and relatively stable reductant [103]; ascorbate, a commonly used reductant in CuAAC but known to produce unwanted byproducts at certain conditions [192,193]; and dithiothreitol (DTT), a strong reductant whose use in CuAAC was recently reported [194]. First, we labeled the mDHFR-43pEthF with a fluorogenic probe, azidocoumarin, using each reductant, and measured the time-course evolution of fluorescence on a microwell plate (Figure 4.7A). Ascorbate was shown to be the most powerful reductant, completing the reaction within 15 min with the highest fluorescence at the plateau. The yield was substantially lower when TCEP or DTT was used. Moreover, the time to completion was

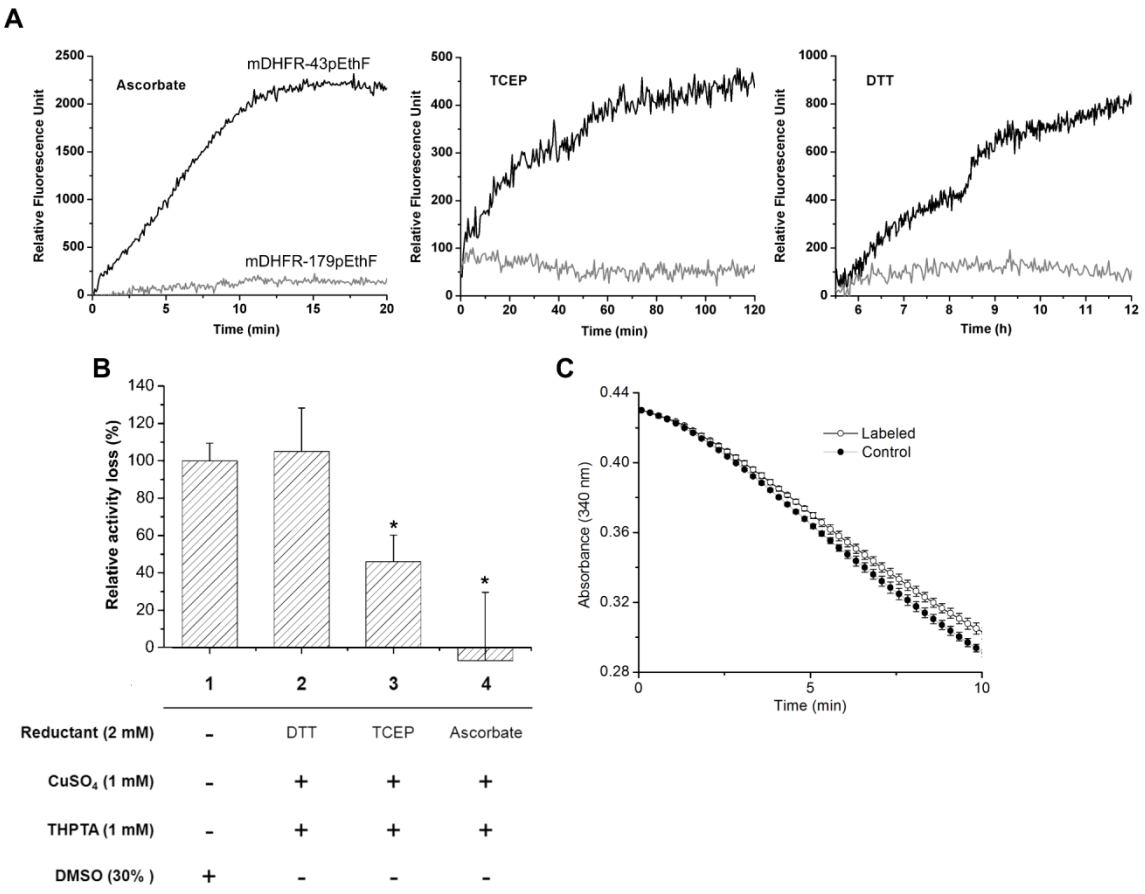

Figure 4.7. Effect of various reductants on CuAAC reaction rates and activities of the mDHFR-43pEthF and the mDHFR-179pEthF. (A) Time course of CuAAC reactions initiated by ascorbate, TCEP, and DTT. Reactions were performed at 25 ^{o}C by adding 2 mM reductant to a phosphate-buffered (pH 8.0) mixture containing 30 µM of the mDHFR-43pEthF (black) or the mDHFR-179pEthF (gray), 60 µM of azidocoumarin, 1 mM of $CuSO_4$, 1 mM THPTA. Fluorescence evolution was recorded at λex = 400 nm and λem = 470 nm. (B) Relative loss of enzymatic activity after incubation with various CuAAC systems in the absence of azidocoumarin (1-4). Incubation times were 15 min for system 1 and 4, 12 h for system 2, and 2 h for system 3. Activity losses were normalized to that in system 1. Error bars represent standard errors (n=3). Two-sided Student's t-tests were applied to the data (*$P < 0.05$). (C) Effect of ascorbate-driven dye labeling of the mDHFR-43pEthF on the enzymatic activity.

prolonged to more than 2 h and 12 h, respectively. Even though ascorbate seemed most effective in reaction kinetics, it does not necessarily mean that it has the best compatibility. To assess an adverse effect of CuAAC systems on enzymatic activity, the mDHFR-43pEthF was incubated with each system, and then subjected to the activity assay (Figure 4.7B). Incubation times were set at 15 min, 2 h, and 12 h, i.e. time for reaction completion, for ascorbate-, TCEP- and DTT-reducing system, respectively. Considering large differences in the conjugation yield observed among the reaction conditions, the mDHFR was incubated in the absence of any dye. The relative reduction in activity was greatest in DTT-reducing system, followed by TCEP- and ascorbate-reducing system. Compared to the activity loss observed after incubation with 30% DMSO, TCEP- and ascorbate-reducing system showed significantly ($P < 0.05$) lower reduction in activity. Notably, the mDHFR-43pEthF treated with ascorbate did not cause any significant reduction in activity compared to that of the untreated control. These results suggest that short incubation with the reductant is critical to minimize adverse effects on enzymatic activity during CuAAC reaction, and ascorbate is the best reductant for CuAAC with an enzyme because it rapidly completes the reaction with high yield. Using the optimized CuAAC condition, an azidocoumarin was conjugated to the mDHFR-43pEthF and then the activity of the dye-conjugated mDHFR-43pEthF was compared to that of the untreated mDHFR-43pEthF (Figure 3.7C). As expected, the dye-conjugation led to only a minor reduction in activity, which is likely due to the slight structural perturbation resulting from the hydrophobic nature of the conjugated dye.

Previously, complete loss of enzymatic activity was observed upon bioconjugation of the E. coli DHFR variant in which the CuAAC reaction was initiated by adding a reactive Cu(I) complex, and incubated overnight [59]. Our optimization study therefore suggests a remedy to

implement enzyme-compatible bioconjugation through in situ reduction of Cu(II) by an appropriate choice of a reductant allowing minimum contact time between the enzyme and reactive species while achieving maximum conjugation yield. Although the CuAAC condition described here works well for the mDHFR, it should, however, be applied to other enzymes with caution. Considering the physicochemical diversity of enzymes and varying sensitivities to reaction components (such as strong inhibition of formate dehydrogenase by copper ions), the CuAAC conditions may need to be slightly adjusted for each enzyme. In case of enzymes greatly inhibited by copper ions, copper-free azide-alkyne cycloaddition can be employed. The construction of multifunctional enzyme complex via copper-free azide-alkyne cycloaddition was performed leading to varying retained activities between 17 to 91% [195].

4.3.5. Comparison of Conjugation Yields at Different Conjugation Sites

To compare the conjugation yield depending on the solvent accessibility of a conjugation site, the phenylalanine at position 179 (F179) was also targeted for pEthF incorporation generating the mDHFR-179pEthF (Figure 4.2B and Figure 4.3B). Contrary to the solvent accessible valine at position 43 (accessibility score: 0.44), a phenyl ring of F179 is buried inside the protein and has a very low solvent accessibility (accessibility score: 0.10). Under the same condition used for the mDHFR-43pEthF, fluorescence signals of the mDHFR-179pEthF were substantially lower than those of the mDHFR-43pEthF (Figure 4.7A). These results strongly indicate that the solvent accessibility of a conjugation site correlates to the conjugation yield. When the crystal structure of a target protein is available, the solvent accessibility prediction tools including ASA-View program can be used to identify a suitable conjugation site leading to a high conjugation yield. Furthermore, in the absence of the protein crystal structure, monitoring

fluorogenic dye conjugation at each site is expected to be used to estimate the solvent accessibility. It should be also noted that the mDHFR-179pEthF had only 30% of original activity of the mDHFR (data not shown). It is known that F179 stabilizes the tertiary structure of the mDHFR by forming a parallel ring stacking interaction with Y33 [196]. Its substitution by even a structurally similar phenylalanine analog appears to adversely impact the aromatic ring stacking, thereby resulting in distorted conformation for ligand binding.

4.3.6. Immobilization of the mDHFR-43pEthF by Site-specific Biotinylation

As a practical application of site-specific bioconjugation of an enzyme, we investigated if the mDHFR can be immobilized onto a streptavidin-coated plate through CuAAC-mediated biotinylation without loss of activity. Biotin-PEG3-azide, a hybrid reagent having a flexible and hydrophilic PEG spacer and a chemoselective azide group, was conjugated to the mDHFR-43pEthF in the ascorbate-reducing system to yield the biotinylated mDHFR (mDHFR-43biotin). Little change in enzymatic activity was observed for the mDHFR-43biotin in comparison to the mDHFR-43pEthF, suggesting that biotinylation as well as the reaction system did not seriously interfere with the activity (Figure 4.8A). Biotinylation was found to be high yielding as revealed by the dye-conjugation analysis (Figure 4.9). The inertness of the mDHFR-43biotin towards the CuAAC-driven dye labeling indicated that most of the accessible pEthFs had been occupied by the biotin. To implement enzyme immobilization through biotin-streptavidin interaction, the streptavidin-coated plate was incubated with the mDHFR-43biotin, in parallel with the mDHFR-43pEthF as a control (Figure 4.8B). Positive enzymatic activity was detected over course of time, but not in the control. To our knowledge, this is the first example of enzyme immobilization through site-specific NNAA incorporation and the CuAAC with retained catalytic activity, and

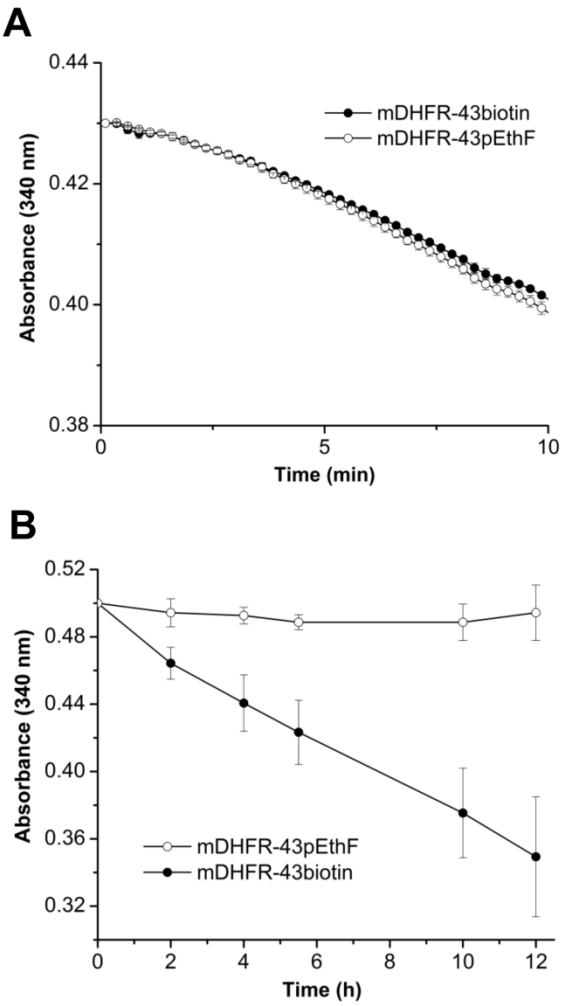

Figure 4.8. Enzymatic activity of the mDHFR after site-specific biotinylation and immobilization. (A) Activity of the mDHFR-43biotin versus the mDHFR-43pEthF. Error bars represent standard errors (n=3). (B) Activity of the immobilized mDHFR-43biotin. Streptavidin-coated wells were incubated with 50 µL of the mDHFR-43biotin and the mDHFR-43pEthF at 1mg/mL, separately, for 30 min at RT. After washing, the enzymatic reaction was initiated at 25 ^{o}C by adding 200 µL of assay buffer, and monitored by spectrometry. Error bars represent standard errors (n=3).

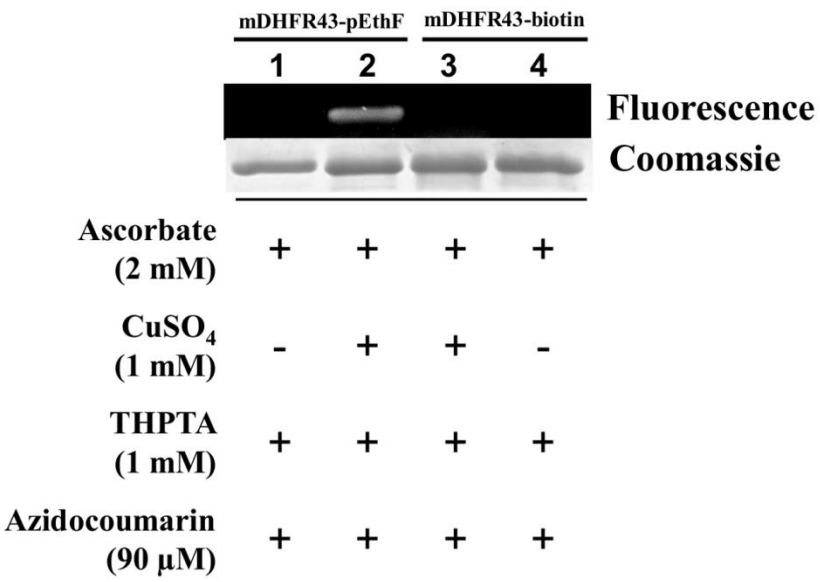

Figure 4.9. Dye labeling of the mDHFR-43pEthF and the mDHFR-43biotin through CuAAC. As a control, reactions were also performed in the absence of copper ions. Protein concentration was 30 µM. Reactions were stopped by 10 mM EDTA at 15 min after initiation, and analyzed by SDS-PAGE. The gel was illuminated by UV (365 nm) to excite the fluorophore (Fluorescence panel), and then stained with Coomassie Brilliant Blue (Coomassie panel) to visualize proteins.

opens the possibility to fabricate highly sensitive biosensors and biocatalysts attributed by controlled orientation and homogeneous chemistry.

4.4. Conclusion

Site-specific bioconjugation of an enzyme was achieved by introducing a NNAA with an alkyne functional group into a specific site followed by conjugation via CuAAC. The effects of CuAAC conditions on catalytic activity were evaluated using the mDHFR as a model enzyme. Under the optimized CuAAC condition utilizing THPTA and ascorbate as a ligand and a reductant, respectively, the fluorescence dye and biotin were efficiently conjugated to the mDHFR in a site-specific manner with retention of substantial catalytic activity. It was also found that the solvent accessibility of a conjugation site correlates to a conjugation yield indicating that the choice of conjugation site is critical to ensure efficient bioconjugation. Furthermore, the site-specific biotinylation was successfully used to immobilize the mDHFR on a streptavidin-coated plate through a highly specific and tight biotin-streptavidin binding, which would enable a spatially controlled and maximally functional enzyme immobilization.

Chapter 5: Substrate Channeling Induced by Controlled Orientation of Active Sites in a Multienzyme Cascade Reaction

Multistep cascade reactions in nature maximize the reaction efficiency by co-assembling related enzymes. Such organization facilitates the processing of intermediates by downstream enzymes, a phenomenon called substrate channeling. It has been reported that the catalytic efficiency of engineered multienzyme cascades can be improved by reducing interenzyme distance which inversely accelerates the substrate channeling. Both intuitively and computationally, the channeling effect is expected to be stronger if orientation of the active sites of enzymes is controlled for direct transfer of intermediates. Here we organized the multienzyme structure in which active sites are oriented towards or away from each other with an aim of understanding the effect of active site positioning on the substrate channeling. The fructose-reducing reaction by mannitol dehydrogenase was coupled to the formate-oxidizing reaction by formate dehydrogenase which supplies the cofactor NADH, an intermediate, to mannitol dehydrogenase. Site-specific incorporation of a non-natural amino acid and chemoselective bioconjugation were employed to control the spatial geometry of those enzymes. The study revealed that the face-to-face orientation of active sites showed 4-fold higher reaction efficiency in comparison to the opposite configuration where active sites were directed away from each other.

5.1. Background and Motivation

The substrate channeling is a molecular mechanism found in nature that facilitates the multienzyme cascade reactions by restricting intermediates to be channeled between active sites of two or more separate enzymes [197–199]. Except for a few exceptions in which intermediates are funneled through a physical tunnel connecting two separate active sites in a single enzyme [200,201], multiple enzymes involved in related cellular processes are co-localized or clustered to form large non-covalent assemblies, thereby increasing local concentrations of intermediates in active sites [202–205]. Engineering efforts to build enzymatic cascade reactions with enhanced catalytic efficiency have proven enzyme clustering as a successful approach. A variety of spatially organized multienzyme structures have been developed using nucleic acids and proteins as a scaffold [206–209]. The computer-aided model has quantitatively demonstrated the benefits of rapid processing of intermediates by co-localized enzymes [210].

Emergence of nano-scale scaffolding technologies has enabled the creation of complex but organized multienzyme structures with spatial programmability, which was previously addressable only by molecular simulation. By systematically varying the distance between enzymes that perform a cascade reaction, Fu *et al* found that the multienzyme reaction displayed the distance-dependent efficiency with greatly improved activity being observed when the enzymes were closely spaced as little as 10 nm [43,211]. DNA-conjugated enzymes were used to organize the enzyme pair onto a DNA origami tile with controlled interenzyme position and spacing. However, due to non-specific conjugation chemistry, the active site of each enzyme was randomly oriented, hindering investigation of enzyme orientation effect on the activity at a fixed interenzyme distance. Importance of enzyme orientation in the multienzyme system has been

described by computational simulations [212], but not demonstrated experimentally due to technical hurdles to control the enzyme orientation relative to a paired enzyme [213].

Here we described catalytic benefits from controlled orientation of active sites of enzymes interacting in a cascade reaction. To this end, we utilized site-specific incorporation of a reactive non-natural amino acid (NNAA) into enzymes followed by bioorthogonal enzyme-to-enzyme conjugation. Enzyme conjugates thus generated were identical in every aspect except for the active site orientation towards each other which depends on the NNAA incorporation site, enabling the evaluation of catalytic efficiency affected by the positioning of active sites. We hypothesized that inward-facing active sites are more likely to facilitate the substrate channeling between enzymes than outward-facing active sites.

NNAAs containing a bioorthogonal group can be incorporated into a target protein during the ribosomal synthesis via expanded genetic codes and engineered translational machinery (Hoesl MG 2896). One of great advantages lies in that a single or multiple NNAA(s) can be introduced to any defined position in the primary sequence of a protein, thereby permitting site-specific and chemoselective bioconjugation with other functional entities [165].

Two bioorthogonal reactions are employed in this study. In strain-promoted azide-alkyne cycloaddition (SPAAC), an internal alkyne activated by ring-strained energy drives cycloaddition with an azide at room temperature without any catalyst. Even though SPAAC is kinetically slower and lacks regioselectivity in comparison to copper-catalyzed azide-alkyne cycloaddition, its high degree of bioorthogonality without harmful byproducts is suitable for protein conjugation involving chemically sensitive enzymes and metal-binding proteins [113,214]. Inverse electron demand Diels-Alder (IEDDA) reaction recently joined the chemistry pool for site-specific protein conjugation [215,216]. IEDDA reaction is the cycloaddition

between tetrazine and strained alkene, and has the fastest reaction rate in a range of 10^4-10^5 $M^{-1}s^{-1}$, thus proceeding efficiently even at low concentrations. Also, it features the orthogonality towards SPAAC [22] as well as natural functionalities in proteins, enabling one-pot dual labeling [23].

5.2. Materials and Methods

5.2.1. Materials

p-Azido-L-phenylalanine (AZF) was purchased from Chem-Impex International (Wood Dale, IL) and dissolved in 0.2 M NaOH to make 100 mM stock solution. Ni-NTA agarose and pQE80 plasmid were obtained from Qiagen (Valencia, CA). Vivaspin centrifugal concentrators with a MWCO of 50 kDa were purchased from Sartorius Corporation (Bohemia, NY). ZipTip with C18 resin was purchased from Millipore Corporation (Billerica, MA). Sequencing grade modified trypsin was obtained from Promega Corporation (Madison, WI). DBCO- PEG_4-carboxyrhodamine, DBCO-amine, TCO-NHS, and tetrazine-DBCO were purchased from Bioconjugate Technology Company (Scottsdale, AZ). PD-10 desalting column and Superdex 200 size exclusion column were obtained from GE Health care (Piscataway, NJ). UNO Q1 anion exchange column and Biologic DuoFlow chromatography system were obtained from Bio-Rad (Hercules, CA). All chemicals were obtained from Sigma-Aldrich Corporation (St. Louis, MO) unless otherwise stated.

5.2.2. Plasmid construction and bacterial strains

A plasmid pEVOL-pAzF [7] encoding an AZF-specific engineered pair of tyrosyl-tRNA synthetase/amber suppressor tRNA derived from *Methanococcus jannaschii* (Plasmid ID: 31186)

was obtained from Addgene (Cambridge, MA), and used without modification. The *fdh* gene, which encodes formate dehydrogenase originating from *Thiobacillus* sp. KNK65MA, with an additional C-terminal histidine sequence was PCR amplified using pET-23b(+) plasmid containing the *fdh* gene as a template [217], and subcloned into pQE80 plasmid to generate pQE80-FDH. Site-directed mutagenic PCR was performed with pQE80-FDH as a template to replace tryptophan codon at positions 172 or valine codon at position 237 with amber codons (UAG), yielding pQE80-FDH-W172amb and pQE80-FDH-V237amb, respectively. *E. coli* TOP10 was transformed with pQE80-FDH for expression of the wild-type FDH (FDH-WT), affording TOP10 [FDH]. As an expression host for AZF-incorporated FDH (FDH-W172AZF or FDH-V237AZF), genomically engineered *E. coli* C321.ΔA.exp [5] was obtained from Addgene (ID: 49018), and co-transformed with pEVOL-pAzF and pQE80-FDH-W172amb or pQE80-FDH-V237amb, affording C321.ΔA.exp [FDH-W172amb] and C321.ΔA.exp [FDH-V237amb], respectively. The *mdh* gene, which encodes mannitol-2-dehydrogenase originating from *Pseudomonas fluorescens* [218], with an additional C-terminal histidine sequence was synthesized by GenScript (Piscataway, NJ), and subcloned into pQE80 to generate pQE80-MDH. Site-directed mutagenic PCR was performed with pQE80-MDH as a template to replace valine codon at positions 273 or 419 with amber codons (UAG), yielding pQE80-MDH-V273amb and pQE80-FDH-V419amb, respectively. *E. coli* TOP10 was transformed with pQE80-MDH for expression of the wild-type MDH (MDH-WT), affording TOP10 [MDH]. As an expression host for AZF-incorporated MDH (MDH-V273AZF or MDH-V419AZF), genomically engineered *E. coli* C321.ΔA.exp [5] was obtained from Addgene (ID: 49018), and co-transformed with pEVOL-pAzF and pQE80-MDH-V273amb or pQE80-MDH-V419amb, affording C321.ΔA.exp

[MDH-V273amb] and C321.ΔA.exp [MDH-V419amb], respectively. All DNA cloning in this study were performed by the restriction-free cloning technique [129].

5.2.3. Site-specific incorporation of AZF into FDH or MDH

The saturated culture of C321.ΔA.exp [FDH-W172amb, FDH-V237amb, MDH-V273amb, or MDH-V419amb] was inoculated into fresh 2×YT medium containing 100 μg/mL ampicillin and 35 μg/mL chloramphenicol at 1:100 (v/v) dilution, and was subjected to vigorous shaking (220 rpm) at 37 °C. When the OD_{600} of 0.5 was reached, AZF solution was added to a final concentration of 1 mM. After 10 min, temperature was shifted to 30 °C, and protein expression was induced by 1 mM IPTG and 0.2% (w/v) *L*-(+)-arabinose. Cells were harvested after 12 h, and pelleted by centrifugation at 5,000 rpm for 10 min before storage at -20°C. To extract and purify FDH or MDH containing AZF, cell pellets were resuspended with the lysis buffer consisting of 50 mM sodium phosphate (pH 7.5), 0.3 M NaCl, 10 mM imidazole, 1 mg/mL lysozyme, DNase, RNase, and protease inhibitor cocktail, and mixed by rotation at 37°C for 1 h followed by at 4°C for 2 h. After centrifugation at 11,000 rpm for 30 min, the clear supernatant was recovered, mixed with Ni-NTA agarose for 1 h, and then washed with the washing buffer consisting of 50 mM sodium phosphate (pH 7.5), 0.3 M NaCl, and 20 mM imidazole on a gravity-flow column to remove impurities. Proteins were eluted by the elution buffer consisting of 50 mM sodium phosphate (pH 7.5), 0.3 M NaCl, and 250 mM imidazole, and then buffer-exchanged to a storage buffer (PBS, pH 7.2) by a PD-10 column. Expression and purification of FDH-WT or MDH-WT were performed similarly except that TOP10 [FDH or MDH] was used as an expression host without adding AZF and *L*-(+)-arabinose.

5.2.4. MALDI-TOF Mass Spectrometry

Proteins in the storage buffer at 0.5 mg/mL were digested with trypsin at 37℃ overnight, and then desalted on a ZipTip C18 according to the manufacturer's protocol. Purified tryptic digests mixed with DHB matrix (20 mg/mL of 2,5-dihydroxybenzoic acid and 2 mg/mL of *L*-(−)-fucose dissolved in 10% ethanol) at 1:1 (v/v) were subjected to mass characterization by Microflex MALDI-TOF M/S (Bruker Corporation, Billerica, MA).

5.2.5. Dye Labeling by SPAAC

FDH-WT, FDH-W172AZF, and FDH-V237AZF at 30 μM in the storage buffer were separately reacted with DBCO- PEG_4-carboxyrhodamine at 100 μM at RT for 2 h, and then loaded onto SDS-PAGE to measure in-gel fluorescence in a BioSpectrum imaging system (UVP, Upland, CA). Upon illumination at λ_{ex} = 480 nm, the emitted light above 510 nm was captured. MDH-WT and variants were treated in the same way for dye labeling by SPAAC.

5.2.6. Enzymatic Activity Assay

Enzymatic reduction of NAD^+ to NADH by FDH-WT and its variants was measured by monitoring increase in $A_{340\ nm}$. The reaction was initiated by mixing 5 μL of 100 nM FDH or variants with 195 μL of the assay buffer consisting of 50 mM formate and various concentrations of NAD^+ in PBS. Enzymatic oxidation of NADH to NAD^+ by MDH-WT and its variants was measured by monitoring decrease in $A_{340\ nm}$. The reaction was initiated by mixing 5 μL of 50 nM MDH or variants with 195 μL of the assay buffer consisting of 50 mM fructose and various concentrations of NADH in PBS. All measurements were made in triplicate at 25˚C in a standard 96-well plate on the Synergy™ four multimode microplate reader (BioTek, Winooski, VT).

Reaction rates were determined by dividing the slope (min^{-1}, OD change in the first one minute upon initiation) by the molar extinction coefficient of NADH, 6,220 $M^{-1}cm^{-1}$, and the path length of 0.52 cm.

5.2.7. Synthesis of FDH-MDH Conjugates

First, a bifunctional chemical linker was conjugated to FDH or MDH variants by SPAAC. Second, FDH-linker was conjugated to MDH-linker by IEDDA reaction. Lastly, the FDH-MDH conjugate was purified by two-step liquid chromatography. Detailed conditions are as follows. FDH-W172AZF or FDH-V237AZF was mixed with 4 molar excess of tetrazine-DBCO in PBS containing 5% (v/v) DMSO, and reacted at RT for 7 h. To remove residual tetrazine-DBCO, the reaction mixture was desalted on a PD-10 column, and buffered-exchanged to 20 mM bis-tris buffered at pH 6.0. MDH-V273AZF or MDH-V419AZF was similarly treated except that TCO-DBCO was used instead of tetrazine-DBCO. TCO-DBCO was prepared beforehand by mixing 2.5 molar excess of TCO-NHS with DBCO-amine in DMSO at RT for 1.5 h and adding excess tris (pH 9.0) to quench. FDH-W172Tetrazine and MDH-V273TCO thus obtained were mixed at 1:1 molar stoichiometry, concentrated to a total protein concentration of 5 mg/mL, and reacted at RT for 2 h. The reaction mixture was directly loaded onto an anion exchange column, UNO Q1, pre-equilibrated with 20 mM bis-tris (pH 6.0), and resolved by applying a salt gradient. A fraction containing FDH-MDH conjugate and unreacted MDH-V237TCO was collected and resolved on a size exclusion column, Superdex 200, to isolate pure FDH-MDH. The conjugation of FDH-V237Tetrazine to MDH-V419TCO was performed in the same way.

5.2.8. Characterization of FDH-MDH Conjugates

Molar compositions of FDH-MDH conjugates were analyzed by band intensities seen in SDS-PAGE using Image J-a public domain Java image processing program. Based upon an approximate 1:1 molar ratio of FDH monomer conjugated to MDH and unconjugated FDH monomer, the molar absorption coefficient of FDH-MDH conjugates was calculated using ExPASy ProtParam tool (http://web.expasy.org/protparam/) with input amino acid sequence obtained by combining MDH sequence (MDH monomer) and FDH sequence twice (FDH dimer), and found to be 180,030 $M^{-1}cm^{-1}$ which was used to determine concentrations of FDH-MDH conjugates throughout the enzymatic assays in this study.

5.2.9. Measurement of Cascade Enzymatic Reactions

The control assay that measures an initial rate of NADH production by FDH activity in the absence of NADH consumption by MDH activity was initiated by mixing 10 µL of FDH-MDH conjugate at an appropriate molar concentration with 190 µL of the assay buffer (50 mM sodium formate, 200 µM NAD^+ in PBS) which lacks D-fructose–a substrate of MDH. The cascade assay that measures an initial rate of NADH production in the presence of NADH consumption by MDH activity was initiated by mixing 10 µL of FDH-MDH conjugate at an appropriate molar concentration with 190 µL of the assay buffer (50 mM sodium formate, 50 mM D-fructose, 200 µM NAD^+ in PBS) which includes D-fructose. Increase in absorbance at 340 nm of the control assay or the cascade assay was monitored upon initiation to obtain NADH production rates defined as the OD change in the first one minute: ΔA_{cont} $[min^{-1}]$ for the control assay and ΔA_{casc} $[min^{-1}]$ for the cascade assay. All measurements were made in triplicate at 25˚C in a standard 96-well plate on the Synergy™ four multimode microplate reader. Similarly, both

the control and the cascade assay were performed with free enzymes instead of FDH-MDH conjugates; one molar equivalent of dimeric FDH (FDH-W172AZF or FDH-V237AZF) mixed with monomeric MDH (MDH-V273AZF or MDH-V419AZF) corresponding to the molar composition of FDH-MDH conjugates, i.e. dimeric FDH conjugated to a single monomeric MDH.

5.3. Results and Discussion

5.3.1. Design and Genetic Incorporation of AZF into FDH and MDH

Formate dehydrogenase (FDH) used in this study originates from *Thiobacillus* and is a homodimer with a molecular mass of 45 kDa for the single subunit [217,219]. Its dimeric form in solution was confirmed by size exclusion chromatography (Fig. 5.1). FDH is a NAD-dependent oxidoreductase that has 10^3 times higher activity of formate oxidation to carbon dioxide than the reverse reaction [217], and has been commonly used for enzymatic regeneration of nicotinamide cofactors [220]. Mannitol dehydrogenase (MDH) used in this study originates from *Pseudomonas fluorescens* and is a monomer with a molecular mass of 55 kDa as revealed in size exclusion chromatography (Fig. 5.1). MDH is a NAD-dependent oxidoreductase that has 2.5 times higher activity of D-fructose reduction to D-mannitol than the reverse reaction [218], and can be utilized for biocatalytic production of D-mannitol through coupling with cofactor regeneration system employing FDH or glucose dehydrogenase [221,222]. In the cascade reaction consisting of FDH coupled to MDH (Scheme 5.1), NADH is regenerated by FDH-mediated formate oxidation, thereby continuously fueling MDH-mediated D-mannitol production. In the presence of excess substrates for both enzymes, i.e. formate and D-fructose, the transfer of NADH between the active sites of FDH and MDH governs the overall cascade

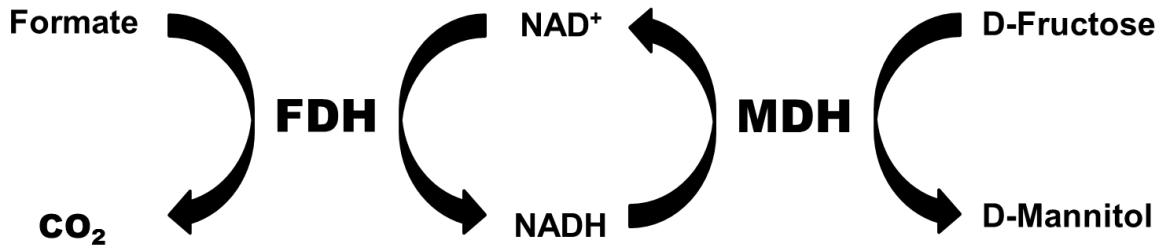

Scheme 5.1. The enzymatic cofactor regeneration system coupled with the D-mannitol synthetic reaction.

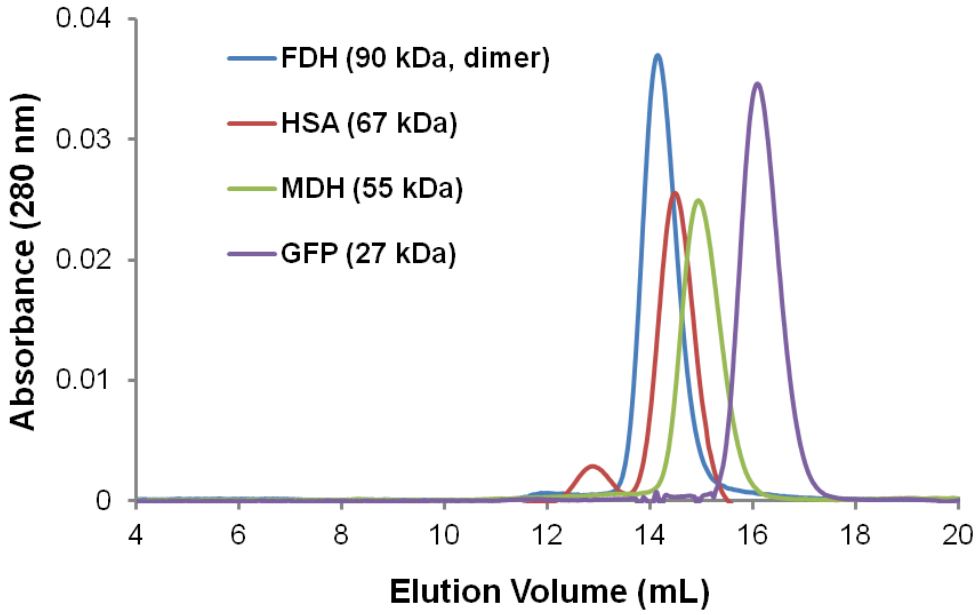

Figure 5.1. Elution profiles of FDH, MDH, and standard proteins in size exclusion chromatography.

reaction efficiency. By inducing a high local concentration of NADH between the active sites rather than its diffusion to the bulk solution, i.e. substrate channeling, enhancements in specific pathway flux and product titers are anticipated.

To investigate the reduced interenzyme distance on NADH pathway as well as the effect of relative orientation of the active sites, we designed FDH-MDH conjugates tethered by a chemical linker with defined orientation of each enzyme. Depending on the site of NNAA incorporation and the structure of a chemical linker, spatial orientation of a single protein towards a specific target as well as the geometry of macroscopic protein assembly can be controlled and customized in accordance with user-defined preferences [149,223–227]. As a first step to construct FDH-MDH conjugates with their active sites in face-to-face (FF) or back-to-back orientation (BB), two surface-exposed positions in FDH and MDH, respectively, were chosen for site-specific genetic incorporation of AZF. Valine at position 237 (V237) is located in proximity to the NAD^+ binding site of FDH and on the same side (Fig. 5.2A, left), while tryptophan at position 172 (W172) is on the opposite side away from the binding site (Fig. 5.2A, right). As a conjugation partner of FDH-V237AZF to generate the FF conjugate, V419 close to and on the same side with the NADH binding site of MDH was substituted by AZF to obtain MDH-V419AZF (Fig. 5.2B, left). The BB conjugate was produced by conjugating FDH-W172AZF to MDH-V273AZF in which the mutation site is positioned on the opposite side of the NADH binding site (Fig. 5.2B, right).

Site-specific genetic incorporation of AZF was performed by introduction of an amber codon into predetermined sites of FDH- and MDH-encoding genes. Host cells were induced to express an orthogonal pair of amber suppressor tRNA and tRNA synthetase as well as the target gene in the presence of AZF in culture medium. Purified FDH and MDH variants were analyzed

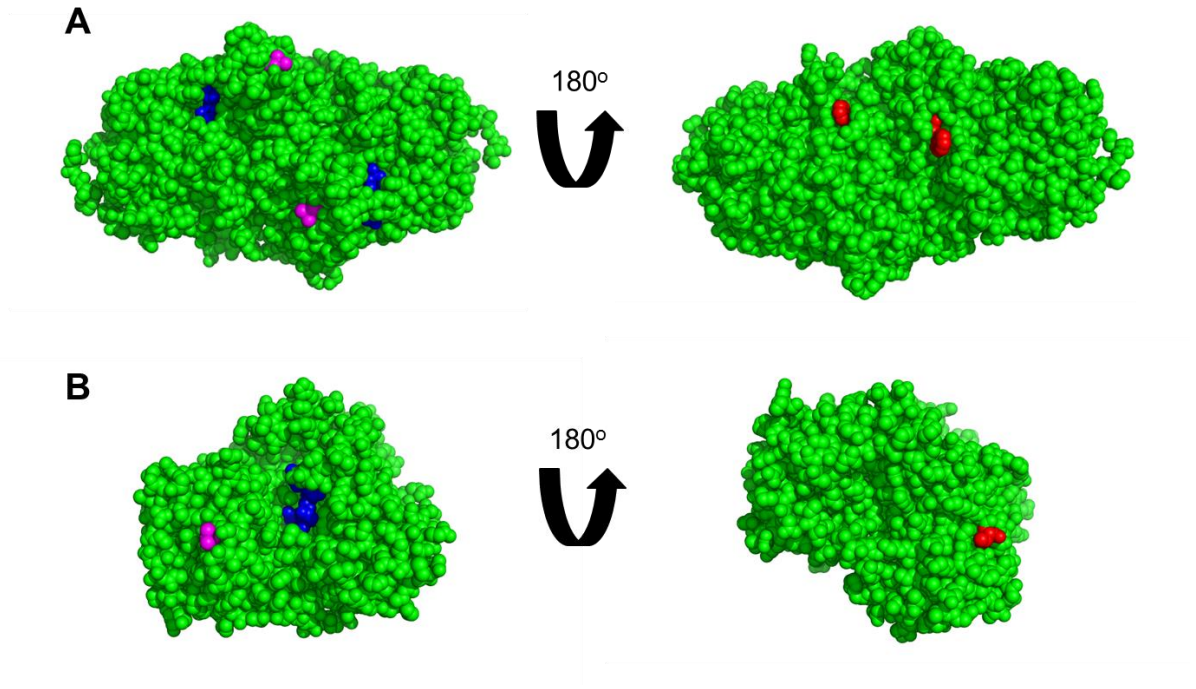

Figure 5.2. Graphical representation of three dimensional structures of FDH and MDH. (A) A dimeric form of FDH in complex with a cofactor (blue) was derived from Protein Data Bank (PDB ID: 3WR5). AZF incorporation sites, V237 and W172, are highlighted in magenta and red, respectively. (B) MDH in complex with a cofactor (blue) was derived from Protein Data Bank (PDB ID: 1LJ8). AZF incorporation sites, V419 and V273, are highlighted in magenta and red, respectively. Images on the right side in (A) and (B) were obtained by rotating images on the left side by 180 ^{o} about the horizontal axis, respectively.

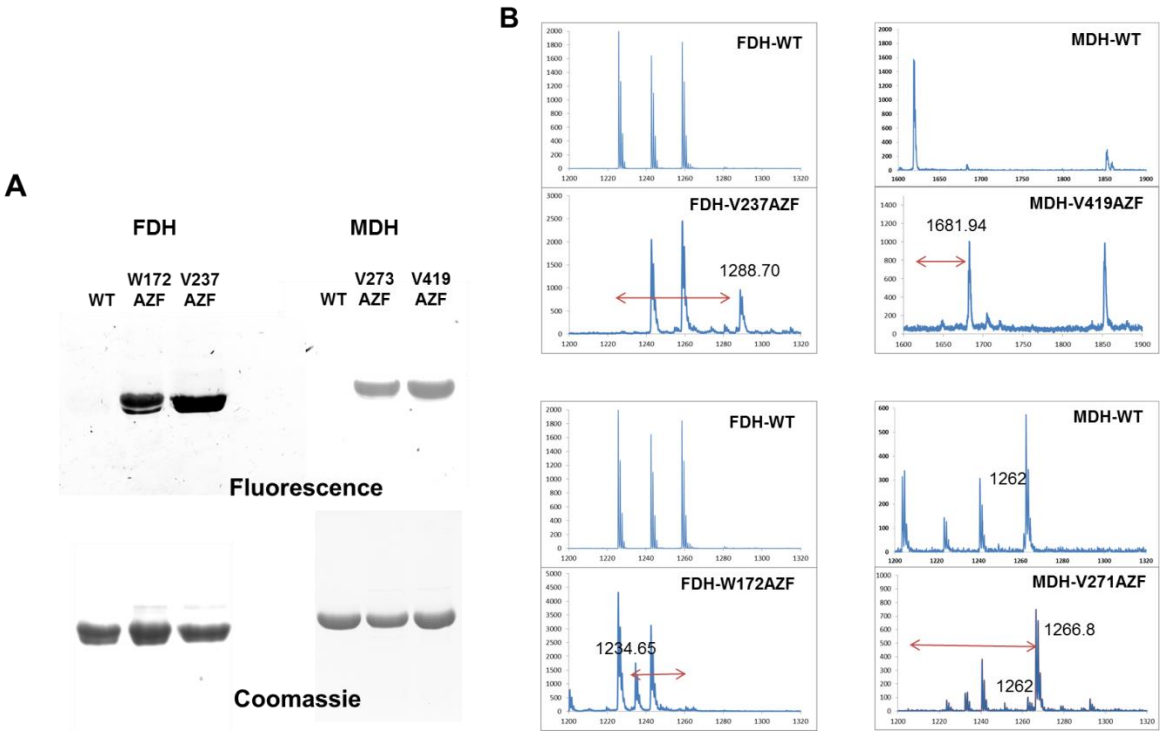

Figure 5.3. Validation of bioorthogonal reactivity and site-specificity of genetically incorporated AZF. (A) In-gel fluorescence analyses of FDH, MDH, and their variants upon completion of reactions with DBCO-PEG_4-carboxyrhodamine. The gel was subjected to UV (390 nm) irradiation to excite the fluorophore (fluorescence panel), and then stained with Coomassie blue (Coomassie panel) to visualize proteins. (B) MALDI-TOF MS analyses of trypsin-digested FDH, MDH, and their variants.

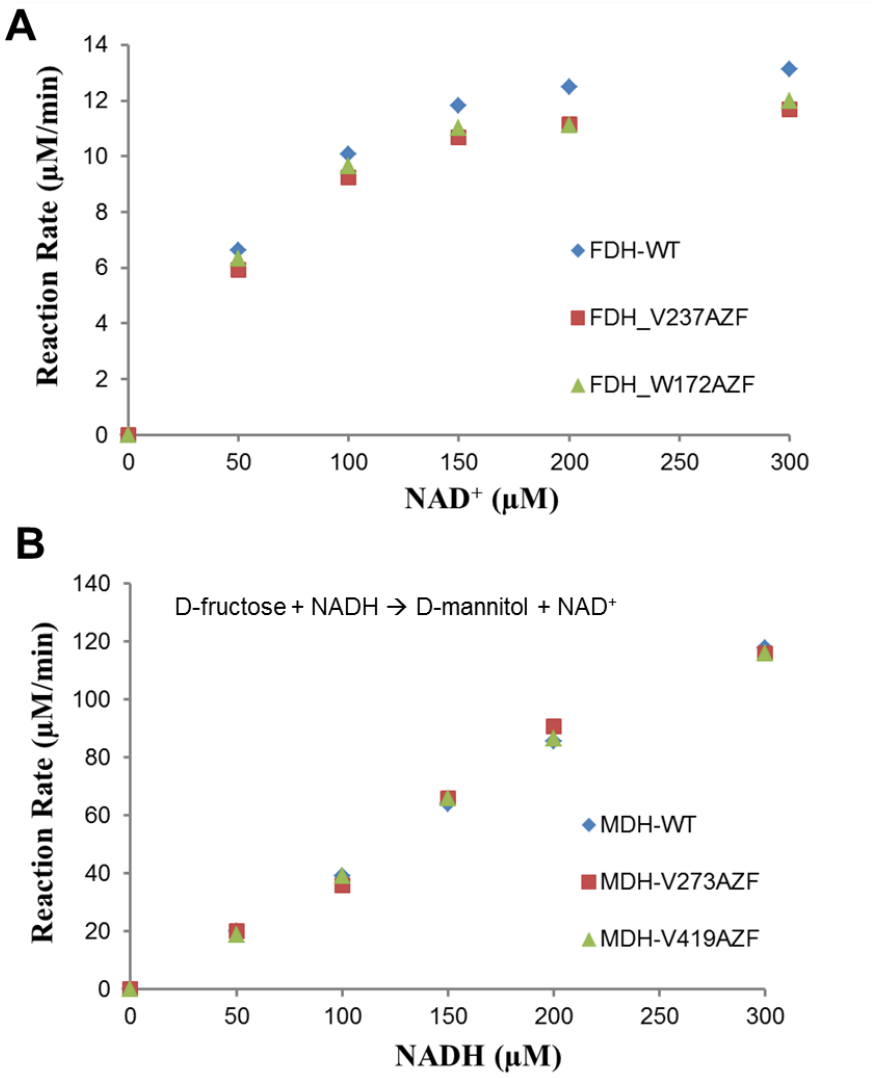

Figure 5.4. Enzymatic activity of FDH, MDH, and their variants. (A) Rates of formate oxidation to carbon dioxide by FDH and variants were plotted as a function of various concentration of a cofactor. (B) Rates of D-fructose reduction to D-mannitol by MDH and variants were plotted as a function of various concentration of a cofactor.

Table 5.1. Kinetic parameters of FDH and its variants

	k_{cat} (min^{-1})	K_m (μM)
FDH-WT	1.60 ± 0.04	67.36 ± 5.51
FDH-W172AZF	1.42 ± 0.04	57.49 ± 5.76
FDH-V237AZF	1.42 ± 0.03	64.38 ± 5.72

Values ± standard errors of regression obtained by fitting to the Michaelis-Menten equation

by dye labeling and mass spectrometry to verify the bioorthogonal reactivity of AZF and site-specific incorporation, respectively. In contrast to the wild-type FDH and MDH showing no fluorescence when mixed with a DBCO-functionalized dye, variants exhibited a strong fluorescence (Fig. 5.3A). MALDI-TOF mass spectra of tryptic fragments demonstrated high fidelity incorporation of AZF in response to the amber codons at position 172 and 237 for FDH and position 273 and 419 for MDH, respectively (Fig. 5.3B). To investigate the effect of AZF incorporation on the native activity, variants were subjected to the enzymatic activity assay in comparison to the wild type (Fig. 5.4). Whereas MDH variants retained enzymatic activities comparable to that of the wild-type, AZF incorporation into FDH slightly affected the native activity, leading to < 15% reduction in k_{cat} and K_m (Table 5.1).

5.3.2. Synthesis and Characterization of FDH-MDH Conjugates

Since genetically encoded AZFs have been found to be situated at chemically well-defined positions and have bioorthogonal reactivity towards SPAAC, variants of FDH and MDH provide a modular platform to generate FDH-MDH conjugates, through a chemical linker, with spatial orientation of the active site of FDH controlled with respective to that of MDH. For instance, FDH-V237AZF, when conjugated to MDH-V419AZF, could have its cofactor binding site directly facing towards the cofactor binding site of MDH-V419AZF, i.e. the face-to-face (FF) conjugate, because both AZFs are positioned on the same side with the active site of respective enzymes (Fig. 5.5A). Likewise, the back-to-back (BB) conjugate whose two active sites are directed away from each other could be produced by connecting FDH-W172AZF with MDH-V273AZF (Fig. 5.5B). To synthesize the FF conjugate, FDH-V237AZF was reacted with a DBCO-tetrazine linker (Fig. 5.6A) through SPAAC, and desalted to remove residual linkers.

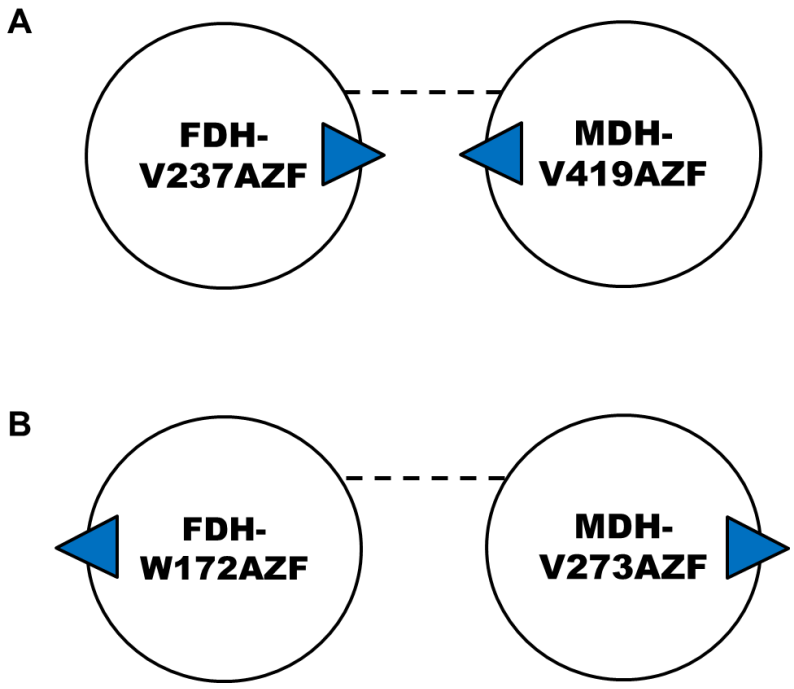

Figure 5.5. Simplified diagrams of FDH-MDH conjugates with different orientation of the active sites. (A) The face-to-face (FF) conjugate generated by linking FDH-V237AZF to MDH-V419AZF via a chemical linker (dotted line) has its cofactor binding sites (triangle) directed inward. (B) The back-to-back (BB) conjugate generated by linking FDH-W172AZF to MDH-V273AZF has its cofactor binding sites directed outward.

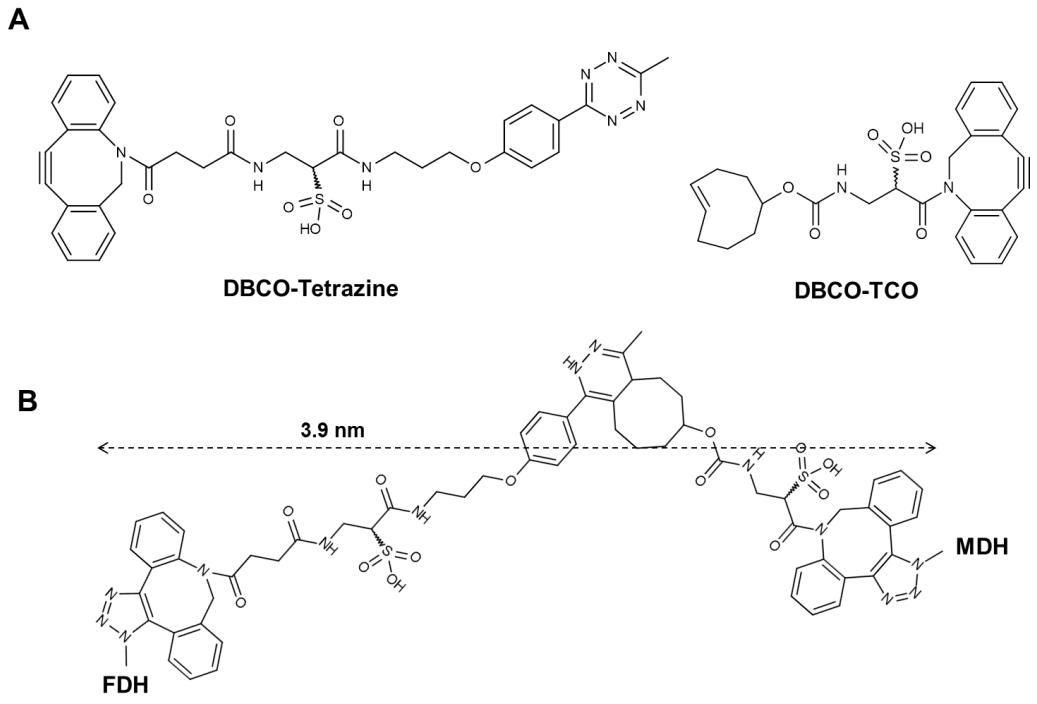

Figure 5.6. Chemical formulae of linkers. (A) DBCO-derivatized bifunctional linkers. The DBCO group reacts with AZF incorporated into FDH and MDH via SPAAC. The conjugation between FDH and MDH is mediated by IEDDA between tetrazine and TCO. (B) The entire structure and length of the conjugated chemical linker bridging FDH and MDH.

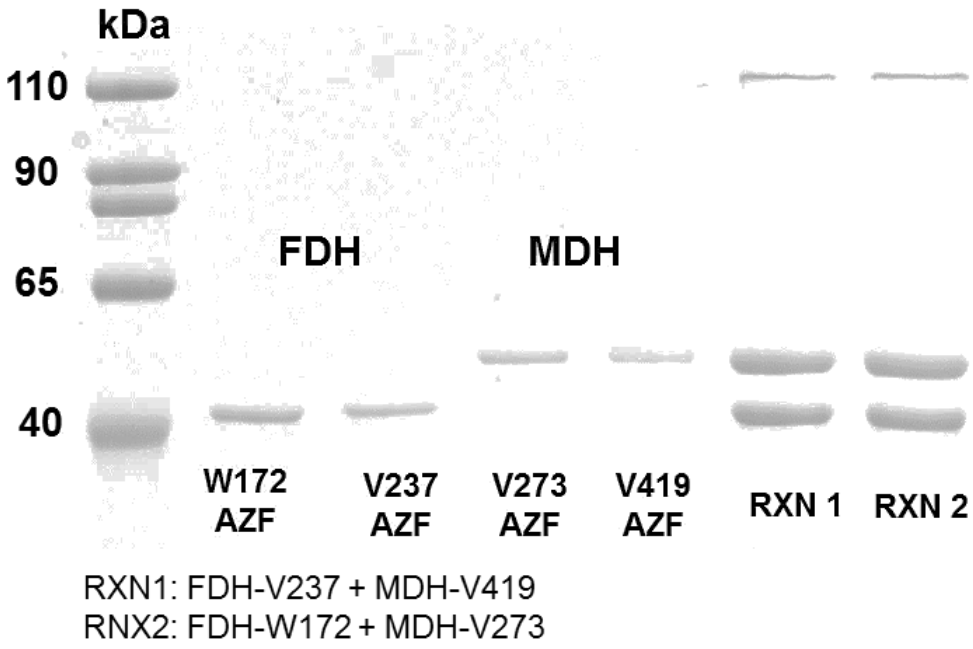

Figure 5.7. SDS-PAGE analysis of FDH and MDH variants and conjugation reaction mixtures.

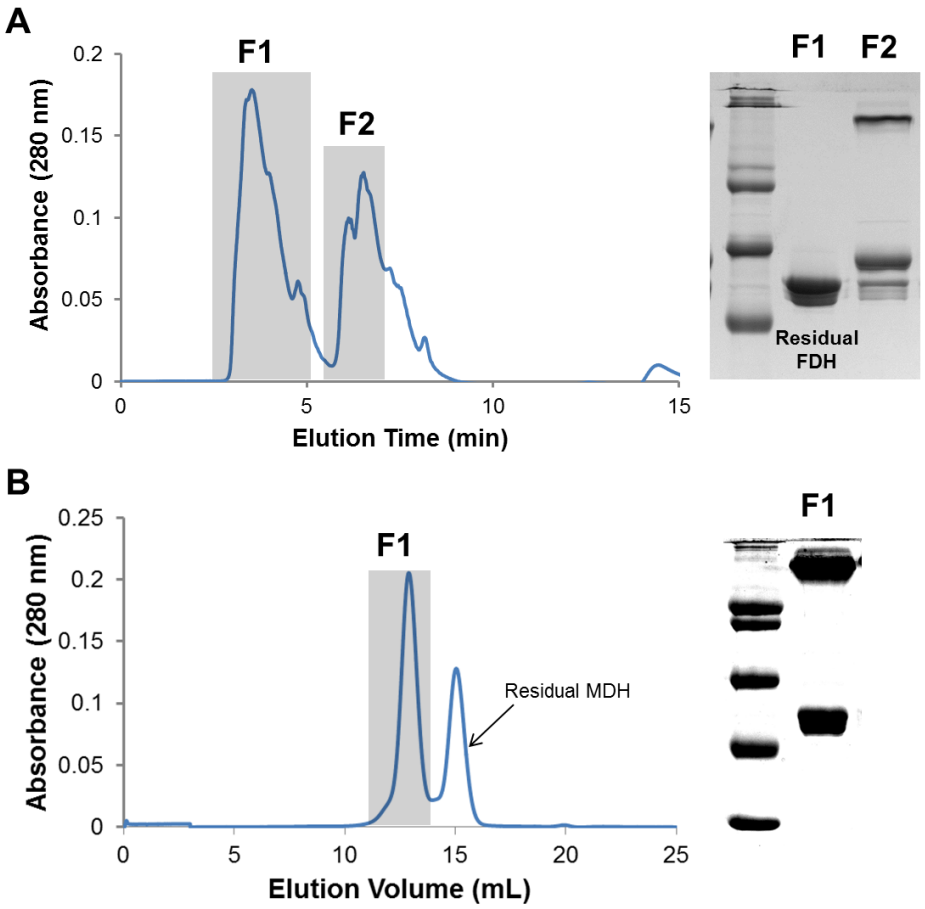

Figure 5.8. Purification of FDH-MDH conjugates by liquid chromatography. (A) Anion exchange chromatography to eliminate residual FDHs (F1) and SDS-PAGE of eluting fractions. (B) Size exclusion chromatography to isolate the pure FDH-MDH conjugate (F1) from residual MDHs.

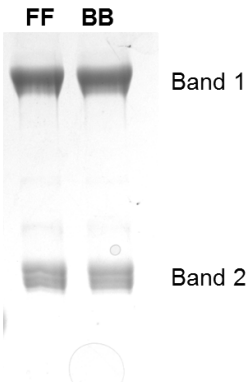

Conjugate	Band	Identity	Intensity (a.u.)	MW (Da)	Mole (Intensity / MW, a.u.)	Mole (rel.)
FDH237-MDH419 (FF)	1	FDH monomer conjugated to MDH	16,995	100,160	0.17	1.0
	2	FDH monomer	8,557	44,780	0.19	1.1
FDH172-MDH273 (BB)	1	FDH monomer conjugated to MDH	15,740	100,160	0.16	1.0
	2	FDH monomer	8,223	44,780	0.18	1.1

Figure 5.9. Densitometric determination of molar stoichiometry of FDH-MDH conjugates. The gel image was analyzed by Image J to estimate band intensity. The MW of the monomeric FDH-MDH conjugate (100,160 Da) is the sum of MWs of monomeric FDH and MDH. Molar composition of each species was calculated assuming that the band intensity is proportional to the amount of protein,

Likewise, MDH-V419AZF was conjugated to a DBCO-TCO linker (Fig. 5.6A). A second bioorthogonal reaction, IEDDA, was carried out to covalently link FDH-V237Tetrazine to MDH-V419TCO. In SDS-PAGE analysis of the reaction mixture, a new single band slightly larger than the 110 kDa-standard protein was detected, indicating the TCO group specifically reacted with the tetrazine functionality (Fig. 5.7). To isolate the FF conjugate from the mixture, the two-step liquid chromatography was performed. In the first step involving an anion exchanger, unreacted FDH-V237Tetrazine was removed from the mixture (Fig. 5.8A). Then, the size exclusion chromatography successfully separated the FF conjugate from unreacted MDH-V419TCO (Fig. 5.8B). The same reaction schemes and purification methods were applied to obtain the BB conjugate which resulted from the crosslink between FDH-W172AZF and MDH-V273AZF. It should be noted that the distance between FDH and MDH upon conjugation, i.e. length of the entire chemical bridge (Fig. 5.6B), was approximately 3.9 nm.

A molar composition of FDH-MDH conjugates could be either one or two MDH molecule(s) per FDH dimer since FDH has two AZFs due to its dimeric form. The elution profile of conjugates observed in the size exclusion chromatogram was a single peak in symmetry, indicating the conjugate was mostly composed of a single species (Fig. 5.8B). To quantitatively evaluate the molar composition, both FF and BB conjugates were subjected to a standard SDS-PAGE and Coomassie staining (Fig. 5.9). In contrast to the unconjugated FDH monomer, the FDH monomer conjugated to MDH exhibited significantly retarded migration at 110 kDa which corresponded to a calculated molecular mass of the conjugate including chemical linkers. Densitometric analyses of the molar composition revealed two molar equivalents of FDH monomer with respect to MDH, demonstrating that most functional dimeric FDHs were conjugated to MDHs in 1-to-1 stoichiometry.

5.3.3. Effect of active site orientation on the cofactor processing in enzyme cascade reactions

In the presence of a saturating amount of the substrate, an efficient transfer of NADH generated by FDH to the active site of MDH is a rate-limiting step in the enzymatic production of D-mannitol (Scheme 5.1). In order to investigate the importance of active site orientation on NADH transport, the rate of NADH production was measured in two reaction conditions by monitoring the absorbance change at 340 nm per minute (ΔA) (Scheme 5.2). In the control assay, the enzymatic reaction was performed in solution devoid of D-fructose to measure the NADH production rate solely by FDH (ΔA_{cont}). In the cascade assay, the same reaction was performed in the presence of all components required for the coupled reaction to measure the NADH production rate affected by the NADH consumption by MDH (ΔA_{casc}). If the processing of NADH by MDH becomes faster due to its increased local concentration contributed by favorable orientation of the active site, it would lead to decrease in ΔA_{casc} (Equation 1).

ΔA_{cont} [min^{-1}] = Rate of NADH production by FDH

ΔA_{casc} [min^{-1}] = Rate of NADH production by FDH – Rate of NADH consumption by MDH (1)

The efficiency of the NADH processing, ε, is defined as

$$\varepsilon = \frac{\text{Rate of NADH consumption by MDH}}{\text{Rate of NADH production by FDH}} = \frac{\text{Rate of NADH production by FDH} - \Delta\text{Acasc}}{\text{Rate of NADH production by FDH}} = 1 - \frac{\Delta\text{Acasc}}{\Delta\text{Acont}} \quad (2)$$

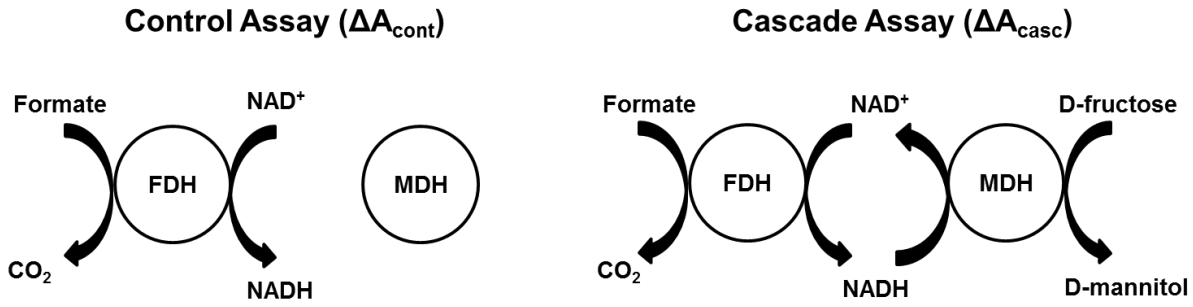

Scheme 5.2. Measurement of the NADH production in the absence or presence of MDH activity.

Both FF and BB conjugates were independently subjected to two assays in Scheme 5.2 at various protein concentrations to obtain ε as a function of protein concentration (Fig. 5.10). At higher protein concentration above 80 nM, the effect of the active site orientation was negligible with both conjugates exhibiting the same efficiencies. This indicates that NADH diffused to the bulk phase fast enough to be processed by nearby conjugates or NADH production is too strong to observe the NADH consumption by MDH. However, at lower concentrations below 40 nM possibly favorable for NADH channeling within a single conjugate, the FF conjugate showed higher efficiency in the NADH processing than the BB conjugate, suggesting that a higher local concentration of NADH available for MDH was attained when the active sites of FDH and MDH were oriented towards each other. In contrast to the BB conjugate in which NADH from the active site of FDH directed towards the bulk phase is more likely to escape the channeling by free diffusion, the FF conjugate would have more NADHs in a confined area between the active site of each enzyme, thereby increasing the chance of NADH processing by MDH.

Next, to investigate if the NADH channeling relative to random Brownian diffusion of NADH provides enhanced reaction efficiency, the same kinetic assays (Scheme 5.2) were performed using unconjugated dimeric FDH and MDH mixed at 1-to-1 molar ratio to calculate ε which was then compared with those of the conjugates to yield the relative efficiency defined as follows:

$$\varepsilon_{rel} = \varepsilon_{FF} / \varepsilon_{free} \text{ or } \varepsilon_{BB} / \varepsilon_{free}$$

Both conjugates were found to have ε_{rel} values more than 1.0 at all concentrations, indicating the cascade reaction efficiency higher than that of free enzymes (Fig. 5.11). Consistent ε_{rel} for

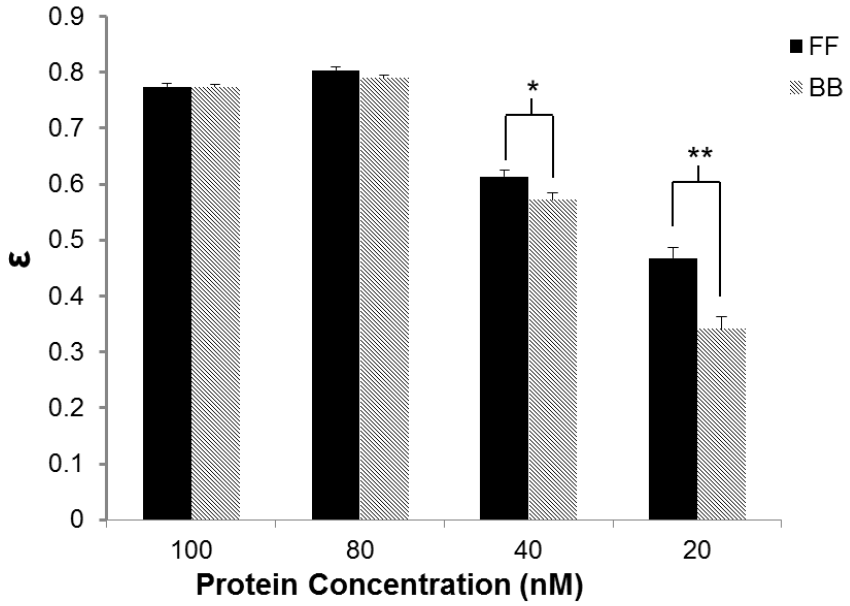

Figure 5.10. The efficiency of the enzymatic cascade reaction as a function of protein concentration. Both ΔA_{cont} and ΔA_{casc} were measured separately for each conjugate, and used to calculate the efficiency (ε) based upon Equation 2 (*$p < 0.1$ and **$p < 0.05$). Error bars represent standard error of the mean with $n = 3$.

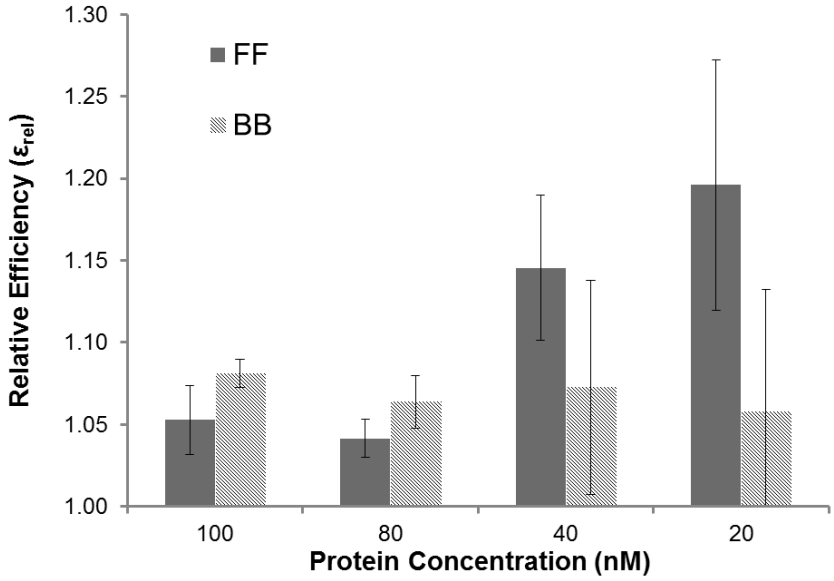

Figure 5.11. Cascade reaction efficiency of FDH-MDH conjugates relative to unconjugated FDH and MDH. The relative efficiency, ε_{rel}, was obtained by dividing ε of each conjugate by that of free enzymes at different protein concentrations. The stoichiometry of dimeric FDH and MDH in free enzyme reactions is 1:1 which corresponds to the molar composition of FDH-MDH conjugates. Error bars represent standard error of the mean with n = 3.

the BB conjugate regardless of protein concentration suggests that improvement in the efficiency originated not significantly from the NADH channeling, but from close interenzyme distance between FDH and MDH as much as the length of the chemical bridge which increased the chance that MDH could recognize freely diffusing NADHs from the covalently partnered FDH rather than FDHs of nearby conjugates. Remarkably, the FF conjugate exhibited increasing ε_{rel} inversely proportional to protein concentrations. Contrary to the BB conjugate, the channeling effect became pronounced when the concentration of the FF conjugate is less than 40 nM, yielding 4 fold higher ε_{rel} than the BB conjugate at 20 nM. These results are consistent with the channeling effect exerted by the FF conjugate at low concentrations in Fig. 5.10, and support the notion that controlled orientation of active sites favorable for the channeling, in particular the face-to-face configuration, restricts free diffusion of intermediates in the bulk solution but accelerates their processing by the downstream enzyme. Nevertheless, overlapping error bars, especially at protein concentrations of 20 and 40 nM, may weaken statistical significance of difference in ε_{rel}. More reliable propensity of induced substrate channeling as a function of protein concentrations would be obtained by increasing the number of observations since the standard error of the mean is inversely proportional to the square root of the sample size.

5.4. Conclusion

Technical challenges in engineering an orientation-controlled multienzyme complex have been overcome by employing the genetic incorporation of NNAAs and chemoselective bioconjugation chemistries. By covalently coupling two enzymes, FDH and MDH, with geometric control and well-defined interenzyme spacing, we could quantitatively measure enhancement in activity of the cascade reaction depending on the active site orientation. The

substrate channeling was shown to be effective when the active site was aligned front to front, leading to increased catalytic efficiency. In contrast, when each enzyme was rotated by 180^{o}, the cascade reaction could not benefit from the channeling effect. Overall, our results, for the first time, provide the experimental evidence of the orientation-dependent acceleration of the multienzyme reaction, and may aid the design of spatially organized multienzyme structures with improved performance.

Chapter 6: Conclusion

6.1. Project Objectives and Summary

Bioconjugation is a popular approach to confer new functions on proteins, but often results in heterogeneous end-products and loss of a native protein function due to non-specific conjugation chemistry. To address this issue, we combined the site-specific NNAA incorporation technique and bioorthogonal chemistries to afford a chemically well-defined and homogeneous conjugate with new add-on functions. **Four research objectives undertaken in the dissertation research were completed:**

1. **Site-specific conjugation of fatty acid to superfolder green fluorescent protein to prolong *in vivo* half-life through albumin binding**
2. **Site-specific albumination of a therapeutic protein with multi-subunit to prolong activity *in vivo***

I demonstrated that a single palmitic acid or human serum albumin could be site-specifically attached to a genetically incorporated NNAA(s) via bioorthogonal chemistries, and act as serum half-life extenders.

3. **Site-specific immobilization of a murine dihydrofolate reductase by copper(I)-catalyzed azide-alkyne cycloaddition with retained enzymatic activity**
4. **Substrate channeling induced by controlled orientation of active sites in a multienzyme cascade reaction**

The mDHFR was immobilized onto a solid support with native activity and controlled orientation, resulting in increased catalytic efficiency. In addition, the multienzyme conjugate was organized to have their active sites aligned towards one another, inducing the substrate channeling and the enhancement in cascade reaction efficiency.

Significance of this dissertation research lies in the fact that attachment of a functional molecule to any defined site of proteins was shown to yield a highly homogeneous bifunctional conjugate with both of their respective functions unharmed. Any existing techniques and molecular design can hardly produce protein conjugates similar with those presented in this dissertation research without the combinatorial approach using the genetic incorporation of NNAAs and site-specific bioconjugation.

The expanded set of genetic codes and increasing number of orthogonal sets of tRNA/aaRS for bioorthogonally reactive NNAAs have significantly enlarged the scope of protein engineering by allowing site-specific, homogeneous, and multiple conjugation of functional molecules to recombinant proteins at desired positions. Such outstanding benefits of NNAA-mediated bioconjugation of proteins have brought about practical applications in biotherapeutics and biocatalysis. With continuing development of bioorthogonal reactions and biosynthetic tools for incorporation of customized NNAAs into proteins in diverse cells and organisms, the NNAA-mediated site-specific bioconjugation is a valuable tool to address challenges in protein engineering.

6.2. Future Work and Suggestions

6.2.1. Multifunctional Therapeutic Proteins

Recent developments have reported site-specific incorporation of two different NNAAs in response to distinct expanded genetic codes, enabling site-specific modification of proteins at multiple positions using mutually orthogonal reactions. For example, two different fluorescent dyes have been shown to be attached to a model protein containing genetically incorporated azide and tetrazine group through SPAAC and IEDDA, respectively. The molecular design presented in Research Objectives I and II can be further expanded to employ incorporation of multiple NNAAs. This implies that a therapeutic protein could be derivatized with another functional entity other than a half-life extender. For instance, anti-cancer therapeutic enzyme, asparaginase, could be conjugated to a tumor-targeting moiety such as an aptamer in addition to a fatty acid using SPAAC and IEDDA. The multiconjugate, aptamer- asparaginase-fatty acid, is likely to exhibit tumor-specificity as well as extended *in vivo* half-life, greatly increasing therapeutic potency with reduced side-effects and injection frequency.

6.2.2. Self-assembled multienzyme clusters

Cellular metabolism is mediated by numerous enzymatic reactions in harmony. Sequential biocatalytic events where an intermediate produced from one enzyme is processed by the other enzyme have evolved in nature. Substrate channeling and enzyme clusters in living cells provided a basis for bioinspired design of synthetic enzyme complexes for biotechnological applications. A number of approaches to co-localize enzymes have been reported, including genetic fusion and co-immobilization / encapsulation via covalent linkage or physical interaction. Self-assembled enzyme complexes driven by oligonucleotide or protein scaffolds are the current trend, providing modular control over cascade reactions. Despite advancing technology for assembling enzymes in an orderly and programmable manner, orientation control of each

enzyme towards optimal substrate channeling has yet to be explored. This is because conventional bioconjugation lacks specificity to modify an enzyme at predetermined residues. Although still in infancy, NNAA-mediated bioconjugation is envisioned to have high potential for construction of substrate-channeled reaction cascade more complex than the two-enzyme system presented in this dissertation study. For example, following the orientation-controlled conjugation of a self-assembling block copolymer to cascade enzymes bearing genetically incorporated NNAA(s), a stimulus-triggered self-assembly would allow the construction of enzyme clusters or nanoparticles in which multi-step cascade reactions occur with substrate channeling and native catalytic activity at their maxima.

References

[1] I. Kwon, S.I. Lim, Non-Natural Amino Acids for Protein Engineering and New Protein Chemistries, Macromol. Chem. Phys. 214 (2013) 1295–1301.

[2] A. Takasu, S. Kondo, A. Ito, Y. Furukawa, M. Higuchi, T. Kinoshita, et al., Artificial extracellular matrix proteins containing phenylalanine analogues biosynthesized in bacteria using T7 expression system and the PEGylation, Biomacromolecules. 12 (2011) 3444–3452.

[3] S. Zheng, I. Kwon, Manipulation of enzyme properties by noncanonical amino acid incorporation, Biotechnol J. 7 (2012) 47–60.

[4] S. Zheng, I. Kwon, Controlling enzyme inhibition using an expanded set of genetically encoded amino acids, Biotechnol Bioeng. 110 (2013) 2361–2370.

[5] M.J. Lajoie, A.J. Rovner, D.B. Goodman, H.-R. Aerni, A.D. Haimovich, G. Kuznetsov, et al., Genomically recoded organisms expand biological functions., Science. 342 (2013) 357–60.

[6] C.C. Liu, P.G. Schultz, Adding new chemistries to the genetic code, Annu. Rev. Biochem. 79 (2010) 413–444.

[7] J.W. Chin, S.W. Santoro, A.B. Martin, D.S. King, L. Wang, P.G. Schultz, Addition of p-azido-L-phenylalanine to the genetic code of Escherichia coli, J Am Chem Soc. 124 (2002) 9026–9027.

[8] D.B. Johnson, J. Xu, Z. Shen, J.K. Takimoto, M.D. Schultz, R.J. Schmitz, et al., RF1 knockout allows ribosomal incorporation of unnatural amino acids at multiple sites, Nat Chem Biol. 7 (2011) 779–786.

[9] T. Mukai, A. Hayashi, F. Iraha, A. Sato, K. Ohtake, S. Yokoyama, et al., Codon reassignment in the Escherichia coli genetic code, Nucleic Acids Res. 38 (2010) 8188–8195.

[10] V. V Rostovtsev, L.G. Green, V. V Fokin, K.B. Sharpless, A stepwise huisgen cycloaddition process: copper(I)-catalyzed regioselective “ligation” of azides and terminal alkynes, Angew Chem Int Ed Engl. 41 (2002) 2596–2599.

[11] C.W. Tornoe, C. Christensen, M. Meldal, Peptidotriazoles on solid phase: [1,2,3]-triazoles by regiospecific copper(i)-catalyzed 1,3-dipolar cycloadditions of terminal alkynes to azides, J Org Chem. 67 (2002) 3057–3064.

[12] E. Lallana, R. Riguera, E. Fernandez-Megia, Reliable and efficient procedures for the conjugation of biomolecules through Huisgen azide-alkyne cycloadditions, Angew Chem Int Ed Engl. 50 (2011) 8794–8804.

[13] J.M. Baskin, J.A. Prescher, S.T. Laughlin, N.J. Agard, P. V Chang, I.A. Miller, et al., Copper-free click chemistry for dynamic in vivo imaging, Proc Natl Acad Sci U S A. 104 (2007) 16793–16797.

[14] M.T. Taylor, M.L. Blackman, O. Dmitrenko, J.M. Fox, Design and synthesis of highly reactive dienophiles for the tetrazine-trans-cyclooctene ligation., J. Am. Chem. Soc. 133 (2011) 9646–9.

[15] M. Vrabel, P. Kölle, K.M. Brunner, M.J. Gattner, V. López-Carrillo, R. de Vivie-Riedle, et al., Norbornenes in inverse electron-demand Diels-Alder reactions., Chemistry. 19 (2013) 13309–12.

[16] D.M. Patterson, L.A. Nazarova, B. Xie, D.N. Kamber, J.A. Prescher, Functionalized cyclopropenes as bioorthogonal chemical reporters., J. Am. Chem. Soc. 134 (2012) 18638–43.

[17] J.B. Haun, N.K. Devaraj, S.A. Hilderbrand, H. Lee, R. Weissleder, Bioorthogonal chemistry amplifies nanoparticle binding and enhances the sensitivity of cell detection., Nat. Nanotechnol. 5 (2010) 660–5.

[18] K. Lang, L. Davis, J. Torres-Kolbus, C. Chou, A. Deiters, J.W. Chin, Genetically encoded norbornene directs site-specific cellular protein labelling via a rapid bioorthogonal reaction., Nat. Chem. 4 (2012) 298–304.

[19] D.S. Liu, A. Tangpeerachaikul, R. Selvaraj, M.T. Taylor, J.M. Fox, A.Y. Ting, Diels-Alder cycloaddition for fluorophore targeting to specific proteins inside living cells., J. Am. Chem. Soc. 134 (2012) 792–5.

[20] K. Lang, L. Davis, S. Wallace, M. Mahesh, D.J. Cox, M.L. Blackman, et al., Genetic Encoding of bicyclononynes and trans-cyclooctenes for site-specific protein labeling in vitro and in live mammalian cells via rapid fluorogenic Diels-Alder reactions., J. Am. Chem. Soc. 134 (2012) 10317–20.

[21] J.W. Chin, Expanding and reprogramming the genetic code of cells and animals., Annu. Rev. Biochem. 83 (2014) 379–408.

[22] M.R. Karver, R. Weissleder, S.A. Hilderbrand, Bioorthogonal reaction pairs enable simultaneous, selective, multi-target imaging., Angew. Chem. Int. Ed. Engl. 51 (2012) 920–2.

[23] A. Sachdeva, K. Wang, T. Elliott, J.W. Chin, Concerted, rapid, quantitative, and site-specific dual labeling of proteins., J. Am. Chem. Soc. 136 (2014) 7785–8.

[24] L.I. Willems, N. Li, B.I. Florea, M. Ruben, G.A. van der Marel, H.S. Overkleeft, Triple bioorthogonal ligation strategy for simultaneous labeling of multiple enzymatic activities., Angew. Chem. Int. Ed. Engl. 51 (2012) 4431–4.

[25] N. Stephanopoulos, M.B. Francis, Choosing an effective protein bioconjugation strategy, Nat Chem Biol. 7 (2011) 876–884.

[26] A.J. de Graaf, M. Kooijman, W.E. Hennink, E. Mastrobattista, Nonnatural amino acids for site-specific protein conjugation, Bioconjug Chem. 20 (2009) 1281–1295.

[27] E. Steen Redeker, D.T. Ta, D. Cortens, B. Billen, W. Guedens, P. Adriaensens, Protein engineering for directed immobilization, Bioconjug Chem. 24 (2013) 1761–1777.

[28] F. Kratz, B. Elsadek, Clinical impact of serum proteins on drug delivery, J Control Release. 161 (2012) 429–445.

[29] C. Chaudhury, C.L. Brooks, D.C. Carter, J.M. Robinson, C.L. Anderson, Albumin binding to FcRn: distinct from the FcRn-IgG interaction, Biochemistry. 45 (2006) 4983–4990.

[30] C. Chaudhury, S. Mehnaz, J.M. Robinson, W.L. Hayton, D.K. Pearl, D.C. Roopenian, et al., The major histocompatibility complex-related Fc receptor for IgG (FcRn) binds albumin and prolongs its lifespan, J. Exp. Med. 197 (2003) 315–322.

[31] S. Havelund, A. Plum, U. Ribel, I. Jonassen, A. Volund, J. Markussen, et al., The mechanism of protraction of insulin detemir, a long-acting, acylated analog of human insulin, Pharm. Res. 21 (2004) 1498–1504.

[32] L.B. Knudsen, P.F. Nielsen, P.O. Huusfeldt, N.L. Johansen, K. Madsen, F.Z. Pedersen, et al., Potent derivatives of glucagon-like peptide-1 with pharmacokinetic properties suitable for once daily administration, J. Med. Chem. 43 (2000) 1664–1669.

[33] A.A. Bhattacharya, T. Grune, S. Curry, Crystallographic analysis reveals common modes of binding of medium and long-chain fatty acids to human serum albumin, J. Mol. Biol. 303 (2000) 721–732.

[34] A.A. Spector, Fatty acid binding to plasma albumin, J. Lipid Res. 16 (1975) 165–179.

[35] L. Pollaro, C. Heinis, Strategies to prolong the plasma residence time of peptide drugs, Medchemcomm. 1 (2010) 319–324.

[36] J.B. Buse, A. Garber, J. Rosenstock, W.E. Schmidt, J.H. Brett, N. Videbaek, et al., Liraglutide treatment is associated with a low frequency and magnitude of antibody formation with no apparent impact on glycemic response or increased frequency of adverse events: results from the Liraglutide Effect and Action in Diabetes (LEAD) trials, J. Clin. Endocrinol. Metab. 96 (2011) 1695–1702.

[37] B. Zinman, A. Philis-Tsimikas, B. Cariou, Y. Handelsman, H.W. Rodbard, T. Johansen, et al., Insulin degludec versus insulin glargine in insulin-naive patients with type 2 diabetes: a 1-year, randomized, treat-to-target trial (BEGIN Once Long), Diabetes Care. 35 (2012) 2464–2471.

[38] Y. Shechter, K. Sasson, V. Lev-Goldman, S. Rubinraut, M. Rubinstein, M. Fridkin, Newly designed modifier prolongs the action of short-lived peptides and proteins by allowing their binding to serum albumin, Bioconjug. Chem. 23 (2012) 1577–1586.

[39] H. Zhao, W.A. van der Donk, Regeneration of cofactors for use in biocatalysis., Curr. Opin. Biotechnol. 14 (2003) 583–9.

[40] C.L. James, R.E. Viola, Production and characterization of bifunctional enzymes. Substrate channeling in the aspartate pathway., Biochemistry. 41 (2002) 3726–31.

[41] M.F. Dunn, V. Aguilar, P. Brzović, W.F. Drewe, K.F. Houben, C.A. Leja, et al., The tryptophan synthase bienzyme complex transfers indole between the alpha- and beta-sites via a 25-30 A long tunnel., Biochemistry. 29 (1990) 8598–607.

[42] X. Huang, H.M. Holden, F.M. Raushel, Channeling of substrates and intermediates in enzyme-catalyzed reactions., Annu. Rev. Biochem. 70 (2001) 149–80.

[43] J. Fu, M. Liu, Y. Liu, N.W. Woodbury, H. Yan, Interenzyme substrate diffusion for an enzyme cascade organized on spatially addressable DNA nanostructures, J Am Chem Soc. 134 (2012) 5516–5519.

[44] C. You, S. Myung, Y.-H.P. Zhang, Facilitated Substrate Channeling in a Self-Assembled Trifunctional Enzyme Complex, Angew. Chemie Int. Ed. 51 (2012) 8787–8790.

[45] S.R. Aggarwal, What's fueling the biotech engine-2011 to 2012, Nat. Biotechnol. 30 (2012) 1191–1197.

[46] S. Jevsevar, M. Kunstelj, V.G. Porekar, PEGylation of therapeutic proteins, Biotechnol J. 5 (2010) 113–128.

[47] R.E. Kontermann, Strategies for extended serum half-life of protein therapeutics, Curr. Opin. Biotechnol. 22 (2011) 868–876.

[48] D.M. Czajkowsky, J. Hu, Z. Shao, R.J. Pleass, Fc-fusion proteins: new developments and future perspectives, EMBO Mol Med. 4 (2012) 1015–1028.

[49] S. Kontos, J.A. Hubbell, Drug development: longer-lived proteins, Chem Soc Rev. 41 (2012) 2686–2695.

[50] M.R. Sherman, M.G. Saifer, F. Perez-Ruiz, PEG-uricase in the management of treatment-resistant gout and hyperuricemia, Adv Drug Deliv Rev. 60 (2008) 59–68.

[51] C. Libon, N. Corvaia, J.F. Haeuw, T.N. Nguyen, S. Stahl, J.Y. Bonnefoy, et al., The serum albumin-binding region of streptococcal protein G (BB) potentiates the immunogenicity of the G130-230 RSV-A protein, Vaccine. 17 (1999) 406–414.

[52] R. Stork, D. Muller, R.E. Kontermann, A novel tri-functional antibody fusion protein with improved pharmacokinetic properties generated by fusing a bispecific single-chain diabody with an albumin-binding domain from streptococcal protein G, Protein Eng Des Sel. 20 (2007) 569–576.

[53] L.L. Baggio, Q. Huang, T.J. Brown, D.J. Drucker, A recombinant human glucagon-like peptide (GLP)-1-albumin protein (albugon) mimics peptidergic activation of GLP-1 receptor-dependent pathways coupled with satiety, gastrointestinal motility, and glucose homeostasis, Diabetes. 53 (2004) 2492–2500.

[54] S. Schulte, Half-life extension through albumin fusion technologies, Thromb. Res. 124 Suppl (2009) S6–8.

[55] H.L. Zhao, C. Xue, Y. Wang, X.Y. Li, X.H. Xiong, X.Q. Yao, et al., Circumventing the heterogeneity and instability of human serum albumin-interferon-alpha2b fusion protein by altering its orientation, J. Biotechnol. 131 (2007) 245–252.

[56] I. Jonassen, S. Havelund, T. Hoeg-Jensen, D.B. Steensgaard, P.O. Wahlund, U. Ribel, Design of the novel protraction mechanism of insulin degludec, an ultra-long-acting basal insulin, Pharm. Res. 29 (2012) 2104–2114.

[57] S. Trussel, C. Dumelin, K. Frey, A. Villa, F. Buller, D. Neri, New strategy for the extension of the serum half-life of antibody fragments, Bioconjug. Chem. 20 (2009) 2286–2292.

[58] T.R. Chan, R. Hilgraf, K.B. Sharpless, V. V Fokin, Polytriazoles as copper(I)-stabilizing ligands in catalysis, Org Lett. 6 (2004) 2853–2855.

[59] B.C. Bundy, J.R. Swartz, Site-specific incorporation of p-propargyloxyphenylalanine in a cell-free environment for direct protein-protein click conjugation, Bioconjug Chem. 21 (2010) 255–263.

[60] K.G. Patel, J.R. Swartz, Surface functionalization of virus-like particles by direct conjugation using azide-alkyne click chemistry, Bioconjug Chem. 22 (2011) 376–387.

[61] N. Budisa, Prolegomena to future experimental efforts on genetic code engineering by expanding its amino acid repertoire, Angew. Chemie. Int. Ed. English. 43 (2004) 6426–6463.

[62] T. Hohsaka, Y. Ashizuka, H. Taira, H. Murakami, M. Sisido, Incorporation of nonnatural amino acids into proteins by using various four-base codons in an Escherichia coli in vitro translation system, Biochemistry. 40 (2001) 11060–11064.

[63] B.C. Jester, J.D. Levengood, H. Roy, M. Ibba, K.M. Devine, Nonorthologous replacement of lysyl-tRNA synthetase prevents addition of lysine analogues to the genetic code, Proc. Natl. Acad. Sci. U. S. A. 100 (2003) 14351–14356.

[64] A.J. Link, D.A. Tirrell, Reassignment of sense codons in vivo, Methods. 36 (2005) 291–298.

[65] L. Wang, A. Brock, B. Herberich, P.G. Schultz, Expanding the genetic code of Escherichia coli, Science (80-.). 292 (2001) 498–500.

[66] J.D. Pedelacq, S. Cabantous, T. Tran, T.C. Terwilliger, G.S. Waldo, Engineering and characterization of a superfolder green fluorescent protein, Nat. Biotechnol. 24 (2006) 79–88.

[67] G. Feng, R.H. Mellor, M. Bernstein, C. Keller-Peck, Q.T. Nguyen, M. Wallace, et al., Imaging neuronal subsets in transgenic mice expressing multiple spectral variants of GFP, Neuron. 28 (2000) 41–51.

[68] M. Okabe, M. Ikawa, K. Kominami, T. Nakanishi, Y. Nishimune, "Green mice" as a source of ubiquitous green cells, FEBS Lett. 407 (1997) 313–319.

[69] I. Kwon, P. Wang, D.A. Tirrell, Design of a bacterial host for site-specific incorporation of p-bromophenylalanine into recombinant proteins, J Am Chem Soc. 128 (2006) 11778–11783.

[70] I. Kwon, D.A. Tirrell, Site-specific incorporation of tryptophan analogues into recombinant proteins in bacterial cells, J. Am. Chem. Soc. 129 (2007) 10431–10437.

[71] I. Kwon, K. Kirshenbaum, D.A. Tirrell, Breaking the degeneracy of the genetic code, J Am Chem Soc. 125 (2003) 7512–7513.

[72] K.E. Beatty, J.C. Liu, F. Xie, D.C. Dieterich, E.M. Schuman, Q. Wang, et al., Fluorescence visualization of newly synthesized proteins in mammalian cells, Angew. Chemie. Int. Ed. English. 45 (2006) 7364–7367.

[73] S. Ahmad, M. Gromiha, H. Fawareh, A. Sarai, ASAView: database and tool for solvent accessibility representation in proteins, BMC Bioinformatics. 5 (2004) 51.

[74] K. Arnold, L. Bordoli, J. Kopp, T. Schwede, The SWISS-MODEL workspace: a web-based environment for protein structure homology modelling, Bioinformatics. 22 (2006) 195–201.

[75] Pymol, The PyMOL Molecular Graphics System, Version 1.2r1 Schrödinger, LLC, (n.d.).

[76] P.H. Hirel, M.J. Schmitter, P. Dessen, G. Fayat, S. Blanquet, Extent of N-terminal methionine excision from Escherichia coli proteins is governed by the side-chain length of the penultimate amino acid, Proc. Natl. Acad. Sci. U. S. A. 86 (1989) 8247–8251.

[77] F. Wang, W. Niu, J. Guo, P.G. Schultz, Unnatural amino acid mutagenesis of fluorescent proteins, Angew. Chemie. Int. Ed. English. 51 (2012) 10132–10135.

[78] J.T. DiPiro, Concepts in Clinical Pharmacokinetics, 5th ed., American Society of Health-System Pharmacists, Bethesda, 2010.

[79] Z. Yang, J. Wang, Q. Lu, J. Xu, Y. Kobayashi, T. Takakura, et al., PEGylation confers greatly extended half-life and attenuated immunogenicity to recombinant methioninase in primates, Cancer Res. 64 (2004) 6673–6678.

[80] M.S. Dennis, M. Zhang, Y.G. Meng, M. Kadkhodayan, D. Kirchhofer, D. Combs, et al., Albumin binding as a general strategy for improving the pharmacokinetics of proteins, J. Biol. Chem. 277 (2002) 35035–35043.

[81] B.M. Tijink, T. Laeremans, M. Budde, M. Stigter-van Walsum, T. Dreier, H.J. de Haard, et al., Improved tumor targeting of anti-epidermal growth factor receptor Nanobodies through albumin binding: taking advantage of modular Nanobody technology, Mol Cancer Ther. 7 (2008) 2288–2297.

[82] H. Cho, T. Daniel, Y.J. Buechler, D.C. Litzinger, Z. Maio, A.M. Putnam, et al., Optimized clinical performance of growth hormone with an expanded genetic code, Proc. Natl. Acad. Sci. U. S. A. 108 (2011) 9060–9065.

[83] T.S. Young, I. Ahmad, J.A. Yin, P.G. Schultz, An enhanced system for unnatural amino acid mutagenesis in E. coli., J. Mol. Biol. 395 (2010) 361–74.

[84] C. Besanceney-Webler, H. Jiang, T. Zheng, L. Feng, D. Soriano del Amo, W. Wang, et al., Increasing the efficacy of bioorthogonal click reactions for bioconjugation: a comparative study, Angew Chem Int Ed Engl. 50 (2011) 8051–8056.

[85] A. Nguyen, A.E. Reyes 2nd, M. Zhang, P. McDonald, W.L. Wong, L.A. Damico, et al., The pharmacokinetics of an albumin-binding Fab (AB.Fab) can be modulated as a function of affinity for albumin, Protein Eng Des Sel. 19 (2006) 291–297.

[86] V. Schellenberger, C.W. Wang, N.C. Geething, B.J. Spink, A. Campbell, W. To, et al., A recombinant polypeptide extends the in vivo half-life of peptides and proteins in a tunable manner, Nat. Biotechnol. 27 (2009) 1186–1190.

[87] W. Gao, W. Liu, T. Christensen, M.R. Zalutsky, A. Chilkoti, In situ growth of a PEG-like polymer from the C terminus of an intein fusion protein improves pharmacokinetics and tumor accumulation, Proc. Natl. Acad. Sci. U. S. A. 107 (2010) 16432–16437.

[88] J. Hopp, N. Hornig, K.A. Zettlitz, A. Schwarz, N. Fuss, D. Muller, et al., The effects of affinity and valency of an albumin-binding domain (ABD) on the half-life of a single-chain diabody-ABD fusion protein, Protein Eng Des Sel. 23 (2010) 827–834.

[89] R.S. Aggarwal, What's fueling the biotech engine-2012 to 2013, Nat. Biotechnol. 32 (2014) 32–39.

[90] B. Elsadek, F. Kratz, Impact of albumin on drug delivery--new applications on the horizon, J. Control. Release. 157 (2012) 4–28.

[91] D. Sleep, J. Cameron, L.R. Evans, Albumin as a versatile platform for drug half-life extension, Biochim. Biophys. Acta. 1830 (2013) 5526–5534.

[92] A. Duttaroy, P. Kanakaraj, B.L. Osborn, H. Schneider, O.K. Pickeral, C. Chen, et al., Development of a long-acting insulin analog using albumin fusion technology, Diabetes. 54 (2005) 251–258.

[93] S. Ikuta, V.T. Chuang, Y. Ishima, K. Nakajou, M. Furukawa, H. Watanabe, et al., Albumin fusion of thioredoxin--the production and evaluation of its biological activity for potential therapeutic applications, J. Control. Release. 147 (2010) 17–23.

[94] C.H. Joung, J.Y. Shin, J.K. Koo, J.J. Lim, J.S. Wang, S.J. Lee, et al., Production and characterization of long-acting recombinant human albumin-EPO fusion protein expressed in CHO cell, Protein Expr. Purif. 68 (2009) 137–145.

[95] B.L. Osborn, L. Sekut, M. Corcoran, C. Poortman, B. Sturm, G. Chen, et al., Albutropin: a growth hormone-albumin fusion with improved pharmacokinetics and pharmacodynamics in rats and monkeys, Eur. J. Pharmacol. 456 (2002) 149–158.

[96] J. Rosenstock, J. Reusch, M. Bush, F. Yang, M. Stewart, Potential of albiglutide, a long-acting GLP-1 receptor agonist, in type 2 diabetes: a randomized controlled trial exploring weekly, biweekly, and monthly dosing, Diabetes Care. 32 (2009) 1880–1886.

[97] G.M. Subramanian, M. Fiscella, A. Lamouse-Smith, S. Zeuzem, J.G. McHutchison, Albinterferon alpha-2b: a genetic fusion protein for the treatment of chronic hepatitis C, Nat. Biotechnol. 25 (2007) 1411–1419.

[98] A.A. Cordes, C.W. Platt, J.F. Carpenter, T.W. Randolph, Selective domain stabilization as a strategy to reduce fusion protein aggregation, J. Pharm. Sci. 101 (2012) 1400–1409.

[99] S.R. Schmidt, Fusion Protein Technologies for Biopharmaceuticals: Applications and Challenges, in: Fusion Protein Technol. Biopharm. Appl. Challenges, First ed., Wiley, New Jersey, 2013: p. 95.

[100] H.L. Zhao, C. Xue, Y. Wang, B. Sun, X.Q. Yao, Z.M. Liu, Elimination of the free sulfhydryl group in the human serum albumin (HSA) moiety of human interferon-alpha2b

and HSA fusion protein increases its stability against mechanical and thermal stresses, Eur. J. Pharm. Biopharm. 72 (2009) 405–411.

[101] T. Plass, S. Milles, C. Koehler, C. Schultz, E.A. Lemke, Genetically encoded copper-free click chemistry, Angew. Chemie. Int. Ed. English. 50 (2011) 3878–3881.

[102] J.L. Seitchik, J.C. Peeler, M.T. Taylor, M.L. Blackman, T.W. Rhoads, R.B. Cooley, et al., Genetically encoded tetrazine amino acid directs rapid site-specific in vivo bioorthogonal ligation with trans-cyclooctenes, J. Am. Chem. Soc. 134 (2012) 2898–2901.

[103] Q. Wang, T.R. Chan, R. Hilgraf, V. V Fokin, K.B. Sharpless, M.G. Finn, Bioconjugation by copper(I)-catalyzed azide-alkyne [3 + 2] cycloaddition, J Am Chem Soc. 125 (2003) 3192–3193.

[104] P.R. Chen, D. Groff, J. Guo, W. Ou, S. Cellitti, B.H. Geierstanger, et al., A facile system for encoding unnatural amino acids in mammalian cells, Angew. Chemie. Int. Ed. English. 48 (2009) 4052–4055.

[105] S.M. Hancock, R. Uprety, A. Deiters, J.W. Chin, Expanding the genetic code of yeast for incorporation of diverse unnatural amino acids via a pyrrolysyl-tRNA synthetase/tRNA pair, J. Am. Chem. Soc. 132 (2010) 14819–14824.

[106] M. King, A. Wagner, Developments in the field of bioorthogonal bond forming reactions-past and present trends, Bioconjug. Chem. 25 (2014) 825–839.

[107] C.D. Spicer, B.G. Davis, Selective chemical protein modification, Nat. Commun. 5 (2014) 4740.

[108] A. Deiters, T.A. Cropp, D. Summerer, M. Mukherji, P.G. Schultz, Site-specific PEGylation of proteins containing unnatural amino acids, Bioorganic Med. Chem. Lett. 14 (2004) 5743–5745.

[109] S.B. Sun, P.G. Schultz, C.H. Kim, Therapeutic applications of an expanded genetic code, Chembiochem. 15 (2014) 1721–1729.

[110] F. Tian, Y. Lu, A. Manibusan, A. Sellers, H. Tran, Y. Sun, et al., A general approach to site-specific antibody drug conjugates, Proc. Natl. Acad. Sci. U. S. A. 111 (2014) 1766–1771.

[111] S.I. Lim, Y. Mizuta, A. Takasu, Y.S. Hahn, Y.H. Kim, I. Kwon, Site-specific fatty acid-conjugation to prolong protein half-life in vivo, J. Control. Release. 170 (2013) 219–225.

[112] Q. Zeng, S. Saha, L.A. Lee, H. Barnhill, J. Oxsher, T. Dreher, et al., Chemoselective modification of turnip yellow mosaic virus by Cu(I) catalyzed azide-alkyne 1,3-dipolar cycloaddition reaction and its application in cell binding, Bioconjug. Chem. 22 (2011) 58–66.

[113] N.J. Agard, J.A. Prescher, C.R. Bertozzi, A strain-promoted [3 + 2] azide-alkyne cycloaddition for covalent modification of biomolecules in living systems, J. Am. Chem. Soc. 126 (2004) 15046–15047.

[114] X. Ning, J. Guo, M.A. Wolfert, G.J. Boons, Visualizing metabolically labeled glycoconjugates of living cells by copper-free and fast huisgen cycloadditions, Angew. Chemie. Int. Ed. English. 47 (2008) 2253–2255.

[115] L. Gabison, M. Chiadmi, M. El Hajji, B. Castro, N. Colloc'h, T. Prange, Near-atomic resolution structures of urate oxidase complexed with its substrate and analogues: the protonation state of the ligand, Acta Crystallogr. Sect. D Biol. Crystallogr. 66 (2010) 714–724.

[116] O. Bessmertny, L.M. Robitaille, M.S. Cairo, Rasburicase: a new approach for preventing and/or treating tumor lysis syndrome, Curr. Pharm. Des. 11 (2005) 4177–4185.

[117] P.M. Navolanic, C.H. Pui, R.A. Larson, M.R. Bishop, T.E. Pearce, M.S. Cairo, et al., Elitek-rasburicase: an effective means to prevent and treat hyperuricemia associated with tumor lysis syndrome, a Meeting Report, Dallas, Texas, January 2002, Leukemia. 17 (2003) 499–514.

[118] C. Geraths, M. Daoud-El Baba, G. Charpin-El Hamri, W. Weber, A biohybrid hydrogel for the urate-responsive release of urate oxidase, J. Control. Release. 171 (2013) 57–62.

[119] S. Jeha, C.H. Pui, Recombinant urate oxidase (rasburicase) in the prophylaxis and treatment of tumor lysis syndrome, Contrib. Nephrol. 147 (2005) 69–79.

[120] A.R. Sood, L.D. Burry, D.K. Cheng, Clarifying the role of rasburicase in tumor lysis syndrome, Pharmacotherapy. 27 (2007) 111–121.

[121] N. Schlesinger, U. Yasothan, P. Kirkpatrick, Pegloticase, Nat. Rev. Drug Discov. 10 (2011) 17–18.

[122] C. Zhang, K. Fan, H. Luo, X. Ma, R. Liu, L. Yang, et al., Characterization, efficacy, pharmacokinetics, and biodistribution of 5kDa mPEG modified tetrameric canine uricase variant, Int. J. Pharm. 430 (2012) 307–317.

[123] J.S. Bomalaski, F.W. Holtsberg, C.M. Ensor, M.A. Clark, Uricase formulated with polyethylene glycol (uricase-PEG 20): biochemical rationale and preclinical studies, J. Rheumatol. 29 (2002) 1942–1949.

[124] C.S. Fishburn, The pharmacology of PEGylation: balancing PD with PK to generate novel therapeutics, J. Pharm. Sci. 97 (2008) 4167–4183.

[125] T. McDonnell, Y. Ioannou, A. Rahman, PEGylated drugs in rheumatology--why develop them and do they work?, Rheumatology. 53 (2014) 391–396.

[126] S. Freitas Dda, P.J. Spencer, R.C. Vassao, J. Abrahao-Neto, Biochemical and biopharmaceutical properties of PEGylated uricase, Int. J. Pharm. 387 (2010) 215–222.

[127] H. Tian, Y. Guo, X. Gao, W. Yao, PEGylation enhancement of pH stability of uricase via inhibitive tetramer dissociation, J. Pharm. Pharmacol. 65 (2012) 53–63.

[128] J.T. Kratzer, M.A. Lanaspa, M.N. Murphy, C. Cicerchi, C.L. Graves, P.A. Tipton, et al., Evolutionary history and metabolic insights of ancient mammalian uricases, Proc. Natl. Acad. Sci. U. S. A. 111 (2014) 3763–3768.

[129] S.R. Bond, C.C. Naus, RF-Cloning.org: an online tool for the design of restriction-free cloning projects, Nucleic Acids Res. 40 (2012) W209–13.

[130] C.N. Pace, F. Vajdos, L. Fee, G. Grimsley, T. Gray, How to measure and predict the molar absorption coefficient of a protein., Protein Sci. 4 (1995) 2411–23.

[131] G.R. Grimsley, C.N. Pace, Current Protocols in Protein Science, in: G.P. Taylor (Ed.), Curr. Protoc. Protein Sci., Wiley, New Jersey, 2004: p. Unit 3.1.

[132] L. Whitmore, B.A. Wallace, Protein secondary structure analyses from circular dichroism spectroscopy: methods and reference databases, Biopolymers. 89 (2008) 392–400.

[133] J.A. Irwin, H.E. Wong, I. Kwon, Different fates of Alzheimer's disease amyloid-beta fibrils remodeled by biocompatible small molecules, Biomacromolecules. 14 (2013) 264–274.

[134] N. Sreerama, S.Y. Venyaminov, R.W. Woody, Estimation of the number of alpha-helical and beta-strand segments in proteins using circular dichroism spectroscopy, Protein Sci. 8 (1999) 370–380.

[135] N. Sreerama, R.W. Woody, A self-consistent method for the analysis of protein secondary structure from circular dichroism, Anal. Biochem. 209 (1993) 32–44.

[136] C. Zhang, K. Fan, X. Ma, D. Wei, Impact of large aggregated uricases and PEG diol on accelerated blood clearance of PEGylated canine uricase, PLoS One. 7 (2012) e39659.

[137] B. Ahren, R.M. Baldwin, P.J. Havel, Pharmacokinetics of human leptin in mice and rhesus monkeys, Int. J. Obes. Relat. Metab. Disord. 24 (2000) 1579–1585.

[138] J.M. Sanders, G.A. Knudsen, L.S. Birnbaum, The fate of beta-hexabromocyclododecane in female C57BL/6 mice, Toxicol. Sci. 134 (2013) 251–257.

[139] M. Simon, R. Frey, U. Zangemeister-Wittke, A. Pluckthun, Orthogonal assembly of a designed ankyrin repeat protein-cytotoxin conjugate with a clickable serum albumin module for half-life extension, Bioconjug. Chem. 24 (2013) 1955–1966.

[140] J.T. Andersen, B. Dalhus, J. Cameron, M.B. Daba, A. Plumridge, L. Evans, et al., Structure-based mutagenesis reveals the albumin-binding site of the neonatal Fc receptor, Nat. Commun. 3 (2012) 610.

[141] Y. Guillaneuf, P.E. Dufils, L. Autissier, M. Rollet, D. Gigmes, D. Bertin, Radical Chain End Chemical Transformation of SG1-Based Polystyrenes, Macromolecules. 43 (2010) 91–100.

[142] Y. Li, J.N. Hoskins, S.G. Sreerama, S.M. Grayson, MALDI-TOF Mass Spectral Characterization of Polymers Containing an Azide Group: Evidence of Metastable Ions, Macromolecules. 43 (2010) 6225–6228.

[143] J.F. Lutz, H.G. Borner, K. Weichenhan, Combining atom transfer radical polymerization and click chemistry: A versatile method for the preparation of end-functional polymers, Macromol. Rapid Commun. 26 (2005) 514–518.

[144] J. Raynaud, C. Absalon, Y. Gnanou, D. Taton, N-heterocyclic carbene-induced zwitterionic ring-opening polymerization of ethylene oxide and direct synthesis of alpha,omega-difunctionalized poly(ethylene oxide)s and poly(ethylene oxide)-b-poly(epsilon-caprolactone) block copolymers, J. Am. Chem. Soc. 131 (2009) 3201–3209.

[145] S. Gregoire, S. Zhang, J. Costanzo, K. Wilson, E.J. Fernandez, I. Kwon, Cis-suppression to arrest protein aggregation in mammalian cells, Biotechnol. Bioeng. 111 (2014) 462–474.

[146] M.J. Lajoie, S. Kosuri, J.A. Mosberg, C.J. Gregg, D. Zhang, G.M. Church, Probing the limits of genetic recoding in essential genes, Science (80-.). 342 (2013) 361–363.

[147] P.S. Banerjee, P. Ostapchuk, P. Hearing, I.S. Carrico, Unnatural amino acid incorporation onto adenoviral (Ad) coat proteins facilitates chemoselective modification and retargeting of Ad type 5 vectors, J. Virol. 85 (2011) 7546–7554.

[148] M.R. Fleissner, E.M. Brustad, T. Kalai, C. Altenbach, D. Cascio, F.B. Peters, et al., Site-directed spin labeling of a genetically encoded unnatural amino acid, Proc. Natl. Acad. Sci. U. S. A. 106 (2009) 21637–21642.

[149] S.I. Lim, Y. Mizuta, A. Takasu, Y.H. Kim, I. Kwon, Site-specific bioconjugation of a murine dihydrofolate reductase enzyme by copper(I)-catalyzed azide-alkyne cycloaddition with retained activity, PLoS One. 9 (2014) e98403.

[150] S.C. Reddington, E.M. Tippmann, D.D. Jones, Residue choice defines efficiency and influence of bioorthogonal protein modification via genetically encoded strain promoted Click chemistry, Chem. Commun. 48 (2012) 8419–8421.

[151] T. Fujita, Y. Yasuda, Y. Takakura, M. Hashida, H. Sezaki, Tissue distribution of 111In-labeled uricase conjugated with charged dextrans and polyethylene glycol, J. Pharmacobiodyn. 14 (1991) 623–629.

[152] M.G. Saifer, L.D. Williams, M.A. Sobczyk, S.J. Michaels, M.R. Sherman, Selectivity of binding of PEGs and PEG-like oligomers to anti-PEG antibodies induced by methoxyPEG-proteins, Mol. Immunol. 57 (2014) 236–246.

[153] M.R. Sherman, L.D. Williams, M.A. Sobczyk, S.J. Michaels, M.G. Saifer, Role of the methoxy group in immune responses to mPEG-protein conjugates, Bioconjug. Chem. 23 (2012) 485–499.

[154] J.T. Andersen, M.B. Daba, G. Berntzen, T.E. Michaelsen, I. Sandlie, Cross-species binding analyses of mouse and human neonatal Fc receptor show dramatic differences in immunoglobulin G and albumin binding., J. Biol. Chem. 285 (2010) 4826–36.

[155] M.M. Schmidt, S.A. Townson, A.J. Andreucci, B.M. King, E.B. Schirmer, A.J. Murillo, et al., Crystal Structure of an HSA/FcRn Complex Reveals Recycling by Competitive Mimicry of HSA Ligands at a pH-Dependent Hydrophobic Interface, Structure. 21 (2013) 1966–1978.

[156] M.S. Hershfield, L.J. Roberts 2nd, N.J. Ganson, S.J. Kelly, I. Santisteban, E. Scarlett, et al., Treating gout with pegloticase, a PEGylated urate oxidase, provides insight into the importance of uric acid as an antioxidant in vivo, Proc Natl Acad Sci U S A. 107 (2010) 14351–14356.

[157] M.P. Gillmeister, M.J. Betenbaugh, P.S. Fishman, Cellular trafficking and photochemical internalization of cell penetrating peptide linked cargo proteins: a dual fluorescent labeling study, Bioconjug Chem. 22 (2011) 556–566.

[158] S.Y. McLoughlin, M. Kastantin, D.K. Schwartz, J.L. Kaar, Single-molecule resolution of protein structure and interfacial dynamics on biomaterial surfaces, Proc Natl Acad Sci U S A. 110 (2013) 19396–19401.

[159] X.T. Zheng, A. Than, A. Ananthanaraya, D.H. Kim, P. Chen, Graphene quantum dots as universal fluorophores and their use in revealing regulated trafficking of insulin receptors in adipocytes, ACS Nano. 7 (2013) 6278–6286.

[160] N. Aissaoui, J. Landoulsi, L. Bergaoui, S. Boujday, J.F. Lambert, Catalytic activity and thermostability of enzymes immobilized on silanized surface: influence of the crosslinking agent, Enzym. Microb Technol. 52 (2013) 336–343.

[161] E. Basle, N. Joubert, M. Pucheault, Protein chemical modification on endogenous amino acids, Chem Biol. 17 (2010) 213–227.

[162] F. Rusmini, Z. Zhong, J. Feijen, Protein immobilization strategies for protein biochips, Biomacromolecules. 8 (2007) 1775–1789.

[163] C. Albayrak, J.R. Swartz, Cell-free co-production of an orthogonal transfer RNA activates efficient site-specific non-natural amino acid incorporation, Nucleic Acids Res. 41 (2013) 5949–5963.

[164] N. Budisa, Expanded genetic code for the engineering of ribosomally synthetized and post-translationally modified peptide natural products (RiPPs), Curr Opin Biotechnol. 24 (2013) 591–598.

[165] C.H. Kim, J.Y. Axup, P.G. Schultz, Protein conjugation with genetically encoded unnatural amino acids, Curr Opin Chem Biol. 17 (2013) 412–419.

[166] S.W. Santoro, J.C. Anderson, V. Lakshman, P.G. Schultz, An archaebacteria-derived glutamyl-tRNA synthetase and tRNA pair for unnatural amino acid mutagenesis of proteins in Escherichia coli, Nucleic Acids Res. 31 (2003) 6700–6709.

[167] J.C. Anderson, P.G. Schultz, Adaptation of an orthogonal archaeal leucyl-tRNA and synthetase pair for four-base, amber, and opal suppression, Biochemistry. 42 (2003) 9598–9608.

[168] M. Sisido, K. Ninomiya, T. Ohtsuki, T. Hohsaka, Four-base codon/anticodon strategy and non-enzymatic aminoacylation for protein engineering with non-natural amino acids, Methods. 36 (2005) 270–278.

[169] S.E. Averick, E. Paredes, D. Grahacharya, B.F. Woodman, S.J. Miyake-Stoner, R.A. Mehl, et al., A protein-polymer hybrid mediated by DNA, Langmuir. 28 (2012) 1954–1958.

[170] K.E. Beatty, F. Xie, Q. Wang, D.A. Tirrell, Selective dye-labeling of newly synthesized proteins in bacterial cells, J Am Chem Soc. 127 (2005) 14150–14151.

[171] D. Banerjee, A.P. Liu, N.R. Voss, S.L. Schmid, M.G. Finn, Multivalent display and receptor-mediated endocytosis of transferrin on virus-like particles, Chembiochem. 11 (2010) 1273–1279.

[172] N.F. Steinmetz, V. Hong, E.D. Spoerke, P. Lu, K. Breitenkamp, M.G. Finn, et al., Buckyballs meet viral nanoparticles: candidates for biomedicine, J Am Chem Soc. 131 (2009) 17093–17095.

[173] N. Soundrarajan, S. Sokalingam, G. Raghunathan, N. Budisa, H.J. Paik, T.H. Yoo, et al., Conjugation of proteins by installing BIO-orthogonally reactive groups at their N-termini, PLoS One. 7 (2012) e46741.

[174] N.J. Agard, J.M. Baskin, J.A. Prescher, A. Lo, C.R. Bertozzi, A comparative study of bioorthogonal reactions with azides, ACS Chem Biol. 1 (2006) 644–648.

[175] E.H. Christen, R.J. Gubeli, B. Kaufmann, L. Merkel, R. Schoenmakers, N. Budisa, et al., Evaluation of bicinchoninic acid as a ligand for copper(I)-catalyzed azide-alkyne bioconjugations, Org Biomol Chem. 10 (2012) 6629–6632.

[176] V. Hong, S.I. Presolski, C. Ma, M.G. Finn, Analysis and optimization of copper-catalyzed azide-alkyne cycloaddition for bioconjugation, Angew Chem Int Ed Engl. 48 (2009) 9879–9883.

[177] A.A. Kislukhin, V.P. Hong, K.E. Breitenkamp, M.G. Finn, Relative performance of alkynes in copper-catalyzed azide-alkyne cycloaddition, Bioconjug Chem. 24 (2013) 684–689.

[178] S.I. Presolski, V.P. Hong, M.G. Finn, Copper-Catalyzed Azide-Alkyne Click Chemistry for Bioconjugation, Curr Protoc Chem Biol. 3 (2011) 153–162.

[179] J.L. Brennan, N.S. Hatzakis, T.R. Tshikhudo, N. Dirvianskyte, V. Razumas, S. Patkar, et al., Bionanoconjugation via click chemistry: The creation of functional hybrids of lipases and gold nanoparticles, Bioconjug Chem. 17 (2006) 1373–1375.

[180] S. Schoffelen, M.H. Lambermon, M.B. van Eldijk, J.C. van Hest, Site-specific modification of Candida antarctica lipase B via residue-specific incorporation of a non-canonical amino acid, Bioconjug Chem. 19 (2008) 1127–1131.

[181] K. Hernandez, R. Fernandez-Lafuente, Control of protein immobilization: coupling immobilization and site-directed mutagenesis to improve biocatalyst or biosensor performance, Enzym. Microb Technol. 48 (2011) 107–122.

[182] T. Hessa, H. Kim, K. Bihlmaier, C. Lundin, J. Boekel, H. Andersson, et al., Recognition of transmembrane helices by the endoplasmic reticulum translocon, Nature. 433 (2005) 377–381.

[183] V. Cody, J. Pace, A. Rosowsky, Structural analysis of a holoenzyme complex of mouse dihydrofolate reductase with NADPH and a ternary complex with the potent and selective inhibitor 2,4-diamino-6-(2’-hydroxydibenz[b,f]azepin-5-yl)methylpteridine, Acta Crystallogr D Biol Crystallogr. 64 (2008) 977–984.

[184] D.D. Young, T.S. Young, M. Jahnz, I. Ahmad, G. Spraggon, P.G. Schultz, An evolved aminoacyl-tRNA synthetase with atypical polysubstrate specificity, Biochemistry. 50 (2011) 1894–1900.

[185] J. Liu, C.A. Castaneda, B.J. Wilkins, D. Fushman, T.A. Cropp, Condensed E. coli cultures for highly efficient production of proteins containing unnatural amino acids, Bioorg Med Chem Lett. 20 (2010) 5613–5616.

[186] D. Schneider, T. Schneider, D. Rosner, M. Scheffner, A. Marx, Improving bioorthogonal protein ubiquitylation by click reaction, Bioorg Med Chem. 21 (2013) 3430–3435.

[187] K. Sivakumar, F. Xie, B.M. Cash, S. Long, H.N. Barnhill, Q. Wang, A fluorogenic 1,3-dipolar cycloaddition reaction of 3-azidocoumarins and acetylenes, Org Lett. 6 (2004) 4603–4606.

[188] W.F. Busby Jr., J.M. Ackermann, C.L. Crespi, Effect of methanol, ethanol, dimethyl sulfoxide, and acetonitrile on in vitro activities of cDNA-expressed human cytochromes P-450, Drug Metab Dispos. 27 (1999) 246–249.

[189] J. Easterbrook, C. Lu, Y. Sakai, A.P. Li, Effects of organic solvents on the activities of cytochrome P450 isoforms, UDP-dependent glucuronyl transferase, and phenol sulfotransferase in human hepatocytes, Drug Metab Dispos. 29 (2001) 141–144.

[190] V. Shah, P. Baldrian, I. Eichlerova, R. Dave, D. Madamwar, F. Nerud, et al., Influence of dimethyl sulfoxide on extracellular enzyme production by Pleurotus ostreatus, Biotechnol Lett. 28 (2006) 651–655.

[191] A.R. Goerke, J.R. Swartz, High-level cell-free synthesis yields of proteins containing site-specific non-natural amino acids, Biotechnol Bioeng. 102 (2009) 400–416.

[192] M.R. Levengood, C.C. Kerwood, C. Chatterjee, W.A. van der Donk, Investigation of the substrate specificity of lacticin 481 synthetase by using nonproteinogenic amino acids, Chembiochem. 10 (2009) 911–919.

[193] P.J. Thornalley, Glutathione-dependent detoxification of alpha-oxoaldehydes by the glyoxalase system: involvement in disease mechanisms and antiproliferative activity of glyoxalase I inhibitors, Chem Biol Interact. 111-112 (1998) 137–151.

[194] N.W. Nairn, K.D. Shanebeck, A. Wang, T.J. Graddis, M.P. VanBrunt, K.C. Thornton, et al., Development of copper-catalyzed azide-alkyne cycloaddition for increased in vivo efficacy of interferon beta-1b by site-specific PEGylation, Bioconjug Chem. 23 (2012) 2087–2097.

[195] S. Schoffelen, J. Beekwilder, M.F. Debets, D. Bosch, J.C. van Hest, Construction of a multifunctional enzyme complex via the strain-promoted azide-alkyne cycloaddition, Bioconjug Chem. 24 (2013) 987–996.

[196] V. Cody, J. Pace, K. Chisum, A. Rosowsky, New insights into DHFR interactions: analysis of Pneumocystis carinii and mouse DHFR complexes with NADPH and two highly potent 5-(omega-carboxy(alkyloxy) trimethoprim derivatives reveals conformational correlations with activity and novel parallel ring s, Proteins. 65 (2006) 959–969.

[197] E.W. Miles, S. Rhee, D.R. Davies, The molecular basis of substrate channeling., J. Biol. Chem. 274 (1999) 12193–6.

[198] D.K. Srivastava, S.A. Bernhard, Metabolite transfer via enzyme-enzyme complexes., Science. 234 (1986) 1081–6.

[199] R.N. Perham, Swinging arms and swinging domains in multifunctional enzymes: catalytic machines for multistep reactions., Annu. Rev. Biochem. 69 (2000) 961–1004.

[200] J.B. Thoden, H.M. Holden, G. Wesenberg, F.M. Raushel, I. Rayment, Structure of carbamoyl phosphate synthetase: a journey of 96 A from substrate to product., Biochemistry. 36 (1997) 6305–16.

[201] D. Kohls, T. Sulea, E.O. Purisima, R.E. MacKenzie, A. Vrielink, The crystal structure of the formiminotransferase domain of formiminotransferase-cyclodeaminase: implications for substrate channeling in a bifunctional enzyme., Structure. 8 (2000) 35–46.

[202] M. Leibundgut, T. Maier, S. Jenni, N. Ban, The multienzyme architecture of eukaryotic fatty acid synthases, Curr. Opin. Struct. Biol. 18 (2008) 714–725.

[203] T.M. Schmeing, V. Ramakrishnan, What recent ribosome structures have revealed about the mechanism of translation., Nature. 461 (2009) 1234–42.

[204] S. An, R. Kumar, E.D. Sheets, S.J. Benkovic, Reversible compartmentalization of de novo purine biosynthetic complexes in living cells., Science. 320 (2008) 103–6.

[205] R. Narayanaswamy, M. Levy, M. Tsechansky, G.M. Stovall, J.D. O'Connell, J. Mirrielees, et al., Widespread reorganization of metabolic enzymes into reversible assemblies upon nutrient starvation., Proc. Natl. Acad. Sci. U. S. A. 106 (2009) 10147–52.

[206] R.J. Conrado, G.C. Wu, J.T. Boock, H. Xu, S.Y. Chen, T. Lebar, et al., DNA-guided assembly of biosynthetic pathways promotes improved catalytic efficiency., Nucleic Acids Res. 40 (2012) 1879–89.

[207] J.E. Dueber, G.C. Wu, G.R. Malmirchegini, T.S. Moon, C.J. Petzold, A. V Ullal, et al., Synthetic protein scaffolds provide modular control over metabolic flux., Nat. Biotechnol. 27 (2009) 753–9.

[208] T.S. Moon, J.E. Dueber, E. Shiue, K.L.J. Prather, Use of modular, synthetic scaffolds for improved production of glucaric acid in engineered E. coli., Metab. Eng. 12 (2010) 298–305.

[209] C.J. Delebecque, A.B. Lindner, P.A. Silver, F.A. Aldaye, Organization of intracellular reactions with rationally designed RNA assemblies., Science. 333 (2011) 470–4.

[210] M. Castellana, M.Z. Wilson, Y. Xu, P. Joshi, I.M. Cristea, J.D. Rabinowitz, et al., Enzyme clustering accelerates processing of intermediates through metabolic channeling., Nat. Biotechnol. 32 (2014) 1011–8.

[211] J. Fu, Y.R. Yang, A. Johnson-Buck, M. Liu, Y. Liu, N.G. Walter, et al., Multi-enzyme complexes on DNA scaffolds capable of substrate channelling with an artificial swinging arm., Nat. Nanotechnol. 9 (2014) 531–6.

[212] P. Bauler, G. Huber, T. Leyh, J.A. McCammon, Channeling by Proximity: The Catalytic Advantages of Active Site Colocalization Using Brownian Dynamics., J. Phys. Chem. Lett. 1 (2010) 1332–1335.

[213] J.-L. Lin, L. Palomec, I. Wheeldon, Design and Analysis of Enhanced Catalysis in Scaffolded Multienzyme Cascade Reactions, ACS Catal. 4 (2014) 505–511.

[214] Y. Kim, S.H. Kim, D. Ferracane, J.A. Katzenellenbogen, C.M. Schroeder, Specific labeling of zinc finger proteins using noncanonical amino acids and copper-free click chemistry., Bioconjug. Chem. 23 (2012) 1891–901.

[215] M.L. Blackman, M. Royzen, J.M. Fox, Tetrazine ligation: fast bioconjugation based on inverse-electron-demand Diels-Alder reactivity., J. Am. Chem. Soc. 130 (2008) 13518–9.

[216] N.K. Devaraj, R. Weissleder, S.A. Hilderbrand, Tetrazine-based cycloadditions: application to pretargeted live cell imaging., Bioconjug. Chem. 19 (2008) 2297–9.

[217] H. Choe, J.C. Joo, D.H. Cho, M.H. Kim, S.H. Lee, K.D. Jung, et al., Efficient CO2-reducing activity of NAD-dependent formate dehydrogenase from Thiobacillus sp. KNK65MA for formate production from CO2 gas., PLoS One. 9 (2014) e103111.

[218] P. Brünker, J. Altenbuchner, K.D. Kulbe, R. Mattes, Cloning, nucleotide sequence and expression of a mannitol dehydrogenase gene from Pseudomonas fluorescens DSM 50106 in Escherichia coli., Biochim. Biophys. Acta. 1351 (1997) 157–67.

[219] H. Nanba, Y. Takaoka, J. Hasegawa, Purification and characterization of an alpha-haloketone-resistant formate dehydrogenase from Thiobacillus sp. strain KNK65MA, and cloning of the gene., Biosci. Biotechnol. Biochem. 67 (2003) 2145–53.

[220] A. Weckbecker, H. Gröger, W. Hummel, Regeneration of nicotinamide coenzymes: principles and applications for the synthesis of chiral compounds., Adv. Biochem. Eng. Biotechnol. 120 (2010) 195–242.

[221] M. Slatner, G. Nagl, D. Haltrich, K.D. Kulbe, B. Nidetzky, Enzymatic Production of Pure D-Mannitol at High Productivity, (2009).

[222] S.M. Bhatt, A. Mohan, S.K. Srivastava, Challenges in Enzymatic Route of Mannitol Production, ISRN Biotechnol. 2013 (2013) 1–13.

[223] B.M. Hutchins, S.A. Kazane, K. Staflin, J.S. Forsyth, B. Felding-Habermann, P.G. Schultz, et al., Site-specific coupling and sterically controlled formation of multimeric antibody fab fragments with unnatural amino acids., J. Mol. Biol. 406 (2011) 595–603.

[224] S.A. Kazane, J.Y. Axup, C.H. Kim, M. Ciobanu, E.D. Wold, S. Barluenga, et al., Self-assembled antibody multimers through peptide nucleic acid conjugation., J. Am. Chem. Soc. 135 (2013) 340–6.

[225] C.H. Kim, J.Y. Axup, A. Dubrovska, S.A. Kazane, B.A. Hutchins, E.D. Wold, et al., Synthesis of bispecific antibodies using genetically encoded unnatural amino acids., J. Am. Chem. Soc. 134 (2012) 9918–21.

[226] D. Guan, Y. Kurra, W. Liu, Z. Chen, A click chemistry approach to site-specific immobilization of a small laccase enables efficient direct electron transfer in a biocathode., Chem. Commun. (Camb). 51 (2015) 2522–5.

[227] M.H. Seo, J. Han, Z. Jin, D.W. Lee, H.S. Park, H.S. Kim, Controlled and oriented immobilization of protein by site-specific incorporation of unnatural amino acid, Anal Chem. 83 (2011) 2841–2845.